University of Alberta

Development of High Efficiency and New Selectivity Liquid Chromatographic Phases for the Separation of Ionic and Hydrophilic Analytes

by

Muhammad Farooq Wahab

A thesis submitted to the Faculty of Graduate Studies and Research
in partial fulfillment of the requirements for the degree of

Doctor of Philosophy

Department of Chemistry

Fall 2013
Edmonton, Alberta

This thesis is dedicated to my parents, Dr. Abdul Wahab and Razia Wahab

ABSTRACT

Separation of low molecular weight ions and hydrophilic analytes is achieved by high performance ion chromatography (IC) and hydrophilic interaction liquid chromatography (HILIC). The goal of this thesis was three-fold: to increase the efficiency of IC separations by employing small particles; to develop new selectivity phases for HILIC; and to understand the factors that can lead to distorted peak shapes.

Long columns packed with large polymeric particles (6.5-13 μm) still dominate IC. This work investigated 3 μm carbon clad zirconia to which benzene sulfonic acid was bonded using diazonium chemistry. A 5 cm agglomerated anion exchanger was developed by adsorbing polycationic latexes to the particle surface. The efficiencies achieved (~ 51,000 /m) were superior to those of commercial column (~ 22,500 /m).

In addition to particle size, column packing process strongly affects the efficiency. Packing studies with sulfonated particles (4.4 μm) showed that dispersed slurries are desirable to avoid particle agglomeration. Dispersed suspensions exhibit shear thickening that can be overcome by heating the slurry during column packing. Near optimum (reduced plate height ~ 2) packing of agglomerated columns was achieved. These studies concluded that the colloidal and rheological aspects of microparticulates must be considered to optimize packing.

A new class of HILIC phases was created by modification of porous graphitic carbon (PGC) using diazonium chemistry. The hydrophobic PGC

surface was converted into a polar HILIC phase by attaching benzoic acid groups. This phase showed unusual selectivity, which was different from 35 stationary phases. The utility of the phase was demonstrated for separations of nucleotides, phenols, and carboxylic acids.

Overloading a column reduces the separation efficiency and alters the peak shape from Gaussian peaks to fronted or tailed peak profiles. Studies with IC columns showed that if the eluent anion is more *strongly* retained than the analyte ion on an ion exchanger, the analyte peak is *fronting*. If the eluent is more *weakly* retained on the stationary phase, the analyte peak always *tails* under overload conditions.

Overall, this work has enhanced the fundamental understanding in the column packing process and offered new materials for the separation of ionic and polar analytes.

ACKNOWLEDGEMENTS

The research work contained in this thesis would not have been possible without the moral support, intellectual discussions and advice from some brilliant minds around me. First, I would like to thank God for making everything possible. I am grateful to Prof. Charles Lucy for his continual support, guidance, patience and additional useful “career tips” throughout the graduate degree program. He provided many opportunities for oral and poster presentations in major scientific conferences. A special thanks goes to Christopher A. Pohl (Dionex, Thermo Fisher) whose insightful discussions gave me a deeper understanding of the packing process and the chemistry of the stationary phases which is not available in the scientific literature. I would to like to personally thank Dr. Harald Ritchie and Jamieson Doug (Thermo Fisher) for the provision of porous graphitic carbon and other proprietary column packing supplies for my work. Helpful discussions on diazonium chemistry with Dr. Richard McCreery and Dr. Mark McDermott are gratefully acknowledged. I am grateful to the machine and glass shops for their technical support. I am extremely grateful to the University of Alberta for the financial support in the form of the FS Chia Scholarship and a Research Assistantship.

I extend my sincere gratitude to Dr. Robert Campbell and Dr. Mark McDermott for a wonderful time in their spectroscopy teaching labs for the last 5 years. I would like to acknowledge past and present Lucy group members especially Mohammed E. A. Ibrahim for collaborating with me on two interesting research projects. Thanks to Chad, Mahmoud, Lei, Jordan and Chuen for a good time in the

laboratory. I wish to thank Mr. Mustafa Kamal, Mr. and Mrs. Ghani for their support during my stay in Edmonton. This thesis also owes its existence to my siblings (Wasim, Baber and Shazia) who were in constant touch with me for the last five years for providing encouragement and moral support. Finally, I also wish to thank all my friends, colleagues, former students, teachers both in Pakistan and Canada.

TABLE OF CONTENTS

CHAPTER ONE. Introduction

LIST OF TABLES

LIST OF FIGURES

LIST OF SYMBOLS AND ABBREVIATIONS

Symbol	Parameters
A	Hamaker constant
Å	Angstroms
ACN	Acetonitrile
ADP	Adenosine 5'-diphosphate
AMP	Adenosine 5'-monophosphate
A_s	Asymmetry
A term	Multipath band broadening term
ATP	Adenosine 5'-triphosphate
AU	Arbitrary units
A^{x-}	A generic anion of charge x^-
B term	Longitudinal diffusion band broadening term
b_k	Langmuir equation coefficient for a k^{th} component
BTMA	Benzyltrimethylammonium (ion)
C	Concentration
^oC	degree Celsius
CCZ	Carbon clad zirconia
CFC	Critical flocculation concentration
C_M	Concentration of the solute in the mobile phase
CMP	Cytidine monophosphoric acid
cps	Counts per second
C_S	Concentration of the solute in the stationary phase

C term	Resistance to mass transfer coefficients
DDAB	Didodecyldimethylammonium bromide
D_M	Diffusion coefficient in the mobile phase
d_p	Particle diameter
DSC	Differential scanning calorimeter
EP	European pharmacopeia
ERLIC	Electrostatic repulsion hydrophilic interaction chromatography
eV	Electron volt
EVB-DVB	Ethylvinylbenzene-divinylbenzene
E^{y-}	Eluent anion with charge y^-
F	Flow rate
FDA	Food and Drug Administration
f(t)	Baseline corrected signal over time
H	Plate height
h	Reduced plate height
h	Hour(s)
HILIC	Hydrophilic interaction liquid chromatography
HPLC	High performance liquid chromatography
I	Ionic strength
i.d.	Internal diameter
IC	Ion chromatography
i_M	Analyte *i* in the mobile phase

i_S	Analyte *i* in the stationary phase
k	Retention factor
$K_{A,E}$	Selectivity coefficient of an analyte anion over an eluent anion on a given resin
k_b	Boltzmann constant
$K_{E,A}$	Selectivity coefficient of an eluent anion over an analyte anion on a given resin
K_α	X-ray radiation emission line
L	Column length
l_b	Bjerrum length
M	Mobile phase
M	Molar
M^+	A monovalent cation
meq	Milliequivalents
min	Minutes
mM	Millimolar
MSA	Methane sulfonic acid
mV	Millivolts
MΩ	Megaohms
N	Efficiency, Plate number
N_{corr}	Corrected efficiency
ODS	Octadecyl silica
Pa	Pascal
PEEK	Polyether ether ketone

PGC	Porous graphitic carbon
pH	Negative logarithm of the hydrogen ion concentration
pK_a	Negative logarithm of the acid dissociation constant
ppb	Parts per billion
PREG	Polar retention effect on graphite
psi	Pounds per square inch
Q	Ion Exchange capacity of a column
q_k	Amount of analyte in mobile phase at equilibrium
q_s	Saturation capacity of the stationary phase
R	Resolution
R	An organic functional group
R	Resin
RPLC	Reversed phase liquid chromatography
RSD	Relative standard deviation
RSF	Relative sensitivity factor
s	seconds
S	Stationary phase
S	Skewness
S	Surface area
SEM	Scanning electron microscopy
T	Temperature
t	time
t_1	Heart cut time (beginning)

t_2	Heart cut time (end)
t_M	Dead time
t_R	Retention time
u	Linear velocity
UHMWPE	Ultrahigh molecular weight polyethylene
UHPLC	Ultrahigh pressure liquid chromatography
UV	Ultraviolet
V_M	Dead volume of a column
V_S	Volume of the stationary phase
w	Weight of the resin inside a column
w_h	Width of a peak at half height
wt/wt	Weight by weight
x	Charge of an anion
XPS	X-ray photoelectron spectroscopy
y	Charge of an eluent
z	Charge of a counter ion
ΔP	Pressure drop
μ_o	Zeroth statistical moment
μ_1	First statistical moment
μ_2	Second statistical moment
µeq	Microequivalents
µL	Microliter
µm	Micrometers

μS	Microsiemens
α	Selectivity factor
η	Viscosity
λ	Packing factor
σ^2	Overall peak variance
σ^2_{col}	Peak variance contribution due to the column
σ^2_{det}	Peak variance contribution due to the detector
$\sigma^2_{extra\ col}$	Peak variance due to extra-column effects
σ^2_{inj}	Peak variance contribution due to the injection loop
σ^2_{other}	Peak variance due to other band broadening terms
σ^2_{tub}	Peak variance contribution due to the tubings
Φ	Volume fraction of a solid
Φ	Flow resistance
ψ	A correction term in the van Deemter coefficient

CHAPTER ONE. Introduction

1.1 Motivation and Thesis Overview

The art and science of separating individual components from complicated mixtures have occupied a key position in chemistry since earliest times. The culmination of over 50 years of scientific contributions has led to the development of modern high performance liquid chromatography (HPLC). The first HPLC paper appeared in 1966 in *Nature.*[1] HPLC has now become a modern and indispensable tool for the analysis of complicated mixtures in scientific laboratories. The ultimate quest by separation scientists, as laid down by Purnell[2] and Knox,[3] is to achieve maximum separating power in a reasonable amount of time. The separation of components is dependent on how long the components are retained, how efficiently they are separated, and on the relative order of elution in the chromatographic process. All of these parameters depend significantly on the stationary phase. Thus, the stationary phase is the heart of any chromatographic system.

This thesis revolves around fundamental and practical aspects of liquid chromatography with an emphasis on developing and characterizing stationary phases and supports for ion chromatography (IC) and hydrophilic interaction liquid chromatography (HILIC). Chapter 2 of this thesis reviews the state-of-the art developments that have taken place in achieving high-speed and high-resolution IC separations.

To date, modern IC columns (standard diameter of 2 to 4.6 mm) are based on functionalized polymers of 5 to 13 μm diameter packed in 15-25 cm columns. Such long columns can take up to 60 minutes for separation of a clean sample. Much of the hype in HPLC has focused on high efficiencies at ultrahigh pressure using sub-2 μm particles. But the key advantage of small particles lies in using short columns to achieve the same efficiency as obtained in 25 cm commercial ion chromatography columns. Chapter 3 explores the potential of 3 μm microparticulates to improve the efficiency of short IC columns.

Chapter 4 addresses the issues associated with packing small charged particles in HPLC columns. Unfortunately, column packing is still considered an art and a secret by column manufacturers. To see improved resolution and efficiency this art must be understood as a science. It is a non-trivial task to pack small charged particles. The small particles, bearing ionized functional groups, show properties very similar to colloids in terms of flow properties and suspension stability. On the other hand, relatively concentrated suspensions of these small particles show interesting properties such as shear thickening properties, which must be mitigated to pack efficient columns.

Achieving unique selectivity is another critical factor in stationary phase design using diazonium chemistry. A new type of phase was developed in Chapter 5 based on porous graphitic carbon to achieve novel selectivity on carbonaceous phases. The porous graphitic carbon was decorated with benzoic acid groups. This phase is the first example of HILIC on modified carbon surface. The surface and chromatographic characterization of this phase is discussed in Chapter 5.

Another factor that affects the resolution and peak efficiency is the concentration of the analyte injected into a column. In many real samples, some components may have a disproportionately high concentration whereas other components are present in trace amounts. In such cases peaks shapes are distorted regardless of the chromatography mode. Chapter 6 discusses these trends and develops simple criteria to predict the overload peak shape with any given eluent in ion chromatography.

The last chapter (Chapter 7) ends the thesis with conclusions and prospects.

1.2 Chromatographic Terminology

A typical HPLC system consists of an eluent reservoir, a pump capable of high pressure eluent delivery at a constant flow rate, a sample injection valve, a chromatography column and a detector. Once the sample mixture enters the column, the components migrate with different speeds depending on their interaction with the stationary phase. This differential migration results in separation of the components in the mixture with each component eluting at a specific *retention time*, t_R. The fraction of an i^{th} component in the mobile and the stationary phase is determined by the equilibrium:

$$i_{\mathrm{M}} \rightleftharpoons i_{\mathrm{S}} \qquad \text{(equation 1.1)}$$

If C_S is concentration of the solute in the stationary phase and C_M is mobile phase concentration, then a quantity called the *retention factor k* of *i* can be defined as:

$$k_i = \frac{C_S}{C_M}\frac{V_S}{V_M} \qquad \text{(equation 1.2)}$$

where V_S is the volume of the stationary phase and V_M is the volume of the mobile phase. Practically, the retention factor is obtained from the chromatogram using:

$$k_i = \frac{t_R - t_M}{t_M} \qquad \text{(equation 1.3)}$$

where t_R is the retention time of the analyte and t_M is the time at which any unretained component elutes from the column (dead time). Another fundamental criterion that helps in method development is the selectivity factor α. The selectivity factor is the relative retention of two components (*i* and *j*) on a given stationary phase, where by convention component *i* is the less retained species.

$$\alpha_{i,j} = \frac{k_j}{k_i} \qquad \text{(equation 1.4)}$$

If a peak is Gaussian, the "efficiency" of separation can be quantified by the number of plates *N* obtained from the chromatographic data according to:

$$N = 5.54 \left(\frac{t_R}{w_h}\right)^2 \qquad \text{(equation 1.5)}$$

where t_R is the retention time of the peak of interest and w_h is the peak width at 50% of the peak height. Equation 1.5 is used in Chapters 3 and 4 for measuring efficiencies for the columns made in this work. However, *N* scales with the length of the column. Therefore this thesis also utilizes the *plate height*, *H*, which is related to *N* and the column length *L* by:

$$H = \frac{L}{N} \qquad \text{(equation 1.6)}$$

Another useful equation in chromatography is the resolution equation:[4]

$$R = \left(\frac{\sqrt{N}}{4}\right)\left(\frac{k}{1+k}\right)\left(\frac{\alpha - 1}{\alpha}\right) \qquad \text{(equation 1.7)}$$

where N is the plate number (efficiency), α is the selectivity factor and k is the retention factor. Two Gaussian peaks of equal height (1:1 ratio) are *baseline resolved* if the resolution between the two components is 1.5. Equation 1.7 is fundamental in chromatography as it helps in the stationary phase design and method development. Equation 1.7 shows that if there is no retention, there will be no separation ($k = 0$, $R = 0$). Therefore, the column must retain the component of interest. It is desirable to keep $0 < k < 10$ because the fraction $\frac{k}{1+k}$ reaches a limiting value of unity for large k values, and so no greater resolution results from long analysis times. As is clear from equation 1.7, N is a critical factor in controlling separation because R has a square root dependence on N. The variable N is mainly dependent on the stationary phase packing and its particle size, and the analyte's diffusion coefficient. Chapters 3 and 4 are devoted to improving the plate numbers by reducing the particle size. Another powerful parameter in the equation is the selectivity factor α. This quantity is controlled by the column chemistry and the eluent in HPLC. Chapter 5 deals with developing a novel selectivity stationary phase.

1.3 Band Broadening Processes in a Chromatographic Column

During the chromatographic separation, as the solute zones migrate on the column the zones broaden.[5, 6] The chromatographic peaks widths can be described using *variances,* σ^2. The variance is related to the measure of peak efficiency, *i.e.* plate height H by:

$$H = \frac{\sigma^2}{L} \qquad \text{(equation 1.8)}$$

The variance is expressed in length unit squared and *L* has dimensions of length. Therefore, *H* also has units of length. The smaller the plate height, the narrower is the peak. When HPLC columns are packed, it is desired that *H* be minimized. These issues are addressed in Chapter 4. A number of equations exist that account for peak variance.[7] Regardless, the van Deemter equation[8] "*remains an incredibly accurate representation of band-broadening processes*".[7] The van Deemter equation describes the plate height as a sum of the peak variance by three contributing terms as a function of linear velocity *u*: the *A* term represents eddy diffusion; the *B* term accounts for the longitudinal molecular diffusion; and the *C* term represents all sources of resistance to mass transfer.

$$H = A + \frac{B}{u} + Cu \qquad \text{(equation 1.9)}$$

The *A* term accounts for the movement of the solute in a chromatographic column where the direction of the solute is changed by the column packing material. The different paths lead to different travelling distances from the front to the column end - this effect results an increase in the peak variance. Poorly packed columns, or voids in a column further increase the multipath band broadening. The *A* term is related to the particle diameter d_p by:

$$A = 2\lambda d_p \qquad \text{(equation 1.10)}$$

The λ term is called the *packing factor* which is related to the geometry of the support particles and how uniformly they are packed. The contribution of the *A* term can be minimized by packing the column as a tightly packed bed.

The *B* term in equation 1.9 accounts for the longitudinal diffusion of the solute in a chromatographic band. This diffusion term is inversely dependent on flow rate in the van Deemter equation since the longitudinal diffusion process increases with the amount of time a solute spends in the mobile phase.

$$B = 2\psi D_M \qquad \text{(equation 1.11)}$$

where ψ term is a correction factor which accounts for the interparticle spaces in a packed column. The *diffusion coefficient* D_M for liquids are small as compared to gases; as a result the *B* term is generally not significant in HPLC except at low flow rates, at elevated temperatures or when extremely efficiently packed columns are employed, *e.g.* in ultrahigh performance liquid chromatography (UHPLC).

In liquid chromatography, the mass transfer term "*C*" is related to the transfer of molecules in and out of the stationary phase, and the mobile phase. The *C* term depends linearly on the linear velocity in the van Deemter equation. The different contributions to the mass transfer term are additive:

$$H_{mass\ trans} = \sum C_i\, u \qquad \text{(equation 1.12)}$$

where the constants C_i depend on the particle diameter d_p in which the mass transfer process is occurring and on the diffusion coefficients D_M of the solute in this layer. The general dependence of the *C* term on particle size is:

$$C \propto \frac{d_p^2}{D_M} \qquad \text{equation (1.13)}$$

At equilibrium, the solute molecules distribute between the mobile phase and the stationary phase. As the mobile phase moves past the stationary phase, the molecules in the stationary phase may lag behind, resulting in an increase of the

peak width. The mass transfer term is minimized by fast transfer kinetics, by using smaller diameter particles (short diffusion distances), and by using a thin layer of a stationary phase on a support (short diffusion distances). The plate heights when plotted against linear velocity yield the van Deemter plot (Figure 1.1).

1.4 Reduced Plate Height (*h*)

To compare columns with different lengths and particle diameters, it is useful to define a dimensionless parameter of efficiency called the *reduced plate height, h*.[9] The reduced plate height is calculated by dividing the plate height *H* with the particle diameter d_p. A reduced plate height of 2 is usually considered the practical limit of achieving highest efficiency with packed columns.[10, 11] Reduced plate heights are used in Chapter 4 to compare the packing efficiency of commercial columns with the columns made in this lab.

1.5 The Small Particle Advantage

Section 1.3 discussed the factors that lead to an increase in the peak width. The *A* and *C* terms in the van Deemter equation are dependent upon the particle size (equations 1.10 and 1.13). Foundational work by Knox[12] laid the conditions for optimizing the speed and resolution in liquid chromatography. Thus it was realized that decreasing the particle size of the stationary phase is one of the most viable approaches to improving chromatographic performance. Namely, the speed of analysis can be increased by using short columns packed with small particles.

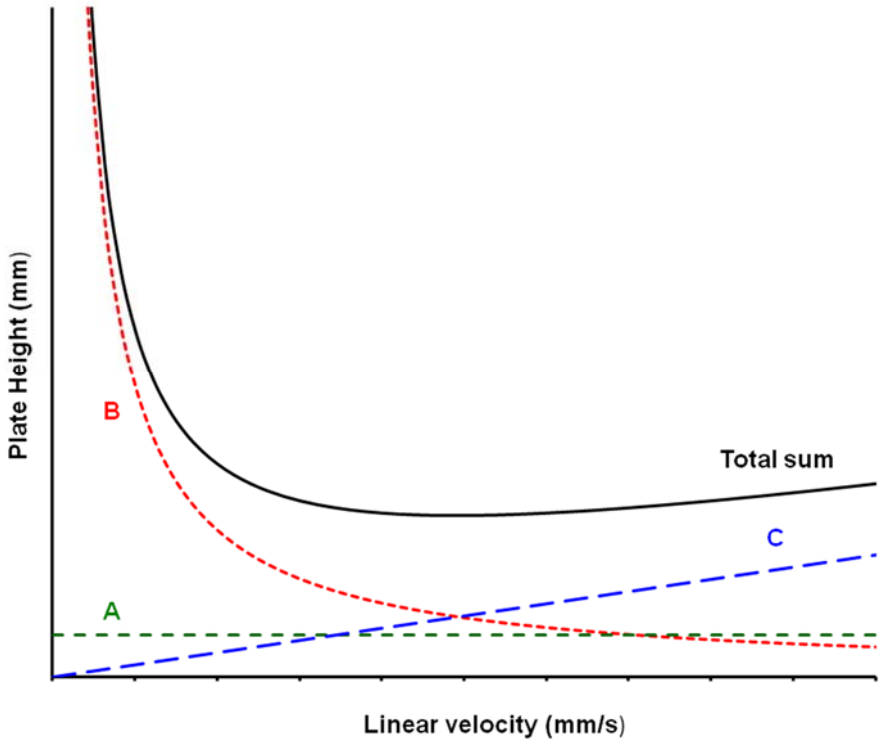

Figure 1.1. A typical van Deemter plot (solid line). The individual components (*A*, *B* and *C*) are shown as dashed curves.

Additionally, very high resolution can be achieved by using longer columns. In the literature, a range of particle sizes (1.7 - 100 μm) have been employed.[13-15] Rapid progress has been made in using small sub-2 μm particles. Recently, particle sizes as small as 0.47 μm were reported.[15] Table 1.1 shows the calculated efficiencies and the pressure offered by a given particle size in a packed column using the *HPLC Simulator* program.[16] The trend is obvious that the smaller the particle size, the higher is the efficiency of separation for a given column length. Thus it may be appealing to use smaller and smaller particles in short columns to achieve high efficiency fast separations. However the ultimate limit on the speed of analysis is technologically limited by the pressure drop which a HPLC or UHPLC system can develop. Darcy's law relates the pressure drop ΔP across a column of length L with the linear velocity u, flow resistance Φ, viscosity η and particle diameter d_p.

$$\Delta P = \frac{u\,\eta\,\phi\,L}{d_p^2} \qquad \text{(equation 1.14)}$$

In equation 1.14 the pressure drop scales inversely with the square of particle diameter. For instance in Table 1.1, a 100 x 4.6 mm i.d. column packed with 1.7 μm particles develops a pressure of ~ 10,000 psi. This pressure is beyond the capability of HPLC pumps which generally have a pressure limit of 5000-6000 psi. Chromatography on sub 2-μm silica particles are becoming routine using UHPLC pumps (pressure tolerance > 10,000 psi).[17] High performance separations using polymeric phases usually have an upper limit of 3000 psi (for reasons to be discussed in Chapter 2). This thesis explores small particles (2 μm < $d_p \leq$ 5 μm)

Table 1.1. Efficiency and pressure offered by the particles in a given column size.

Particle diameter/ µm	Column dimension	Efficiency *N* [a]	Pressure/ psi [a]
10	**150 x 4.6 mm i.d.**	**3900**	**400**
	50 x 4.6 mm i.d.	1300	140
5	**150 x 4.6 mm i.d.**	**11,700**	**1700**
	50 x 4.6 mm i.d.	3900	570
3	**150 x 4.6 mm i.d.**	**23,410**	**4700**
	50x4.6 mm i.d.	7800	1600
1.7	**150 x 4.6 mm i.d.**	**44,100**	**14700**
	100 x 4.6 mm i.d.	29,400	9800
	50 x 4.6 mm i.d.	14,700	4900

[a] Calculated efficiency and pressure at a flow rate of 2.0 mL/min using a 84% methanol - water mixture on Agilent Zorbax SB C-18 column. Analyte is p-nitrotoluene. The software *HPLC Simulator* predicts the efficiencies and pressure based on equations 1.9 (modified with reduced velocities) and 1.14, respectively. Values have been rounded off. The *HPLC Simulator* and its description is detailed in Reference 16.

with shorter column lengths (5 to 10 cm) for the separation of anions on commercial HPLC instruments. The pressure issues in high performance ion chromatography with small particles are dealt in detail in Chapter 2.

1.6. Band Broadening and Extra-column Effects

For fundamental studies related to determining the column efficiencies and plate height, extra-column effects must be considered.[7, 18] Likewise to optimize practical analysis with both HPLC and UHPLC it is important to minimize any extra-column effects.[19] The *apparent* peak variance has several contributions from other parts of the separation system besides the column, *e.g.*, from the injection port, the connecting tubings, and the detector cell.[20] The overall variance of the peak σ^2 is therefore a sum of the following:

$$\sigma^2 = \sigma_{inj}^2 + \sigma_{tub}^2 + \sigma_{col}^2 + \sigma_{det}^2 + \sigma_{other}^2 \qquad \text{(equation 1.15)}$$

where σ^2_{inj}, σ^2_{tub}, σ^2_{col}, σ^2_{det}, and σ^2_{other} represent the variance originating from the injector, connection tubings, column, and detector respectively. The σ^2_{other} can include other band broadening contributions such as the detector rise time. In commercial HPLC instruments the tubings are plumbed so that the $\sigma^2_{extra\ col}$ does not exceed 10% of the apparent peak variance.[21] Early eluting and unretained peaks are most vulnerable to extra-column band broadening effects.[7] Extra-column effects can easily be detected when the early peaks have much lower efficiency than later eluting peaks. These effects are usually observed on short columns (*e.g.*, which have small dead volumes) and high efficiency small particles, which are explored in Chapters 3 and 4. The most convenient way to

determine the "true" efficiency of the peak is to measure the peak variance with and without the column on the same HPLC system. After removing the column, the injection valve is connected directly with the detector using the same tubing. The variance of the peak, determined without the column, represents the total extra-column effect, *i.e.*, the sum $(\sigma_{inj}^2 + \sigma_{tub}^2 + +\sigma_{det}^2 + \sigma_{other}^2)$ in equation 1.15. Rearrangement of equation 1.15 to $\sigma_{col}^2 = \sigma^2 - (\sigma_{inj}^2 + \sigma_{tub}^2 + +\sigma_{det}^2 + \sigma_{other}^2)$ enables determination of the true column broadening behaviour. This approach is employed in Chapter 4.

1.7 Stationary Phase Supports in HPLC

1.7.1 An Ideal Stationary Phase for Liquid Chromatography (LC)

There is a variety of characteristics that an ideal LC stationary phase should possess.[22, 23] As HPLC requires working at higher pressures (typically >2000 psi), any chromatographic support must be mechanically stable so that it can withstand long term exposure to high pressures without cracking or crushing. This feature is required to make a stable bed. A chromatographic bed made of soft materials will eventually compact and form a void at the column head. The particles should not shrink or compress with different eluents. This factor is also related to the bed stability. The stationary phase must be chemically compatible with the eluents for which it is being designed. Ideally it should be able to tolerate aggressive mobile conditions, *e.g.*, at high temperature, and low or high pH. In short, the stationary phase should not chemically react with analytes or with the mobile phase.

Physically, the particles should be available in a narrow size distribution to facilitate formation of a tight packed bed (small *A* term in the van Deemter equation).[24] Ideally, fines (small irregular sized particles) should be absent to minimize the back pressure. Most particles in liquid chromatography are porous to increase the surface area. The pore diameter must be larger than 8 times the analyte size to allow free diffusion of the solute into and out of the particle.[25] The surface of the stationary phase should be chemical modifiable, yet have the chemical stability to tolerate the mobile phases. Additionally, the surface chemistry should be reproducible.

1.7.2. Silica Based Supports

Silica based phases are the classical stationary phases in liquid chromatography. More than 90% of the packings in normal and reversed phases are based on silica.[26, 27] A number of advantages are associated with silica. First, silica based packings are mechanically strong. Some commercial columns for UHPLC are packed at 30,000 psi and no mechanical damage is seen. Silica particles are commercially available with narrow size dispersions. The typical size distribution is 15-19% RSD for porous silica particles.[28] The surface areas can range from 160 to 700 m^2/g for commercial columns.[29] Silica does not swell or shrink in organic solvents. Finally, silica surface is modifiable *via* silane chemistry.[5] All of these properties make silica nearly an "ideal" stationary phase.

However, at low pH (< 2) loss of the surface modification (called bonded phase) occurs[30] due to the hydrolysis of the attached ligand. The bonded phase

loss occurs *via* cleavage of the siloxane bond (-Si-O-Si-) that connects the silanes to the surface of silica.[5] The rate of acid hydrolysis is highly pronounced at elevated temperatures (> 60 ºC). This results in retention time loss and degradation of the peak shape.

Also, silica is soluble in mobile phases having high water content or high pH. Silica dissolves slowly in pure water, as silicic acid as shown in equation 1.16.[31] Silica's solubility increases with temperature and the mobile phase pH.[32]

$$SiO_{2\,(s)} + 2H_2O_{\,(l)} \longrightarrow Si(OH)_{4\,(aq)} \qquad \text{(equation 1.16)}$$

The solubility of silica at high pH is one of the main drawback of silica supports, and is the primary reason that silica phases are not used in this thesis. When column manufacturers mention the pH stability to more than 8, it is usually a "soft" limit in the sense that high organic content is always used if the mobile phase pH is high.[9] These drawbacks make silica a less than an ideal phase.

1.7.3 Alternatives to Silica Based Supports

Due to the chemical stability issues with silica (Section 1.7.2), the stationary phases explored in this thesis are based on non-silica based supports which are mechanically robust as well as have a wider range of chemical compatibilities. As stated in Section 1.2, the driving force in the stationary phase development is tweaking of the parameters within the resolution equation (equation 1.7). Interesting selectivities can be easily achieved by employing non-silica supports.

Polymers are an obvious alternative to silica phases due to their wider pH stability window.[33] Other novel materials that can overcome the pH issues

associated with silica have been explored in the chromatography literature. Some of the durable supports which have been proposed include titania,[34] zirconia,[35] alumina,[36] carbon clad zirconia,[37] carbon clad silica,[38] carbon clad alumina,[38] boron doped diamonds,[39] carbon cores with porous diamond coatings[40] and porous graphitized carbon (PGC).[41] The zirconia, titania and carbon based supports have already been commercialized. This thesis explores the use of polymeric, carbon clad zirconia and porous graphitic carbon packings for achieving high efficiency and different selectivities for separating ions and polar analytes. The following sections give an overview of polymeric and carbon HPLC phases.

1.7.3.1 Polymeric Packings

Polymeric supports have been employed for reversed phase chromatography, ion exchange and size-exclusion chromatography.[5] In ion chromatography nearly all supports are based on cross-linked polystyrene, ethylvinylbenzene or substituted methacrylates.[42] The cross-linking imparts mechanical strength to the particles. The key advantage of using polymers is their robustness with respect to pH (0 to 14).[42] For instance in anion separations using suppressed IC, the NaOH eluent may have a pH as high as 13. However polymeric particles are not without drawbacks.[9] Polymers are mechanically weaker than inorganic oxides such as silica, titania, or zirconia. As a result, the pressure limits of polymer columns are lower. Also, the separation efficiencies (*N*) with polymeric phases are lower than with silica due to hindered mass transfer kinetics.[9] Another issue is the shrinking or swelling in organic solvents. This issue

can be overcome by increasing the cross-linking of the polymer. Modern polymeric IC phases have up to 55% cross-linking which gives them 100% solvent compatibility with common HPLC solvents such as acetonitrile.[42]

A common type of polymeric IC packing is the latex agglomerated phase.[33, 43, 44] Chapters 3, 4, and 5 employ agglomerated phases for separating anions with high pH mobile phases. In a typical commercial agglomerated phase, as shown in Figure 1.2, a polystyrene or ethylvinylbenzene core particle is cross-linked with divinylbenzene to form a rigid co-polymer. The co-polymer is sulfonated under mild conditions to introduce sulfonic acid groups on the surface of the particles (negative surface charge). The polymer beads are then exposed to a suspension of nanometer (60 - 100 nm) sized polymer particles bearing quaternary ammonium groups. The positively charged latexes are very strongly held by electrostatic forces.[45] The thin layer of the latex on a relatively large sized particle (5 - 13 μm) ensures fast mass transfer kinetics leading to high efficiency separations. For example, as will be shown in Chapter 4, reduced plate heights of 3 can be obtained on 13 μm agglomerated support particle.

1.7.3.2 Carbon Based Packings

Carbon based stationary phases are one of the most promising HPLC phases because of their unique properties. Carbon overcomes all the drawbacks of silica stationary phases discussed in the Section 1.7.2. Knox and co-workers[41] pioneered the synthesis of highly robust porous graphitic carbon (PGC) with

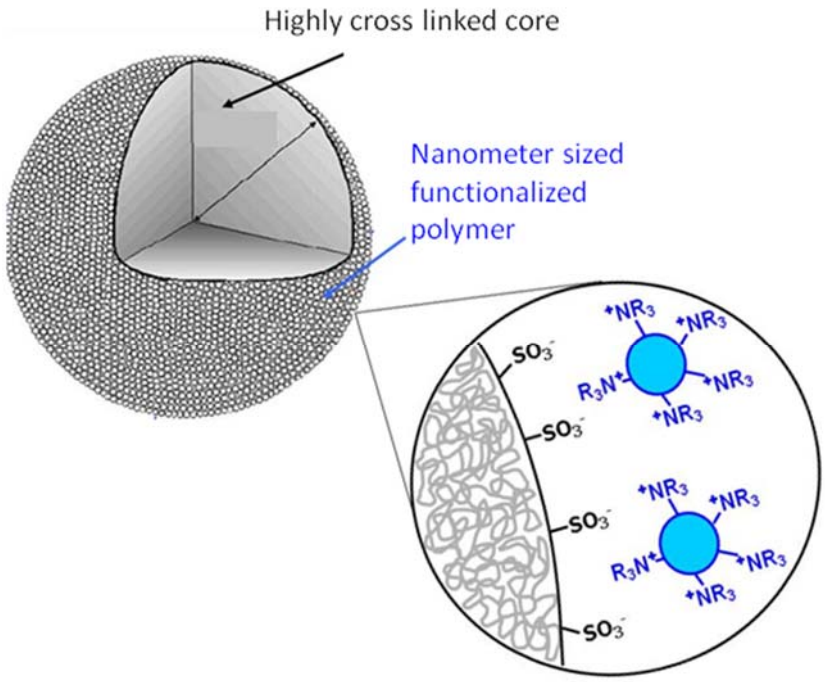

Figure 1.2. A schematic diagram of an agglomerated phase. The negatively charged surface of the highly cross-linked core (5-13 μm) is coated with nanometer (>60 nm) sized polymer polycationic particles (latex). The core can be solid or macroporous.

reproducible surface properties for HPLC. PGC consists of layers of graphitic sheets (sp^2 hybridized carbon atoms). PGC is inert to highly acidic or alkaline mobile phases. Additionally, PGC possesses high chemical and thermal (up to 200 °C) stability. All liquid chromatography solvents are compatible with PGC. PGC can tolerate high pressure (~ 5800 psi) without any mechanical damage. This phase is now commercially available as Hypercarb™ in 3, 5 and 10 µm particle sizes for reversed phase chromatography.

The surface chemistry of carbon is radically different from that of other HPLC phases. Thus PGC offers a different separation selectivity compared to silica or other inorganic oxide based phases.[46] To further impart mechanical strength to carbon supports, the Carr group[37, 38] introduced carbon coated zirconia. Carbon clad zirconia is commercially available in 2 to 3 µm size. This phase consists of porous zirconia particles onto which 5-6 monolayers of graphitized carbon have been deposited *via* vapour deposition. The heated zirconia particles are exposed to organic vapours in an inert atmosphere. The high temperature leads to the decomposition of the organic compounds into elemental carbon, leading to formation of carbon coated zirconia particles. The carbon clad zirconia modified particles are employed in Chapter 3.

Given that carbon is inert to most chemicals; it is not easy to covalently modify the carbon surface. Newer hybrid high efficiency polymer-carbon based stationary phase have recently been developed for reversed phase applications at high pH and high temperature.[40, 47] Direct covalent functionalization of carbon

surface using aryl radical chemistry is highly promising.[48, 49] Chapters 3 and 5 employ aryl diazonium chemistry to develop HPLC stationary phases.

1.8 Chromatographic Modes

1.8.1 Reversed Phase Liquid Chromatography (RPLC)

Reversed phase liquid chromatography (RPLC) is the most common separation mode in HPLC.[50] In RPLC, the stationary phase is less polar than the mobile phase. The most common RPLC supports consist of C-8 or C-18 alkyl chains bonded to silica. This functionalization makes the silica surface more hydrophobic than the native surface of silica. The usual eluent consists of water, buffers, and organic solvents such as methanol or acetonitrile. RPLC is best suited for the separation of hydrophobic or moderately polar molecules. However, very polar or ionic compounds are weakly retained in RPLC ($k << 1$).[5] In such cases, other modes of chromatography must be employed. This thesis focuses on the development of stationary phases that are specially designed for separating ions and highly polar compounds.

1.8.2 Ion Chromatography (IC)

Ion chromatography is a versatile separation technique for analyzing inorganic anions, cations (heavy metal ions, transition metal complexes, alkali and alkaline earth metals), biomolecules, carbohydrates, and small organic acids. [42, 51] IC employs highly alkaline or acidic eluents (pH 0 to 14) which are not compatible with silica phases. Therefore polymeric substrates such as discussed in

Section 1.7.3.1 are employed in IC. Since anion exchange chromatography is the most widely used ion-exchange technique, further discussion will focus on it. In anion exchange chromatography, the resin consists of a polymeric support bearing quaternary ammonium groups. Anionic analytes will interact electrostatically with these fixed positive charges. The eluting ion E^{y-} is also negatively charged. The equilibrium of the ion exchange of the anion (A^{x-}) between the stationary phase (resin, R) and mobile (M) phase is:

$$yA^{x-}{}_{(M)} + xE^{y-}{}_{(R)} \rightleftharpoons yA^{x-}{}_{(R)} + xE^{y-}{}_{(M)} \quad \text{equation (1.17)}$$

where A^{x-} and E^{y-} are the analyte and eluent anions bearing negative charges x and y. The equilibrium constant (selectivity coefficient) is:

$$K_{A,E} = \frac{[A_R^{x-}]^y [E_M^{y-}]^x}{[A_M^{x-}]^y [E_R^{y-}]^x} \quad \text{equation (1.18)}$$

The larger the value of the equilibrium constant, the larger is the retention factor of the ion. We employ the reciprocal of the selectivity coefficient in equation 1.18 when predicting the peak shapes of anions under column overloading conditions (Chapter 6).

Besides the selectivity coefficient, other factors which control IC retention include the capacity of the resin Q, the weight w of the resin within the column, the volume of the mobile phase V_M in the column, the concentration of the eluent [E^{y-}], and the charges on the analyte (x) and the eluent (y). From the fundamental thermodynamic definitions of retention factor and capacity, equation 1.18 can be converted into equation 1.19.[52]

$$\log k = \frac{1}{y}\log K_{A,E} + \frac{x}{y}\log\frac{(Q)}{y} + \log\left(\frac{w}{V_m}\right) - \frac{x}{y}\log[E^{y-}] \quad \text{equation (1.19)}$$

For a given column, the selectivity coefficient, column capacity, weight of the resin, and the volume of the mobile phase in the eluent (the dead volume) are constant. This allows equation 1.19 to be simplified to:

$$\log k = constant - \frac{x}{y}\log[E^{y-}] \qquad \text{equation (1.20)}$$

Equation 1.20 shows that IC retention is strongly affected by the charge of the analyte ion (x) as well as the charge of the eluent anion (y). The typical eluents in IC are borate, hydroxide, and carbonate-bicarbonate solutions.

1.8.2.1 IC Instrumentation

Figure 1.3 shows the schematic of a modern IC system such as used in this thesis. The IC system is very similar to a standard HPLC system with a high pressure pump, microliter injector, column and detector. The unique features of an IC are that: (a) the eluent may be generated online using pure water *via* electrodialytic principles; and (b) the analytes are detected by suppressed conductivity.[53, 54] The description that follows illustrates the typical instrumental set up for separating anions, which is the focus of Chapters 3, 4 and 6. Pure water is pumped by a high pressure pump into an eluent generator.[55] The eluent generator (Figure 1.4) is an electrolytic flow cell in which the cathode and anode are separated by a cation exchange membrane. At the cathode, hydroxide ions are generated by the electrolysis of water. To maintain charge neutrality, Na^+ migrate from a reservoir containing concentrated NaOH and traverses the cation exchange membrane. The Na^+ and OH^- combine in the HPLC flow stream to form the hydroxide eluent, which then flows through the injector to the column. The OH^-

participates in the ion exchange equilibrium (equation 1.17) on the column to separate the various analyte anions within an injected sample plug.

Prior to detection, the high background conductivity of the eluent must be suppressed to enable detection of the analyte ions by conductivity. To do this the effluent from the column passes through a suppressor (Figure 1.5). The suppressor is commonly a membrane chemical reactor, which changes the ionic counter ion for the eluent and the analyte anions (Figure 1.5). For instance, if NaOH is being used as an eluent, Na^+ in the effluent stream exchanges across a cation exchange membrane within the suppressor with H^+ ions from a regenerating stream. The electrolytically generated H^+ from the suppressor combines with the OH^- in the eluent to form water which has an extremely low background conductivity (0.055 μS/cm).[55] At the same time the exchange of cations converts the analyte anions into their corresponding acids, *e.g.*, Cl^- is converted into HCl and NO_3^- is converted to HNO_3. These strong acids fully dissociate and are highly conducting due to the very high equivalent conductance of the proton (349.8 Scm^2/mol) as compared to other cations such as Na^+ (50.1 Scm^2/mol). The process of background suppression improves the detection limits. Part per trillion detection limits are routine for common anions in suppressed conductivity IC. Chapter 2 deals with the recent developments that have taken place in the IC instrumentation for achieving fast and high resolution separations.

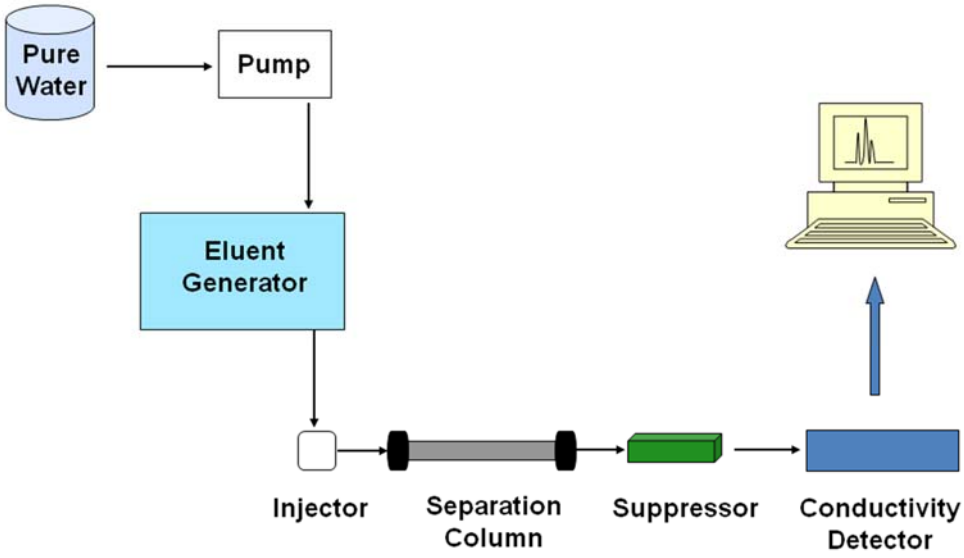

Figure 1.3. A schematic outline of the IC instrument for suppressed conductivity detection used in this work.

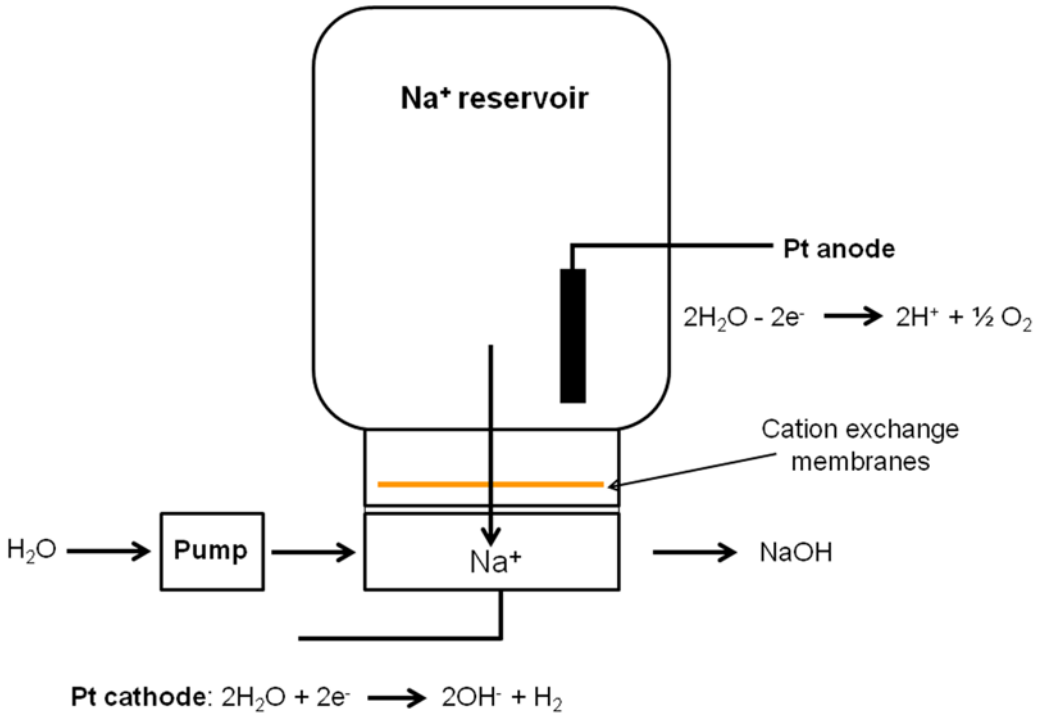

Figure 1.4. A schematic diagram of an eluent generator. Figure from Ref. 46.

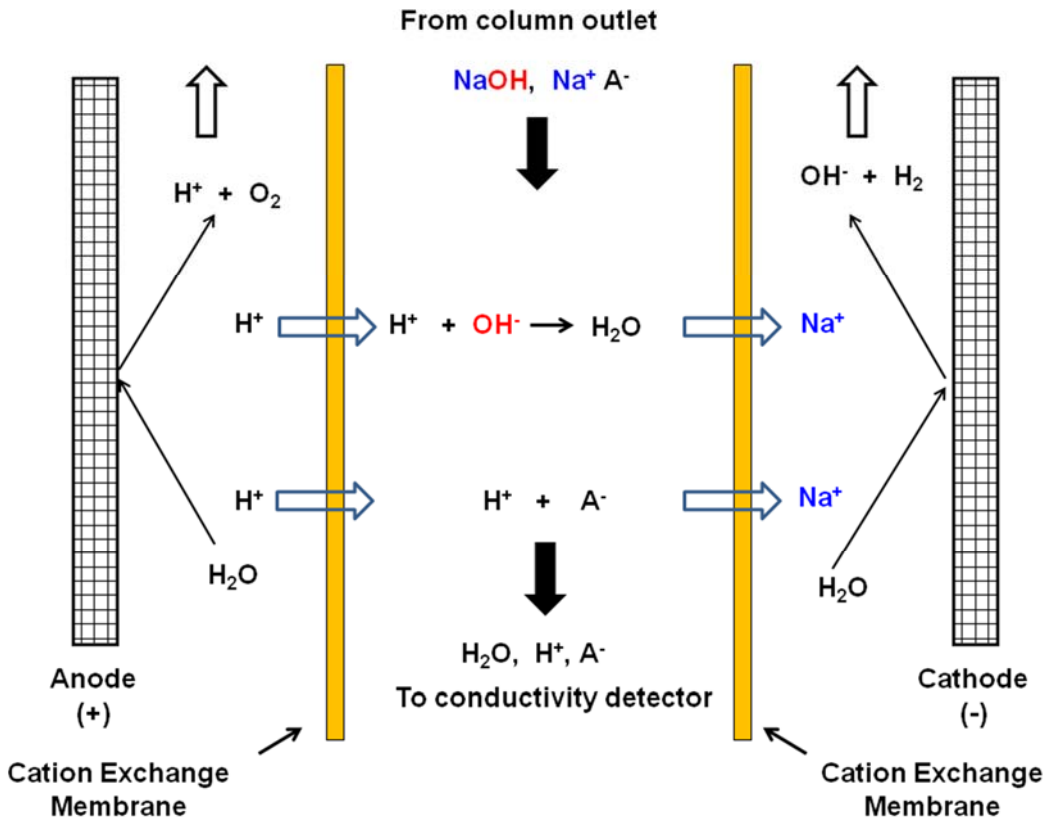

Figure 1.5. A schematic diagram of an electrolytically regenerated suppressor used in this work. The electrodes in suppressors are made of Pt meshes or Pt coated Ti. Figure is adapted from Ref. 55

1.8.3 Hydrophilic Interaction Liquid Chromatography (HILIC)

As stated in Section 1.6, RPLC shows very poor retention of hydrophilic compounds. However, as early as 1975, it was shown that very polar compounds (*e.g.,* carbohydrates) could be retained on polar stationary phases if the mobile phase contained a large percentage of an organic modifier.[56] In 1990 Alpert coined the term hydrophilic interaction liquid chromatography (HILIC) to describe this broad mode of liquid chromatography.[57] Soon afterwards, HILIC gained high popularity as a chromatographic technique for separating highly polar compounds such as amino acids, carbohydrates, peptides, carboxylic acids and biomolecules.[58, 59] Figure 1.6 shows the idealized mechanism of retention in HILIC. When a high percentage of organic solvent such as acetonitrile is present in the mobile phase, a stagnant water-enriched layer forms on the hydrophilic stationary phase. Hydrophilic solutes partition between the water enriched layer and the organic-rich mobile phase. The elution order is from least polar to most polar analyte. This elution order is opposite to that of RPLC.

While the partitioning process depicted in Figure 1.6 is the predominant retention mechanism in HILIC,[60] other interactions including hydrogen bonding, adsorption, ion exchange, dipole-dipole and π-π interactions may also contribute to retention.[59] Thus, HILIC commonly exhibits multimodal retention. Chapter 5 exploits these additional interactions to develop a new class of HILIC phase on surface modified PGC.

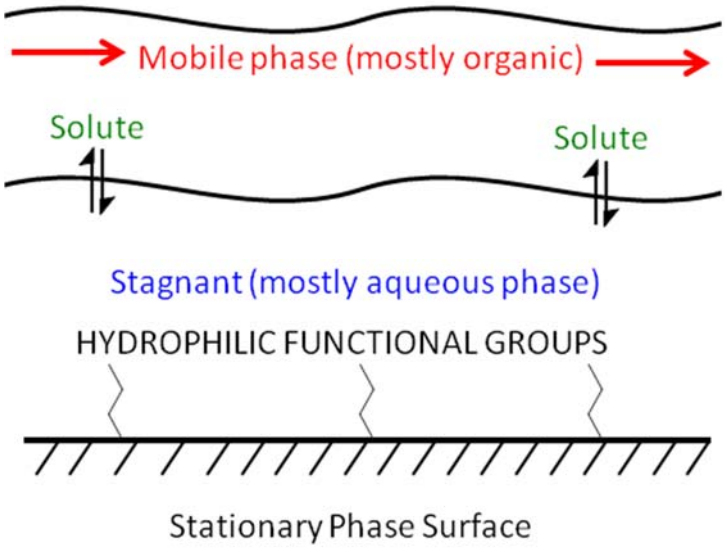

Figure 1.6. The idealized partitioning mechanism of retention in HILIC. The red arrows indicate the flow direction of the mobile phase. This is a modified version of Figure 3 in Reference 60.

1.9 Thesis Summary

This thesis addresses some fundamental and practical aspects of liquid chromatography with an emphasis on the development of columns with high efficiency or different selectivity. Chapter 2 highlights the trials, tribulations and triumphs that now enable fast and high resolution ion chromatographic separations. In Chapter 3, the potential of small particles in ion chromatography is explored. In Chapter 4, I demonstrate the colloidal nature of IC packings, the challenges that colloidal nature causes for packing of high efficiency IC columns, and how these challenges can be overcome. Chapter 5 discusses the synthesis and properties of a new class of HILIC phase based on the synthetic routes developed in Chapter 3. Finally, Chapter 6 is an exploration into why odd peak shapes are sometimes observed in IC. Elution profiles of anions on a variety of IC columns and eluents are explained using classical non-linear isotherm behaviour. Chapter 7 provides the overall conclusions regarding the thesis work.

1.10 References

1. C. H. Horvath, S. R. Lipsky, *Nature* **1966**, *211*, 748-749.
2. J. H. Purnell, *Journal of the Chemical Society* **1960**, 1268-1274.
3. J. H. Knox, *Journal of the Chemical Society* **1961**, 433-441.
4. J. P. Foley, *Analyst* **1991**, *116*, 1275-1279.
5. L. R. Snyder, J. J. Kirkland, J. W. Dolan, *Introduction to Modern Liquid Chromatography*, 3rd ed.; John Wiley & Sons, Inc., Hoboken, New Jersey, 2010.
6. C. A. Lucy, *Lecture Notes on Analytical Separations Course, University of Alberta, Edmonton*, 2008.

7. K. M. Usher, C. R. Simmons, J. G. Dorsey, *Journal of Chromatography A* **2008**, *1200*, 122-128.

8. J. J. van Deemter, F. J. Zuiderweg, A. Klinkenberg, *Chemical Engineering Science* **1956**, *5*, 271-289.

9. U. D. Neue, *HPLC Columns Theory, Technology and Practice*; Wiley VCH Inc. USA, 1997.

10. J. J. DeStefano, T. J. Langlois, J. J. Kirkland, *Journal of Chromatographic Science* **2008**, *46*, 254-260.

11. J. H. Knox, *Journal of Chromatographic Science* **1980**, *18*, 453-461.

12. J. H. Knox, M. Saleem, *Journal of Chromatographic Science* **1969**, *7*, 614-622.

13. D. T. T. Nguyen, D. Guillarme, S. Rudaz, J.-L. Veuthey, *Journal of Separation Science* **2006**, *29*, 1836-1848.

14. R. E. Majors, *LC GC North America* **2005**, *23*, 1248.

15. B. Wei, B. J. Rogers, M. J. Wirth, *Journal of the American Chemical Society* **2012**, *134*, 10780-10782.

16. P. G. Boswell, D. R. Stoll, P. W. Carr, M. L. Nagel, M. F. Vitha, G. A. Mabbott, *Journal of Chemical Education* **2013**, *90*, 198-202.

17. Y. Wang, F. Ai, S.-C. Ng, T. T. Y. Tan, *Journal of Chromatography A* **2012**, *1228*, 99-109.

18. J. M. Miller, *Chromatography Concepts and Contrasts*, 2nd ed.; John Wiley & Sons, Inc., Hoboken, New Jersey, 2005.

19. F. Lestremau, D. Wu, R. Szucs, *Journal of Chromatography A* **2010**, *1217*, 4925-4933.

20. F. Gritti, C. A. Sanchez, T. Farkas, G. Guiochon, *Journal of Chromatography A* **2010**, *1217*, 3000-3012.

21. H. A. Claessens, C. A. Cramers, M. A. J. Kuyken, *Chromatographia* **1987**, *23*, 189-194.

22. G. Schomburg, *TrAC Trends in Analytical Chemistry* **1991**, *10*, 163-169.

23. U. Trüdinger, G. Müller, K. K. Unger, *Journal of Chromatography A* **1990**, *535*, 111-125.

24. E. Grushka, N. Grinberg (editors), *Advances in Chromatography,* CRC Press, Taylor & Francis Group, Boca Raton, 2012, Vol. 50.

25. Salvatore Fanali, Paul R. Haddad, Colin Poole, Peter Schoenmakers, D. K. Lloyd (editors), *Liquid Chromatography: Fundamentals and Instrumentation,* Elsevier Inc., Waltham, MA, 2013.

26. A. Berthod, *Journal of Chromatography A* **1991**, *549*, 1-28.

27. S. C. Moldoveanu, V. David, *Essentials in Modern HPLC Separations*; Elsevier: Amsterdam, USA, 2013.

28. F. Gritti, T. Farkas, J. Heng, G. Guiochon, *Journal of Chromatography A* **2011**, *1218*, 8209-8221.

29. M. E. A. Ibrahim, Y. Liu, C. A. Lucy, *Journal of Chromatography A* **2012**, *1260*, 126-131.

30. L. Ma, P. W. Carr, *Analytical Chemistry* **2007**, *79*, 4681-4686.

31. G. B. Alexander, W. M. Heston, R. K. Iler, *The Journal of Physical Chemistry* **1954**, *58*, 453-455.

32. H. A. Claessens, M. A. van Straten, *Journal of Chromatography A* **2004**, *1060*, 23-41.

33. H. Small, *Journal of Chemical Education* **2004**, *81*, 1277-1284.

34. J. J. Pesek, M. T. Matyska, J. Ramakrishnan, *Chromatographia* **1997**, *44*, 538-544.

35. C. J. Dunlap, P. W. Carr, C. V. McNeff, D. Stoll, *Analytical Chemistry* **2001**, *73*, 598 A-607 A.

36. U. Bienvogelsang, A. Deege, H. Figge, J. Kohler, G. Schomburg, *Chromatographia* **1984**, *19*, 170-179.

37. T. P. Weber, P. T. Jackson, P. W. Carr, *Analytical Chemistry* **1995**, *67*, 3042-3050.

38. C. Paek, A. V. McCormick, P. W. Carr, *Journal of Chromatography A* **2011**, *1218*, 1359-1366.

39. G. W. Muna, V. M. Swope, G. M. Swain, M. D. Porter, *Journal of Chromatography A* **2008**, *1210*, 154-159.

40. L. A. Wiest, D. S. Jensen, C.-H. Hung, R. E. Olsen, R. C. Davis, M. A. Vail, A. E. Dadson, P. N. Nesterenko, M. R. Linford, *Analytical Chemistry* **2011**, *83*, 5488-5501.

41. J. H. Knox, B. Kaur, G. R. Millward, *Journal of Chromatography* **1986**, *352*, 3-25.

42. C. Pohl, *LC GC North America* **2013**, *31*, 16-22.

43. H. Small, *LC GC North America* **2013**, *31*, 8-15.

44. H. Small, T. S. Stevens, W. C. Bauman, *Analytical Chemistry* **1975**, *47*, 1801-1809.

45. James S. Fritz, D. T. Gjerde, *Ion Chromatography*, 3rd ed.; Wiley-VCH: Weinheim, 2000.

46. C. West, C. Elfakir, M. Lafosse, *Journal of Chromatography A* **2010**, *1217*, 3201-3216.

47. G. Saini, D. S. Jensen, L. A. Wiest, M. A. Vail, A. Dadson, M. L. Lee, V. Shutthanandan, M. R. Linford, *Analytical Chemistry* **2010**, *82*, 4448-4456.

48. G. L. C. Paulus, Q. H. Wang, M. S. Strano, *Accounts of Chemical Research* **2012**, *46*, 160-170.

49. P. Allongue, M. Delamar, B. Desbat, O. Fagebaume, R. Hitmi, J. Pinson, J.-M. Savéant, *Journal of the American Chemical Society* **1997**, *119*, 201-207.

50. J. L. Rafferty, L. Zhang, J. I. Siepmann, M. R. Schure, *Analytical Chemistry* **2007**, *79*, 6551-6558.

51. J. Weiss, *Handbook of Ion Chromatography*, 3rd ed.; Wiley-VCH: New York, 2004; Vol. I.

52. J. E. Madden, P. R. Haddad, *Journal of Chromatography A* **1998**, *829*, 65-80.

53. D. L. Strong, P. K. Dasgupta, K. Friedman, J. R. Stillian, *Analytical Chemistry* **1991**, *63*, 480-486.

54. D. L. Strong, P. K. Dasgupta, *Analytical Chemistry* **1989**, *61*, 939-945.

55. Y. Liu, K. Srinivasan, C. Pohl, N. Avdalovic, *Journal of Biochemical and Biophysical Methods* **2004**, *60*, 205-232.

56. J. C. Linden, C. L. Lawhead, *Journal of Chromatography* **1975**, *105*, 125-133.

57. A. J. Alpert, *Journal of Chromatography* **1990**, *499*, 177-196.

58. Y. Guo, S. Gaiki, *Journal of Chromatography A* **2005**, *1074*, 71-80.

59. P. Hemstrom, K. Irgum, *Journal of Separation Science* **2006**, *29*, 1784-1821.

60. B. Buszewski, S. Noga, *Analytical and Bioanalytical Chemistry* **2012**, *402*, 231-247.

CHAPTER TWO. Advances in High-Speed and High-Resolution Ion Chromatography*

2.1 Introduction

Just four decades ago, the analysis of an individual ion required that the analyst perform a time consuming titration or gravimetric measurement. Each additional ion to be analyzed magnified the effort required. In 1975 Hamish Small and coworkers in Dow Chemical Company[1] introduced ion chromatography (IC) (Section 1.8.2). This technique enabled the simultaneous analysis of multiple ions with low detection limits using suppressed conductivity detection. Compared to the hours of labour needed for classical methods, IC yielded rapid measurements. For instance, Li^+, Na^+ and K^+ could be baseline resolved in 134 minutes.[2] Similarly five anions such as fluoride, chloride, phosphate, nitrate and sulfate could be analyzed in 20 minutes.[1, 2]

Today, ion chromatography is widely used for the analysis of inorganic ions and many ionizable organic compounds. More than 70 commercial IC columns are available.[3, 4] However until recently developments by IC column manufacturers focused on increasing the ion-exchange capacity, reliability and selectivity of stationary phases[5] rather than on the speed of analysis. Thus, up to just a few years ago the typical separation time of anions differed little from that demonstrated by Small and co-workers in 1975.[1, 2]

---

* A version of this chapter has been published as an invited article. Charles A. Lucy and M. Farooq Wahab, *LC-GC (Special Issue on Ion Chromatography)* **2013**, *31 (S4b)*, 38-42.

2.2 Recent Developments in High-Speed Ion Chromatography

In contrast, in the last decade rapid developments have taken place in the speed of analysis in reverse phase liquid chromatography. Smaller particles enabled faster analysis by allowing shorter column lengths while maintaining high efficiency and resolution.[6] Introduction of sub-2 μm particles required ultrahigh pressure (UHPLC, up to 15,000 psi) metallic pumps due to the dramatically greater backpressure generated by these smaller particle diameters.[6, 7]

Why has ion chromatography lagged behind this trend? Firstly, ion chromatography was *hardware* limited.[8] The stainless steel pumps, tubing and fittings used in HPLC and UHPLC are not compatible with the highly corrosive acidic or alkaline eluents required in IC. Early IC systems were constructed with glass columns and Delrin components.[9] The introduction of polyether ether ketone (PEEK) pumps and tubing increased the pressure capabilities of IC to near that of conventional HPLC systems (5000 psi). Second, severe baseline drift and ghost peaks were experienced with gradient elution in IC due to the inherent background conductivity of carbonate eluents and impurities in the carbonate or hydroxide eluents. Generation of ultrahigh purity eluents such as carbonate free NaOH was made possible through membrane based electrodialytic eluent generators (Section 1.8.2.1).[10, 11] The fragility of eluent generators restricted the upper pressure limit to 3000 psi.[12] The maximum flow rate in IC was further limited by the suppressor to 1-3 mL/min (for 2 to 4 mm i.d. columns, respectively) to protect the suppressor membranes from leaking. Thus the standard IC hardware was pressure and flow rate limited as late as 2011.

Due to these pressure and flow rate limits, IC columns continued to be characterized by large particle sizes (7-13 μm) and long (200-250 mm) columns. For instance, Figure 2.1(A) shows a typical ion chromatogram using a 250 mm IonPac AS22 column packed with 6.5 μm particles. The seven common anions are separated in ~12 minutes with 9600 plates at a column pressure of < 2000 psi.

However there is actually excessive resolution in Figure 2.1(A) - leading to "wasted" time which is highlighted in blue in Figure 2.1(A). Clearly some of this excess resolution could be traded for analysis time by shortening the column while keeping the particle size and other parameters the same. The first such column was the 150 mm IonPac AS22-Fast introduced at Pittcon 2010. Figure 2.1(B) shows a 7 minute separation on the AS22-Fast - a 40% reduction in run time. The efficiency is reduced from 9600 to 5000 due to the shorter length, but is still sufficient for baseline resolution. The lower backpressure of the shorter column also allows use of higher flow rates while staying within the pressure limits of the IC instrumentation. Figure 2.1(C) shows a 4.5 minute separation of the 7 common inorganic anions using a 150 mm AS22-Fast at 2 mL/min. Using even shorter columns while keeping the particle size the same can further reduce the analysis time. For instance Haddad's group used 30 to 50 mm columns packed with 7.5 μm resins to demonstrate 15 minute separations of highly retained perchlorate and thiocyanate ions.[13] Such ions are typically retained for more than 1 hour on standard 250 mm IC columns.

The next evolution in the speed of IC analysis was associated with the *re-design* of the commercial hardware for capillary columns (~ 0.4 mm i.d.). Such

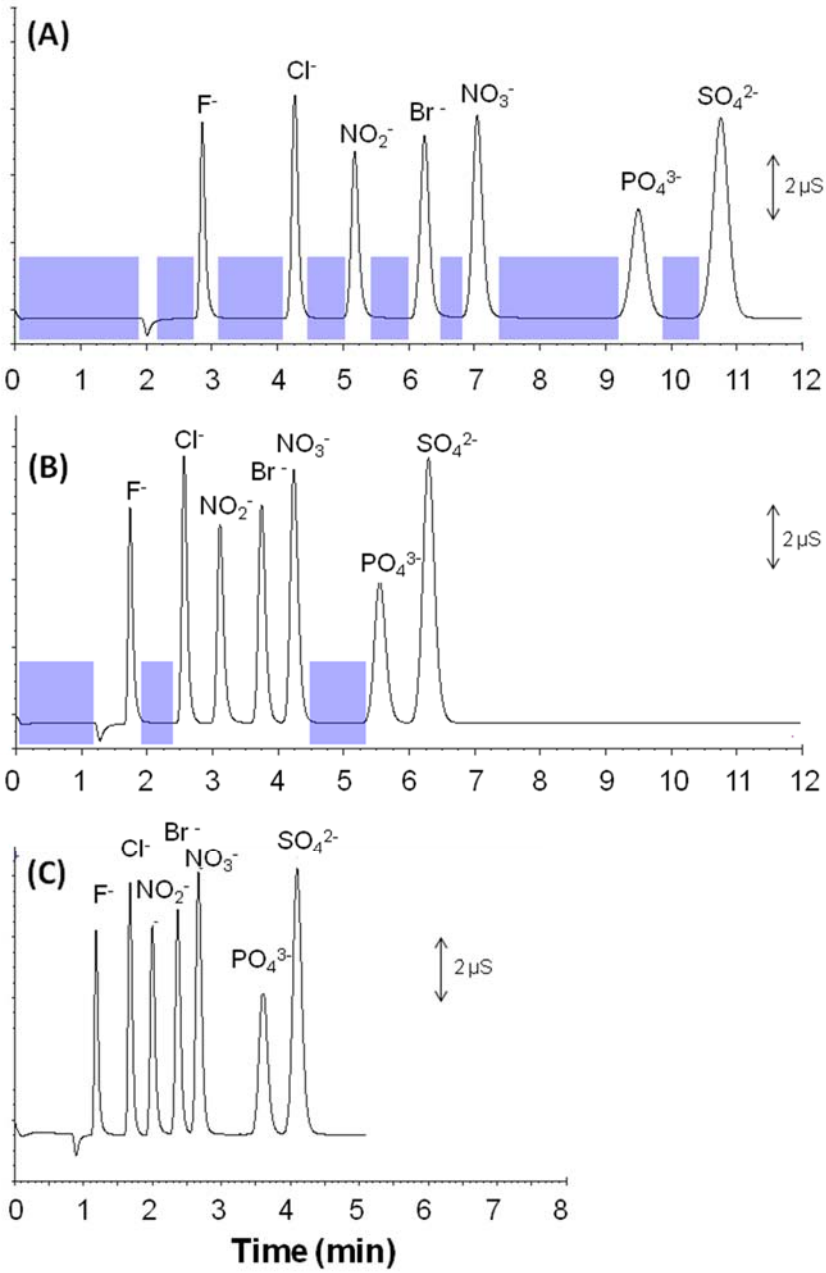

Figure 2.1. Comparison of separations obtained using 250 and 150 mm columns with the same particle size (6.5 µm) and column diameter: (a) 250 mm × 4 mm i.d. AS22 (flow rate: 1.2 mL/min), (b) 150 × 4 mm i.d. AS22-Fast (flow rate 1.2 mL/min), (c) 150 × 4 mm i.d. AS22-Fast (2.0 mL/min). The typical working pressure of AS22 and AS22-Fast is ~ 1900 psi. The excessive resolution is shown in blue boxes. Eluent: 4.5 mM sodium carbonate, 1.4 mM sodium bicarbonate; injection volume: 10 µL; suppressed conductivity detection. (Courtesy of Thermo Fisher with permission.)

columns allow the same linear velocity (*u,* cm/min) as a normal 4 mm i.d. column at a 100-fold lower volumetric flow rate,[14] enabling extended operation with a single bottle of eluent. An immediate consequence of the lower volumetric flow rates needed for capillary IC was a decrease in the surface area of the electrodialytic membrane in the eluent generator,[15, 16] which yielded a higher burst pressure for the membrane. Thus a capillary IC system such as the Thermo Fisher ICS 5000 has a pressure limit of 5000 psi (compared to a limit of 3000 psi for conventional IC systems). Capillary separation systems also produce greater column efficiencies (reduced plate heights < 2) than large bore counterparts.[14] Figure 2.2 shows the separation of the 7 common anions in less than 2 minutes using a 150 mm capillary column packed with 4 µm particles.[17] At 25 µL/min, the back pressure was only 3480 psi. For the sake of comparison, this capillary separation in Figure 2.2 takes ~ 17 s/ion *vs.* 38 s/ion for the AS22-Fast column in Figure 2.1(C). Thus, capillary systems have the potential of high speed IC separations by employing smaller particles in 150 mm capillaries. A number of such "fast" IC capillaries are available for cations (IonPac CS12A) and anions (IonPac AS18-Fast) from Thermo Fisher. In January 2013, a redesign of the eluent generators for conventional flow IC yielded the Thermo Fisher ICS 5000+ which also has a 5000 psi pressure limit.[18]

Given the ubiquitous presence of UHPLC systems in the industry, chromatographers have begun to ask "Can IC be as fast as UHPLC?" Although the terms "fast" and "ultra-fast" separations are relative, a survey of the literature and commercial catalogues shows that these terms imply sub-minute separations.

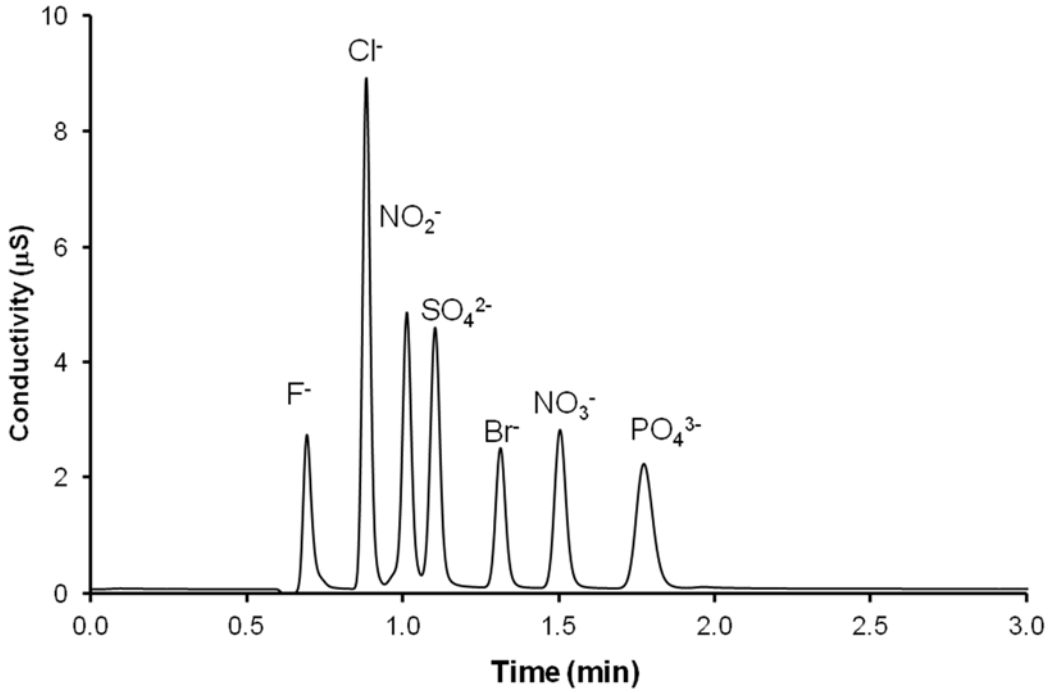

Figure 2.2. Fast separation of seven common anions on IonPac AS18 capillary column (150 x 0.4 mm) packed with 4 µm particles. Eluent: 35 mM OH^- with a flow rate of 25 µL/min. Suppressed conductivity detection. (Reprinted with permission from reference 17, American Chemical Society.)

Sub-minute IC separations were pioneered by the groups of Paull[19] and Lucy.[20] For instance Figure 2.3 shows the ultra-fast separation of seven common anions in just 40 *seconds* using an *ultra-short* 13 mm column packed with 1.8 µm C-18 silica particles.[21]

Although significant developments have taken place in achieving fast separations in commercial IC columns, we have yet to see sub-minute IC separations in commercial columns. Technology exists to synthesize 2 µm highly cross linked polymer particles which can withstand high pressure (> 5000 psi).[22] However, there are still significant challenges in using smaller particles. Firstly, as columns become more efficient, extra-column band broadening effects come into play (Section 1.6),[21] which is particularly challenging in IC where post-column devices such as suppressors are essential. Secondly, optimum packing of sub-2 µm particles is a non-trivial task. As will be discussed in Chapter 4, even 4.4 µm charged polymeric particles display unexpected behaviour in the packing process.[23] Third, the mechanical strength of PEEK limits current IC to a 5000 psi pressure limit. Ion chromatography certainly has the opportunity to catch up with the efficiencies and speed of UHPLC.

2.3 Recent Developments in High-Resolution Ion Chromatography

The above discussion has demonstrated fast separations of a few ions in relatively *simple* samples by employing smaller particles and/or very short columns. However speed becomes a secondary factor when analyzing difficult

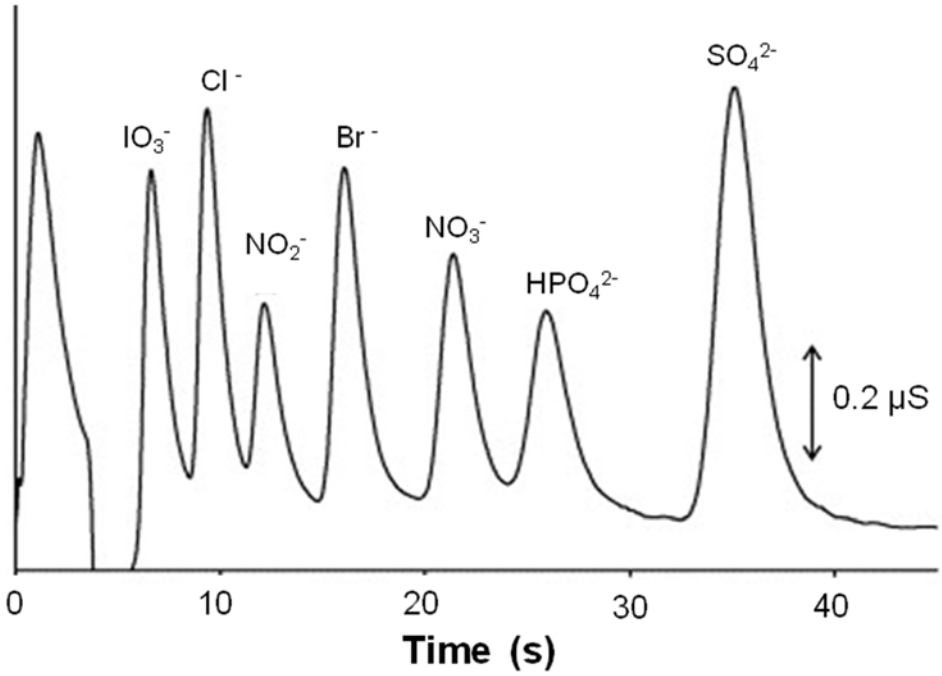

Figure 2.3. Ultrafast separation of seven common anions on very short column (13 x 4.6 mm i.d.) with suppressed conductivity detection. Column: Cationic surfactant (didodecyldimethylammonium bromide, DDAB) coated Extend-C18 column operated at 2.0 mL/min. Particle size: 1.8 µm. Eluent is 4-hydroxybenzoic acid 2.5mM at pH 10.1. (Reproduced with permission from reference 21.)

and ill-characterized samples such as food, biological samples or environmental waste. In these cases, the target is to fully resolve all the ions of interest.

As discussed in Section 1.2, the factors that affect the resolution (R) between pairs of analytes in a given separation are described by:

$$R = (\frac{\sqrt{N}}{4})(\frac{k}{1+k})(\frac{\alpha-1}{\alpha}) \qquad \text{(Equation 2.1)}$$

The plate number N is easily increased by using longer columns or smaller particles. The selectivity factor α and retention factor k becomes important for high resolution. Both of these variables are dependent on the stationary phase chemistry and the eluent.[5, 24] Software packages for the simulation and optimization of separations are available.[25] For instance, *Virtual Column* uses a database of experimental retention data to predict retention using the linear solvent strength model-empirical approach. Resolution maps are also generated by the software for the critical pairs of ions. Retention times were predicted within 3% of the observed behaviour for 33 anionic and cationic analytes across a variety of column formats and complex gradients.[26]

Thus by using specially designed high capacity columns and utilizing small particles one can achieve very high resolution. One such specifically designed high capacity capillary column is the IonPac AS11-HC. Figure 2.4 illustrates a high resolution separation of 44 inorganic and organic ions in 40 min using a long 250 mm capillary and 4 μm particles, corresponding to a separation speed of ~ 53 s/ion.

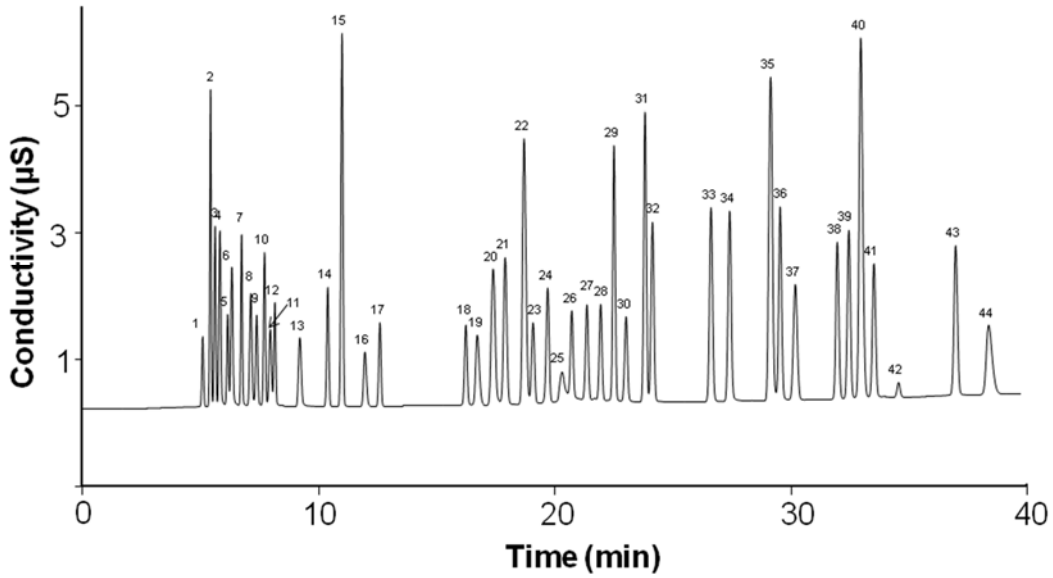

Figure 2.4. High resolution gradient separation of 44 anions on a specially tailored high capacity capillary column (IonPac AS11-HC, 250 mm x 0.4 mm i.d., 4 µm particle size). Eluent: KOH: 1-14 mM KOH in 16 min, 14-55 mM KOH in 24 min, 15 µL/min. Injection volume: 0.4 µL.
Peaks: quinate (1), fluoride (2), lactate (3), acetate (4), 2-hydroxybutyrate (5), propionate (6), formate (7), butyrate (8), 2-hydroxyvalerate (9),pyruvate (10), isovalerate (11), chlorite (12), valerate (13), bromate (14), chloride (15), 2-oxovalerate (16), nitrite (17), ethylphosphonate (18), rifluoroacetate (19), azide (20), bromide (21), nitrate (22), citramalate (23), malate (24), carbonate (25), malonate (26), citraconitate (27), maleate (28), sulfate (29), alpha-ketoglutarate (30), oxalate (31), fumarate (32), oxaloacetate (33), tungstate (34), molybdate (35), phosphate (36), phthalate (37), arsenate (38), citrate (39), chromate (40), iso-citrate (41), cis-aconitate (42), trans-aconitate (43), iodide (44). (Courtesy of Thermo Fisher Scientific with permission.)

However, in most real samples not all ions are in similar concentration. For example, bromate is a human carcinogen, whose concentration is regulated by various government environmental agencies around the world.[27] In IC, bromate elutes early, close to the chloride peak. In clean, low ionic strength samples, baseline resolution is satisfactory, as shown in the lower trace in Figure 2.5. In high ionic strength water samples, as in seawater or waste water, the resolution of bromate with the adjacent peak is severely compromised (upper trace Figure 2.5).[28] The high concentration of the matrix ions overloads the analytical column. The resulting wide fronted or tailed peak *broadens* and *shifts* the retention time of the trace bromate peak (~ 10 part per billion).[29] Eventually the broadening compromises accurate quantification and degrades the resolution of bromate from the overloaded peak.

One of the ingenious ways to obtain high resolution separation in complex matrices is *matrix elimination ion chromatography*,[28, 30, 31] based on high resolution two dimensional ion chromatography (2D-IC). In this *heart cutting* approach for bromate analysis (EPA Method 302.1), the bromate ion is separated in the first dimension using a high capacity IC column capable of handling the high ionic strength matrix. A ~ 2 mL portion of the suppressed eluent (the heart cut portion) containing the bromate (t_1 to t_2 in Figure 2.5) is passed through a "concentrator column" positioned in place of the sample loop of the injection valve for the second dimension (2-D) separation. The trapped analyte is eluted off the concentrator column and separated using a second dimension IC column of *different selectivity* than the 1st dimension column. For high resolution

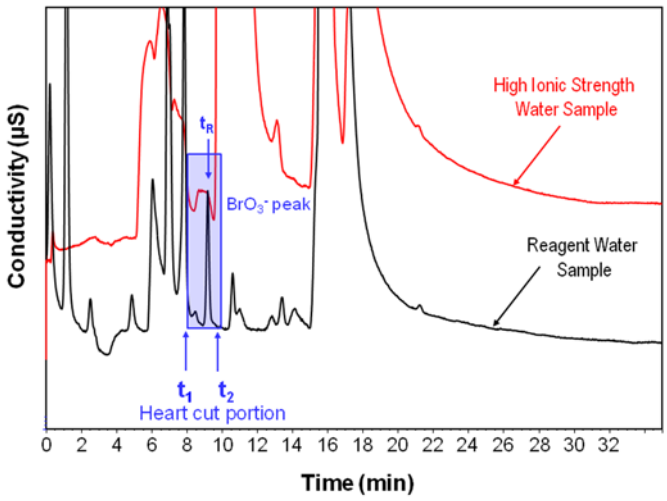

Figure 2.5. First dimension analysis of the bromate peak in reagent water and high ionic strength water. The bromate concentration is 15 µg/L. The bromate retention time (t_R) is 9.2 minutes. The start of the cut window (t_1) is 8.0 minutes and the end of the cut window (t_2) is 9.8 minutes. Column: IonPac AS19, (250 mm x 4 mm) column; Eluent: 10 mM KOH step changed to 65 mM KOH following the elution of bromate at 1.0 mL/min. Injection volume: 1.0 mL (Courtesy of Thermo Fisher with permission.)

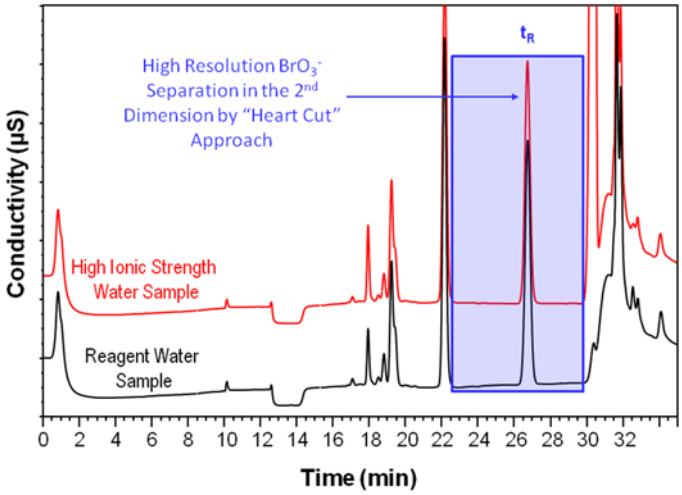

Figure 2.6. High resolution separation of bromate ion in second dimensional analysis of 15 µg/L bromate in reagent water and high ionic water matrix. Column: lonPac AS24 analytical column (250 x 2 mm i.d.) and AG24 guard column (50 x 2 mm i.d.) were used for the second dimension analysis. Eluent: Isocratic10 mM KOH changed to 65 mM potassium hydroxide following the elution of bromate for approximately 10 minutes and re-equilibrate at 10 mM hydroxide prior to injection, Eluent Flow: 0.25 mL/min. (Courtesy of Thermo Fisher with permission.)

applications, a second dimensional column with a lower cross sectional area is used to enhance sensitivity.[29] Figure 2.6 shows the second dimensional high resolution separation of trace levels (15 ppb bromate) in both reagent and high ionic strength water sample. This heart cutting matrix elimination approach is generic and can easily be applied on IC samples that give poor resolution of trace components due to matrix overload. For instance, perchlorate has similarly been resolved in highly complex water samples.[32] Research is ongoing on comprehensive 2D ion chromatography for complete analysis of complex ionic samples.[33] Also, to aid this development, fundamental studies of overload behaviour in IC were undertaken and will be reported in Chapter 6.

2.4 Conclusions

Until recently the speed of ion chromatography were limited by the pressure and flow rate limits of the IC hardware. These conditions required the use of large particles and long columns. Numerous recent advances have enabled fast IC separations by reducing the column length while using the large particles, or by reducing the particle size to 4 μm. However, commercial IC has not yet achieved the ultrafast sub-minute separations that have been demonstrated by sub-2 micron particles in very short columns. Thus further advances in IC speed for simple samples are anticipated.

For complex matrices, the enhanced pressure capabilities of modern IC are enabling greater 1-dimension peak capacities. Commercial equipment has made targeted 2-dimensional IC separations routine.

2.5 References

1. H. Small, T. S. Stevens, W. C. Bauman, *Analytical Chemistry* **1975**, *47*, 1801-1809.

2. H. Small, *Journal of Chemical Education* **2004**, *81*, 1277-1284.

3. http://www.dionex.com/en-us/products/columns/ic-rfic/lp-71774.html, (accessed February 2013)

4. Metrohm, http://www.metrohm.com/com/Produkte2/IC/Columns.html, (accessed February 2013)

5. R. W. Slingsby, C. A. Pohl, *Journal of Chromatography* **1988**, *458*, 241-253.

6. P. W. Carr, X. Wang, D. R. Stoll, *Analytical Chemistry* **2009**, *81*, 5342-5353.

7. M. E. Swartz, *Journal of Liquid Chromatography & Related Technologies* **2005**, *28*, 1253-1263.

8. C. A. Lucy, *Journal of Chromatography A* **1996**, *739*, 3-13.

9. C. A. Lucy, *Journal of Chromatography A* **2003**, *1000*, 711-724.

10. D. L. Strong, P. K. Dasgupta, K. Friedman, J. R. Stillian, *Analytical Chemistry* **1991**, *63*, 480-486.

11. D. L. Strong, C. U. Joung, P. K. Dasgupta, *Journal of Chromatography* **1991**, *546*, 159-173.

12. Y. Liu, K. Srinivasan, C. Pohl, N. Avdalovic, *Journal of Biochemical and Biophysical Methods* **2004**, *60*, 205-232.

13. É. Tyrrell, R. A. Shellie, E. F. Hilder, C. A. Pohl, P. R. Haddad, *Journal of Chromatography A* **2009**, *1216*, 8512-8517.

14. H. Eghbali, C. Bruggink, Y. Agroskin, C. A. Pohl, S. Eeltink, *Journal of Separation Science* **2012**, *35*, 3461-3468.

15. B. Yang, F. Zhang, X. Liang, *Central European Journal of Chemistry* **2012**, *10*, 472-479.

16. B. Yang, M. Takeuchi, P. K. Dasgupta, *Analytical Chemistry* **2008**, *80*, 40-47.

17. B. Wouters, C. Bruggink, G. Desmet, Y. Agroskin, C. A. Pohl, S. Eeltink, *Analytical Chemistry* **2012**, *84*, 7212-7217.

18. Thermo Fisher Scientific, *http://www.dionex.com/en-us/webdocs/30193-PS-Dionex-ICS-5000+-HPIC-29Oct2012-PS70199_E.pdf,*, (accessed February 2013)

19. D. Connolly, B. Paull, *Journal of Chromatography A* **2002**, *953*, 299-303.

20. P. Hatsis, C. A. Lucy, *Analyst* **2002**, *127*, 451-454.

21. S. Pelletier, C. A. Lucy, *Journal of Chromatography A* **2006**, *1125*, 189-194.

22. K. Li, H. D. H. Stover, *Journal of Polymer Science Part a-Polymer Chemistry* **1993**, *31*, 3257-3263.

23. M. F. Wahab, C. A. Pohl, C. A. Lucy, *Journal of Chromatography A* **2012**, *1270*, 139-146.

24. C. Liang, C. A. Lucy, *Journal of Chromatography A* **2010**, *1217*, 8154-8160.

25. J. E. Madden, M. J. Shaw, G. W. Dicinoski, N. Avdalovic, P. R. Haddad, *Analytical Chemistry* **2002**, *74*, 6023-6030.

26. B. K. Ng, R. A. Shellie, G. W. Dicinoski, C. Bloomfield, Y. Liu, C. A. Pohl, P. R. Haddad, *Journal of Chromatography A* **2011**, *1218*, 5512-5519.

27. R. J. Joyce, H. S. Dhillon, *Journal of Chromatography A* **1994**, *671*, 165-171.

28. R. Lin, K. Srinivasan, C. Pohl, *LC GC Europe* **2011**, *24*, 322.

29. H. P. Wagner, B. V. Pepich, K. S. Chris Pohl, Brian De Borba, R. Lin, D. J. Munch, EPA Method 302.0, **2009**

30. Ayushi, S. D. Kumar, A. V. R. Reddy, *Journal of Chromatographic Science* **2012**, *50*, 81-83.

31. P. Zakaria, C. Bloomfield, R. A. Shellie, P. R. Haddad, G. W. Dicinoski, *Journal of Chromatography A* **2011**, *1218*, 9080-9085.

32. H. P. Wagner, B. V. Pepich, Chris Pohl, Douglas Later, Robert Joyce, Kannan Srinivasan, Brian DeBorba, Dave Thomas, A. Woodruff, D. J. Munch, EPA Method 314.1, **2005**

33. S. S. Brudin, R. A. Shellie, P. R. Haddad, P. J. Schoenmakers, *Journal of Chromatography A* **2010**, *1217*, 6742-6746.

CHAPTER THREE. Ion Chromatography on Carbon Clad Zirconia Modified by Diazonium Chemistry and Functionalized Latex Particles*

3.1 Introduction

Ion chromatography (IC) is a widely used technique for the analysis of charged species such as inorganic ions and small ionizable molecules.[1, 2] Typically IC stationary phases are functionalized polymers that tolerate a wide pH range (0-14). The polymers are easily functionalized to tailor the surface properties.[3-6] As shown in Figure 1.2, agglomerated anion exchange phases consist of a polymer core bearing sulfonic acid groups with an agglomerated layer of nanometer sized polymer particles (latex) functionalized with alkyl quaternary ammonium groups.[1, 3, 7-9] The agglomerated nanoparticles are pH stable, and cannot be removed from the core by either strong bases or water-miscible solvents.[1, 10] However polymeric particles are not commercially available in the 3 μm range and swell in organic solvents leading to poor hydraulic performance and blockage of flow paths within the column.[11] Also, polymeric phases have lower mechanical strength and thermal stability compared to inorganic oxides such as silica and zirconia.[12]

Silica based stationary phases yield high efficiency and fast separation of small ions. Coating a 30 mm column packed with 3 μm particles with the cationic surfactant didodecyldimethylammonium bromide (DDAB) enabled separations of nine inorganic anions in 100 s.[13] However surfactants such as DDAB can

* A version of this chapter has been published as M. Farooq Wahab, Christopher A. Pohl and Charles A. Lucy, *Analyst*, **2011**, *136*, 3113-3120.

precipitate within the columns.[14] Secondly, the alkaline eluents needed for high sensitivity in suppressed IC attack silica columns (Sec. 1.7.2). Thus, there is continued interest in investigating new supports for ion chromatography. This chapter explores new approaches to introduce a strong acid functionality onto 3 μm carbon clad zirconia particles. Diazonium chemistry is used to introduce negative charge to the particles and then cationic latex nanoparticles are adsorbed to produce an agglomerated phase. So far, only 4 - 5 μm agglomerated resin phases for anion separation have been reported in 0.4 - 4 mm i.d. columns.[8] This process of surface modification converts the carbon surface into an efficient anion exchanger.

3.1.1 Conversion of Carbon Clad Zirconia into an Anion Exchanger

Figure 3.1 shows the strategy for creating agglomerated anion exchange phases using carbon clad zirconia (CCZ) particles. These particles consist of a zirconium dioxide core coated with carbon.[15] The ZrO_2 core lends the particles very high mechanical strength, which does not shrink or swell. The graphitized carbon coating is chemically inert and pH stable. Diazonium chemistry is a popular means to covalently modify carbon electrodes.[16] In Figure 3.1 (A), the diazonium salt undergoes a one electron reduction to produce an aryl free radical with the loss of nitrogen. This step may be induced thermally or *via* chemical reduction.[17–19] Next negatively charged functionalities must be introduced to the CCZ surface as shown in Figure 3.1(B). Previous work explored hydrogen peroxide treatment[20] and on-column electrolytic reduction of diazonium salts on porous graphitic carbon particles.[21] CCZ phases have also been converted into anion-exchangers by coating surfactants on the stationary phases,[22] by attaching tertiary amine followed by

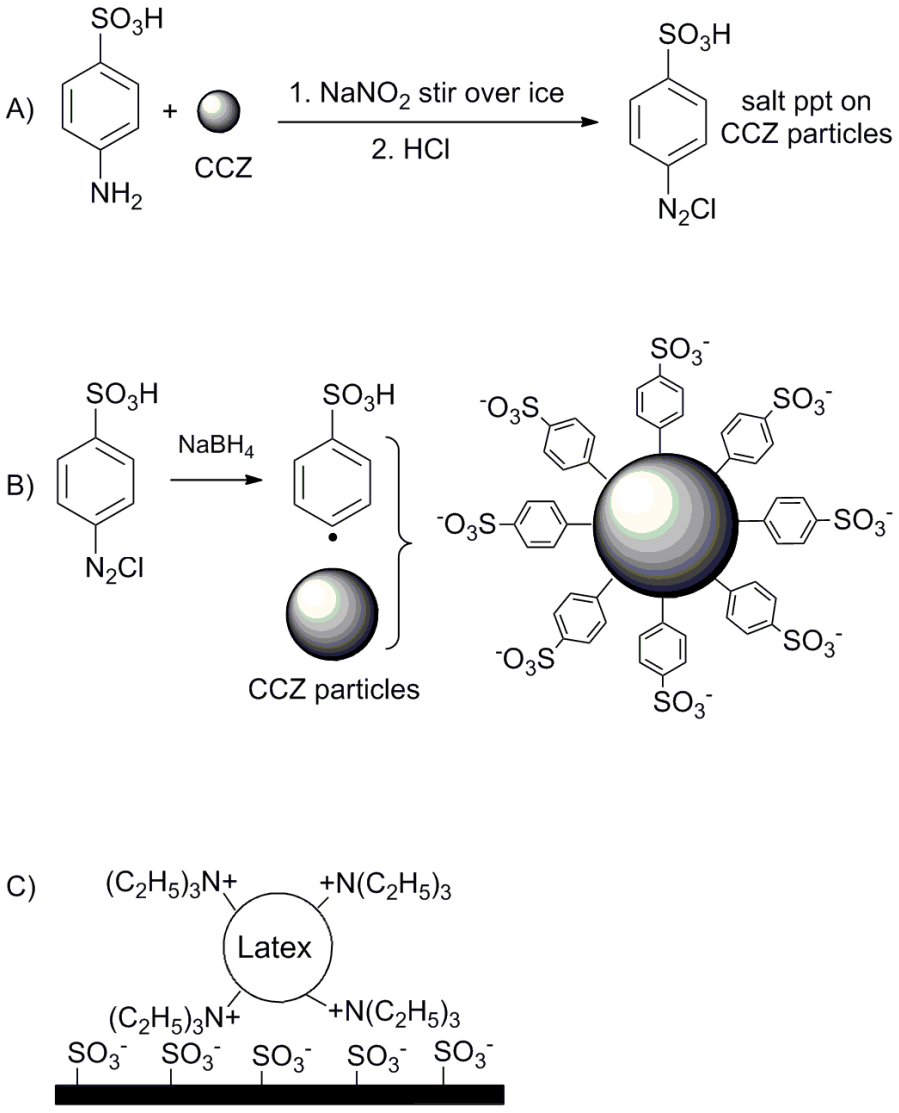

Figure 3.1. The strategy for creating negatively charged anchor sites on carbon clad zirconia (A, B) using *in situ* generated phenylsulfonic acid radicals on the particles. The precipitation step concentrates the salt on the carbon surface. The phenylsulfonic acid provides sites for the latex to agglomerate onto the particles (C).

methyl iodide treatment on CCZ,[23] and by nitric acid oxidation followed by agglomeration (Figure 3.1(C)). Plate heights of 0.024 mm for nitrate were observed for agglomerated 2 μm nitric acid treated CCZ particles.[24]

3.2 Experimental

3.2.1 Materials and Reagents

Carbon clad zirconia (CCZ, 3 μm, 30 m^2/g, ZirChrom-CARB, was purchased from Zirchrom Corporation (Anoka, MN, USA). Batch 75–111 was used for column preparation. Sodium nitrite (Reagent Plus), sodium bromide, trifluoroacetic acid (99%) and hypophosphorous acid were purchased from Sigma Aldrich (St. Louis, MO). Hydrochloric acid (37–38%) and anhydrous sodium carbonate were purchased from Caledon Laboratories (Georgetown, ON, Canada). Distilled deionized (≥17.7 MΩ-cm) water was from a Nanopure system (Barnstead, Dubuque, IA, USA). Magna plain nylon (Krackeler Scientific Inc., Albany, NY, USA) supported filters (0.22 μm) were used for washing and vacuum filtration of the particles.

The 72 nm latex AS12A-Micro1B bearing quaternary ammonium triethyl functionality was prepared by Dionex Corporation (Sunnyvale, CA, USA). Commercial latex bearing trialkyl quaternary ammonium groups is called AS12A; it has a diameter of 140 nm. Sodium acetate and oxalic acid were purchased from Caledon. Sodium chloride, 98% sodium borohydride and sodium nitrate were from EMD Chemicals Inc. (Gibbstown, NJ, USA). HPLC grade ammonium formate was from Fluka (St. Louis, MO, USA), sodium benzenesulfonate was purchased from

Eastman Kodak Co. (Rochester, NY, USA), and succinic acid was from BDH Laboratory Supplies (AnalaR, Poole, England). Fumaric acid was from Aldrich (St. Louis, MO, USA). Spherical iron powder < 10 μm with 99.9% purity on metal basis was purchased from Alfa Aesar (Ward Hill, MA, USA). The slurry and packing solvent was HPLC grade 2-propanol from Fisher Scientific (Fair Lawn, NJ, USA).

Empty PEEK columns (50 x 4 i.d. mm) with stainless steel frits (2 μm), Zitex membranes (G-108) and Ultrahigh Molecular Weight Polyethylene frits (UHMWPE) of 10 μm were gifted by Dionex Corporation. A Haskel (DSF-122-87153, Burbank, CA) high pressure air driven pump was connected to a nitrogen tank and was used for packing the column. The packing apparatus is discussed in greater detail in Section 3.2.5 and 4.2.4.

3.2.2 Apparatus

The chromatography system was a Dionex ICS-3000 equipped with dual pumps with an electrolytic carbonate-bicarbonate generation RFICTM system, a 10 μL injection loop, a 4 mm ASRS-3000 electrolytic suppressor and a conductivity detector. Separations were performed at room temperature. The suppressor was regenerated using the external mode, by pumping deionized water to the suppressor from a second pump (ICS-3000 DP pump) at a flow rate of equal to or slightly greater than the column flow rate setting.

Connecting tubing was kept short to minimize extra-column broadening (Section 1.6) on a 50 mm column. Peak efficiencies at half peak height and retention times were calculated by Chromeleon^{TM} 6.80 SP3 software. The latex solution was

pumped through the column using a Shimadzu LC-600 pump followed by 25% aqueous ACN wash. Efficiencies for the commercial AS12A column are from the Virtual Column^{TM} database (Dionex SP 6.8). A UV detector (Waters Lamda Max Model 481) was used for breakthrough curves. The reported chromatograms are after the capacity measurement experiments.

3.2.3 Strategies to Introduce Sulfonic Acid Functional Group on the Carbon Surface

A mixture of 4 mmol (0.69 g) sulfanilic acid was slurried in 5 mL water with 0.2 g of carbon clad zirconia in a container cooled by crushed ice. Then a 5 mL aqueous solution containing ~ 0.27 g sodium nitrite was added to the sulfanilic acid and the carbon clad zirconia slurry. The mixture was stirred till the solution became deep orange. Addition of 1.7 mL concentrated HCl precipitated diazonium chloride onto the particles. Various reducing agents were tested for efficacy in grafting phenyl sulfonic acid onto CCZ. Hypophosphorous acid: 5 mL of the hypophosphorous acid was added dropwise and the mixture was stirred for 1 h over ice. Iron powder: addition of 0.28 g of Fe powder (additional 0.8 mL conc. HCl was present), followed by stirring over ice for 1 h. Reduction *via* borohydride: 9.9 mmol of $NaBH_4$ in 5 mL water was added dropwise, and allowed to stir for 1 h over ice. In a separate approach, 5 mmol ground sodium borohydride was sonicated with CCZ in ACN and the resulting suspension was rotary evaporated. The resulting mixture was scraped and added to the *in situ* formed sulfanilic diazonium salt (4 mmol sulfanilic acid) suspension. (Caution: *Do not isolate 4-phenylsulfonic acid*

diazonium chloride, as it is unstable in the solid dry state).

An alternate method for diazonium functionalization was tested using the Cabot Corporation patent,[17] except that a larger amount of sulfanilic acid was taken per gram of particles. Briefly, in 11 g of water, 4 g of ethanol was added. To this mixture 1 mmol of sulfanilic acid was added, followed by 0.2 g carbon clad zirconia. The mixture was placed in a water bath pre-heated to 50 ^{o}C, and then the temperature was increased to 65 ^{o}C. When the temperature reached 65 ^{o}C, 0.35 g of 20% wt/wt $NaNO_2$ (308 μL) was added over 2 min. The reaction mixture was allowed to react at 65 ^{o}C for 1.5 h.

After either of the above reactions, the particles were stringently washed to remove side products and adsorbed organics. The particles were washed and filtered on 0.22 μm Magna nylon filters with deionized water, 1% wt/wt NaOH, reagent grade acetone, anhydrous ethanol, and HPLC grade methanol. Additionally, in the reduction with iron powder, the particles were brought in contact with conc. HCl to dissolve any unreacted Fe. Samples of the sulfonated CCZ particles (in methanol suspension) were vacuum dried on the rotary evaporator and stored in a vacuum dessicator prior to analysis.

X-ray photoelectron spectroscopy (XPS) measurements of modified carbon clad zirconia powders were performed on an AXIS 165 spectrometer (Kratos Analytical) at the Alberta Centre for Surface Engineering and Science (ACSES), University of Alberta. The base pressure in the analytical chamber was $< 3 \times 10^{-8}$ Pa. A monochromatic Al Kα source ($h\nu = 1486.6$ eV) was used at a power of 210 W. The analysis spot was 400 x 700 μm. The resolution of the instrument is 0.55

eV for Ag 3d and 0.70 eV for Au 4f peaks. Survey scans were collected for binding energy from 1100 eV to 0 with an analyzer pass energy of 160 eV and a step of 0.35 eV. Charge compensation with an electron flood gun was used to prevent sample charging (when required). The composition was calculated from the peak areas in the spectra using the instrument software with Scofield values of RSF (relative sensitivity factors) and normalized to 5 elements C, N, O, Zr and S. Elemental analysis was performed on Carlo Erba CHNS-O EA1108 Elemental Analyzer.

3.2.4 Preparation and Packing of the Column Material

Modification of 2.2 g of carbon clad zirconia was performed by scaling up the borohydride reduction (10 mmol) and starting with 40 mmol of sulfanilic acid and an equivalent amount of sodium nitrite in the presence of hydrochloric acid. The particles were washed and the sulfonation reaction was then repeated a second time to react any remaining sites on the carbon surface. The particles were filtered, washed with water, 0.5% wt/wt NaOH, water, acetone, ethanol and MeOH and vacuum dried in a dessicator. A slurry of 1.8 g of the sulfonated CCZ in 45 mL isopropanol was sonicated in the ultrasonicator and packed into empty PEEK columns (50 mm x 4 mm i.d.) with stainless steel frits (2 μm). A 40 mL slurry reservoir (Lab Alliance, USA) was connected to the Haskel Pump and the pressure was increased to 6200 psi in 3 min. This pressure was maintained for 3.5 h. After this the pressure was released, and the column inlet and outlet frit was replaced with Zitex membranes (G-108) and UHMWPE frits. (Sulfonated CCZ prepared using 44

mmol sulfanilic acid and 44 mmol $NaNO_2$ had the same sulfur acid loading).

The packed column was flushed with a 4% v/v aqueous solution of AS12A-Micro1B latex in 10 mM Na_2CO_3. To ensure uniform coating, 20 mL latex solution was passed through the column, the column was reversed and another 20 mL of latex solution was passed through the column. (Note: Surfactants within the latex solution generate bubbles in the pump head making it advisable to monitor the collected volume rather than rely on the nominal flow rate). The column was allowed to sit overnight, and washed with 25% v/v aqueous acetonitrile in both directions and later with Na_2CO_3 solution.

3.2.5 Breakthrough Curves

The column capacity was estimated by breakthrough curves[25] using nitrate as the UV absorbing ion. The agglomerated column was converted into the Cl^- form by flushing with 20 mM NaCl for 30 min, followed by a water wash for 20 min at a flow rate 0.80 mL/min. Then, 1.0 mM sodium nitrate solution was passed though the column at 0.80 mL/min. The dead time of column was determined by injecting water while 1.0 mM NO_3^- was flowing. The column capacity was calculated by:

$$Q = CF\ (t_{bkt} - t_M) \qquad \text{equation 3.1}$$

where Q is the column capacity (μeq/mL), C is the concentration (μeq/mL) of nitrate, F is the flow rate (mL/min), t_{bkt} is the breakthrough time (min) and t_M is the dead time.

3.3 Results and Discussion

3.3.1 Surface Characterization of the Stationary Phase

Agglomerated ion exchange particles provide high efficiency ion chromatographic separations.[8] An agglomerated anion exchange phase (Figure 3.1) consists of: a) a negatively charged core support particle; and b) polycationic latexes that are electrostatically bound to the support. Agglomerated IC columns have been created using silica particles and monoliths, but they require eluents that are not suited to suppressed conductivity detection.[26]

Herein the synthesis and performance of 3 μm agglomerated anion exchange particles based on carbon clad zirconia (CCZ) particles grafted with phenylsulfonic acid is described. Latexes bearing quaternary ammonium triethylamine groups are then electrostatically adsorbed onto the particles to generate the anion exchanger. As the porous CCZ have a nominal pore size of 30 nm, it is anticipated that the 72 nm latex particles only adsorb on the outer surface of the CCZ to yield a pellicular support.

As shown in Figure 3.1, the surface of the CCZ particle must be negatively charged to electrostatically anchor the polycationic latexes. However, raw CCZ does not possess sufficient charge. Equilibrating CCZ with a 4% latex solution in 10 mM Na_2CO_3 resulted in little adsorption of latex, as indicated by the small increase in surface nitrogen (from 0.45 to 0.98%) observed using XPS (Table 3.1). Nitric acid and chlorosulfonic acid have been used to introduce negative charge on CCZ.[24] However, agglomerated ion exchangers based on CCZ particles modified in these fashions could not baseline resolve inorganic anions.

Table 3.1. Surface composition by XPS of surface modified carbon clad zirconia particles in atomic percentage

Sample	%Zr (3d)	%O (1s)	%C (1s)	%S (2p)	%N (1s)
Carbon Clad Zirconia (Raw Material)	14.61	36.77	48.13	-	0.45
AS12A-Micro 1B Coat (Raw Unmodified Material)	9.42	23.65	65.77	0.20	0.98
Sulfonation* (Cabot Corporation's Patent)[17]	11.21	34.38	52.21	1.14	1.06
Sulfonated Column Material	12.73	36.10	47.50	2.09	1.57
AS12A-Micro 1B Coated Column Material	6.10	18.58	70.87	1.68	2.77

* Combustion analysis yielded 1.89 % wt/wt C and 0.34 wt/wt S

Due to the limitations of these approaches, the diazonium approach was explored herein. Reduction of diazonium salts to produce free phenyl radicals (bearing the functional group of choice) is well known in the electrochemistry literature.[16] Borohyride has been shown to be an effective reducing agent for such reactions.[18,19] The diazonium salt in Figure 3.1 can conveniently be prepared by reacting a suitable primary aromatic amine with nitrite in acidic medium. As we wish to introduce a negative charge onto the CCZ, sulfanilic acid was used as the primary amine. Sulfanilic acid is compatible with diazonium chemistry[27] and the sulfonic acid group is essentially permanently ionized ($pK_a = 0.7$).[28] However, sulfanilic acid has very limited solubility under the acidic conditions used in the conventional diazonium salt synthesis, necessitating heating of the reaction mixture and using ethanol to solubilize the amine and the corresponding diazonium salt.[17] To circumvent these solubility issues, an "*inverted method*" was used to prepare 4-phenylsulfonic diazonium chloride.[27] Instead of solubilizing the aromatic amine in warm concentrated acid or organic solvent, the sulfanilic acid was directly reacted with sodium nitrite so that the sulfonic acid itself provides the hydrogen ions to form a water soluble product. This reaction was followed by addition of HCl as shown in Figure 3.1(A), which precipitated the diazonium ion as a chloride salt onto the CCZ surface. Next the salt was reduced with borohydride. The reaction was complete as soon as the borohydride addition was complete (5–10 min). Using the inverted method and $NaBH_4$, the surface loading was increased to 2.1% *vs.* the 1.1% atomic S (XPS) achieved using the Cabot's patented method (Table 3.1).

To optimize the grafting density, other reducing agents were tested for

reduction of the diazonium salt (Figure. 3.1(B)). Heating the precipitated diazonium on the CCZ at 40 °C for 1 h in the absence of reducing agent resulted in minimal introduction of sulfur to the CCZ surface (Table 3.2). Hypophosphorous acid has been used successfully by some,[29] while others have found it ineffective.[30] In our hands hypophosphorous acid led to low sulfur loading as measured by elemental analysis (Table 3.2). Iron powder has also been reported to be useful as a reducing agent,[31, 32] but it too yielded low sulfur loading with an additional problem of removal of the iron particles from the CCZ mixture.

Reacting the diazonium salt coated CCZ with sodium borohydride once yielded 0.32% wt/wt S by elemental analysis. Repeating the $NaBH_4$ reduction increased the loading of sulfonic acid to 0.42% wt/wt S. This is the same material analyzed by XPS in Table 3.1. SEM (Figure 3.2 A and B) showed no mechanical damage of the particles due to the two times sulfonation and associated 2 h of stirring. Repetition of the reaction a third time resulted in no improvement in the S loading. The S loading corresponds to 132 μmol $–SO_3H$ groups per gram or 4.4×10^{-10} mol $–SO_3H/cm^2$ of CCZ.

Bélanger and co-workers reported 3.4×10^{-10} mol $–SO_3H/cm^2$ on a glassy carbon electrode modified electrochemically.[33] Electrochemical grafting is a superior method than most chemical approaches for carbon. Typical capacities of surface sulfonated polymeric resins range from 5 to 100 μeq/g.[34] The numbers in Table 3.2 compare well with the sulfonation efficiency of sulfanilic acid diazonium salt.

The importance of washing after modification of carbon surfaces *via*

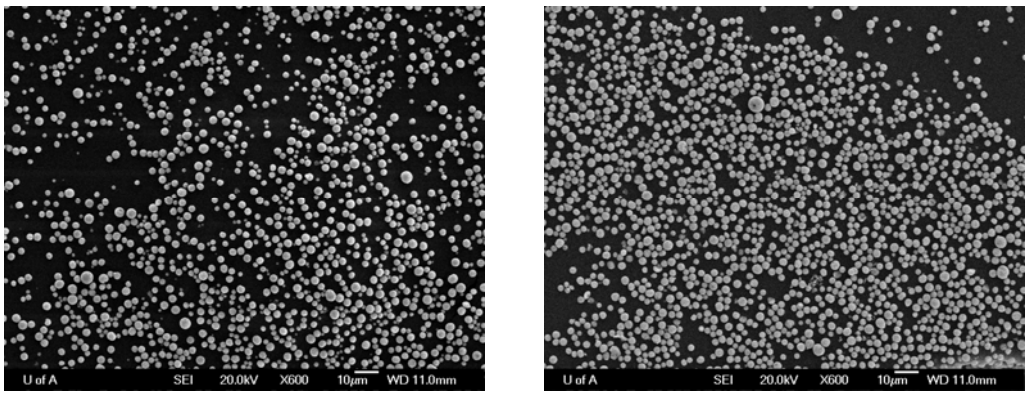

Figure 3.2(A). An overview of carbon clad zirconia particles (left), twice sulfonated carbon clad zirconia particles (right). No mechanical fracture or change in morphology can be seen for particles. The particles were subjected to 2 x sulfonation, 2 h magnetic bar stirring, exposure to solvents and 1% NaOH.

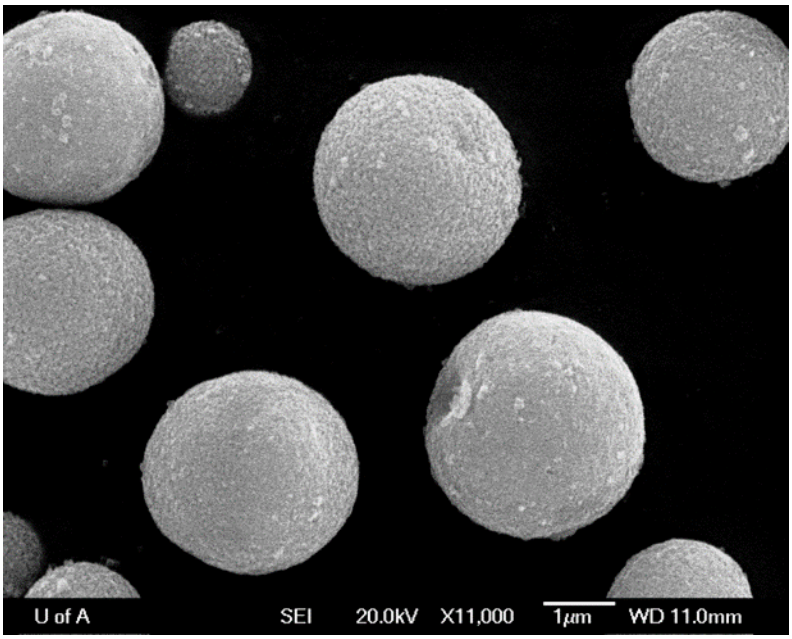

Figure 3.2(B). Higher magnification of 2x sulfonated carbon clad zirconia.

Table 3.2 Carbon and sulfur composition by combustion analysis (% wt/wt)[a]

Sample	Carbon	Sulfur	µeq - SO_3H/g
Carbon Clad Zirconia	1.10	-	-
Thermal Reaction at 40 ºC[a]	1.90	0.26	80
Hypophosphorous Acid	1.68	0.22	69
Iron Powder	1.81	0.27	84
Borohydride Reduction-I (Diazonium salt coated particles)	1.85	0.32	99
Borohydride Reduction –II (Borohydride coated particles)	1.94	0.33	103
Column Material (Two times sulfonation with borohydride)	2.04	0.42	132
Latexed Column Material (Two times sulfonated material in contact with latex)	2.43	0.43	-
AS12A-Micro 1B Coat (Raw unmodified material)	1.68	-	-

[a] Average results of three replicate analyses except the thermal reaction (n=2). The % relative standard deviation for C are ≤ 2.8% and for S ≤ 8.3 %. The thermal reaction was done with 0.1 g carbon clad zirconia starting with 8.3 mmol of sulfanilic acid.

diazonium salts cannot be overemphasized. McDermott and co-workers observed that up to 64% of the nitrophenyl groups "grafted" onto gold were lost upon sonication or refluxing in acetonitrile.[35] Thus apparently attached functional groups are simply adsorbed onto the modified surfaces. Incomplete washing would give a deceptively high grafting density. In our work, the modified CCZ were washed with a variety of solvents of differing polarity (e.g., water, acetone, ethanol, and methanol). Subsequent washing with 1% wt/wt NaOH, resulted in a few drops of orange to black colored filtrate, indicating that some adsorbed side products had remained despite the aggressive wash with organic solvents. Further washing with NaOH resulted in a clear filtrate. The overall effect of sulfonic acid grafting on the particles, regardless of the approach, was that the initially highly hydrophobic phase (which tends to float on water despite having a specific gravity of 5.7) became hydrophilic and disperses very well in water (Figure 3.3).

After sulfonation, the particles were brought in contact with cationic latex nanoparticles. The XPS spectra in Figure 3.4 provide additional insight about the agglomeration step. The counter ion on the sulfonated phase is sodium; after the adsorption of cationic nanoparticles, the sodium ion was exchanged. We note the disappearance of Na 1s peak, showing the replacement of Na by positively charged latex followed by a subsequent increase in the % N content (Table 3.1).

3.3.2 Packing and Latexing Considerations

In the packing of small particles, the particle-particle interaction becomes significant (These effects are discussed in depth in Chapter 4). Flocculating

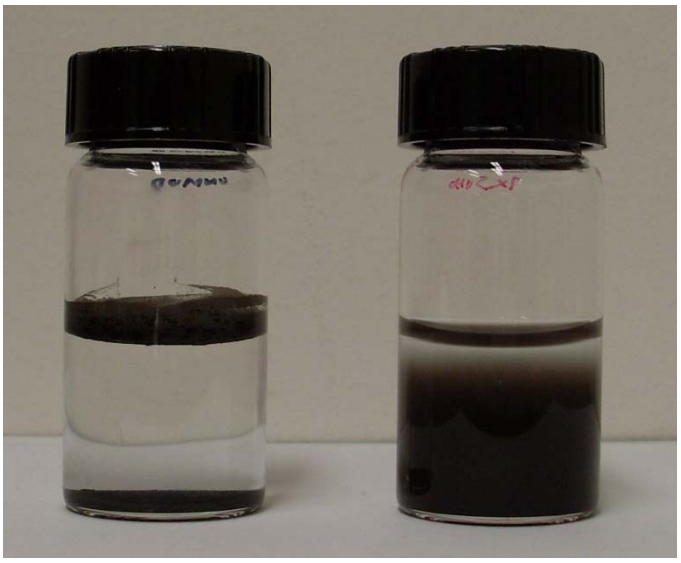

Figure 3.3. Effect of grafting phenylsulfonic acid 1x sulfonated *via* borohydride reduction of diazonium salt) on carbon clad zirconia (specific density ~5). A highly hydrophobic carbonaceous stationary phase (left) now disperses very well in water (right).

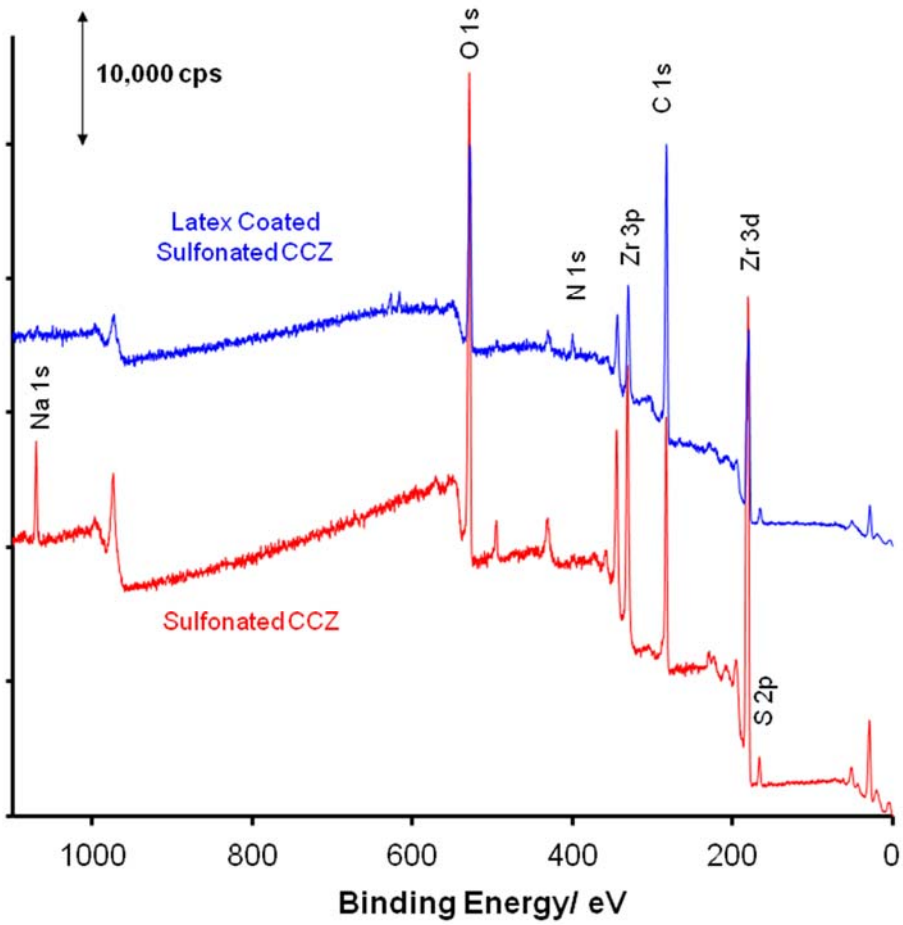

Peak Positions	O 1s	N 1s	C 1s	Zr 3d	S 2p
Position Binding Energy (eV)	**530.53**	**400.68**	**285.18**	**182.63**	**168.98**

Figure 3.4. XPS survey scan of phenylsulfonic acid grafted CCZ (bottom, red) and triethyl quaternary ammonium latex coated sulfonated CCZ (top, blue).

particles settle rapidly and form a loose cake. The slurry solvent should provide very weak attraction between the particles such that the particles settle slowly and the sediment layer is dense.[36] We noted that in water, particles settled faster than in isopropanol and the settled cake in isopropanol was more difficult to disturb by sonication as compared to water (Figure 3.5) showing that the settled bed is probably more compactly settled than in water (along with viscosity effects). Therefore, isopropanol was chosen as the driving and the slurry solvent for packing. This simple vial test is highly useful for judging the quality of the slurry medium, as will be discussed in Chapter 4.

Bed frits, if compressed or damaged during the packing process, give rise to unusually high back pressures (>3000 psi) even at 0.1 mL/min. High back pressure was observed after packing the column when UHMWPE frits were employed during the packing due to compression in the frit center (visual inspection). To avoid frit compression, we used stainless steel bed supports (which easily tolerate 6000 psi) during the packing process.

The latexing step should be done after packing the particles in a column. The AS12A-Micro-1B latex has a very low cross-link (0.5%). When high pressures (6000 psi) are used for packing, the latex compression effect would be highly pronounced if the agglomeration step was done before the column packing.[24] The lower the cross-link of the latex or the higher the packing pressure, the more severe is this effect. The source of the low efficiency in this case will not be related to coating uniformity, per se, but rather due to compression of the latex at the particle-particle contact points. So coating with low cross-link latex of any size will produce

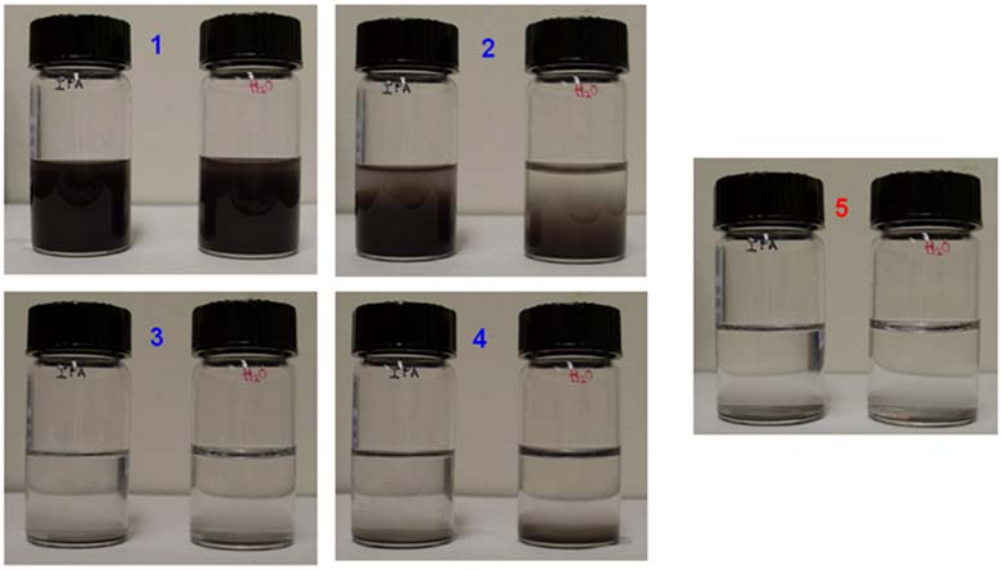

Figure 3.5. Sedimentation behaviour of sulfonated 3µm CCZ in isopropyl alcohol (left) and water (right), for batch 75-112: (1) Freshly sonicated slurry of 1xsulfonated carbon clad zirconia in 2-isopropanol (IPA) and water; (2) After 20 minutes, settling is faster in water; (3) after 9 hours; (4) brief simultaneous sonication of both vials shows that the sediment is easily disturbed in water; (5) Slurry when allowed to sit for 12 hours after sonication. Note that with zirconia core's high density; it eventually settles quickly suggesting that balanced density method of packing may not be practically possible.

poor peak shapes, if the latex layer is applied prior to packing. Therefore in this study, sulfonated particles were always first packed and then agglomerated with latex, as described in Section 3.2.

3.3.3 Column Capacity

A 50 × 4 mm i.d. column was packed with twice sulfonated carbon clad zirconia, and then equilibrated with a 4% v/v suspension of AS12A-Micro-1B latex in 10 mM Na_2CO_3, and finally thoroughly washed with 25% ACN and Na_2CO_3 to remove the surfactants within the latex solution. The capacity of the column was determined using the breakthrough curve method.[25] The capacity was 3.3 ± 0.08 μeq per column (n = 4). This capacity initially seems low compared to commercial agglomerated columns. For example, the IonPac AS12A column has a capacity of 52 μeq/column. However, this difference is predominantly due to the differences in column length (50 mm vs. 200 mm for the IonPac AS12A) and surface area. Also, the latex diameter used herein (72 nm) is approximately half that used in the commercial column (140 nm). Since the commercial polymeric phase is highly macroporous in nature it provides an adequate surface area for the latexes.[37] On the other hand carbon clad zirconia is essentially non-porous for the latexes because of the 30 nm pore size.

3.3.4 Separation of Organic Anions

The separation of carboxylates on any zirconia based columns is challenging due to the strong retention of these Lewis bases on Lewis acid sites on

the exposed zirconia surface.[38] Phosphate and fluoride are the strongest displacing ligands in the eluotropic series for zirconia.[39] Thus, to prevent strong adsorption of carboxylates, high concentrations of fluoride or phosphate buffers are typically used in the eluent.[39] However, fluoride and phosphate eluents would yield a high background conductivity in suppressed conductivity detection. The carbonate ion is not listed in the eluotropic series on zirconia columns.[39] However, recent studies showed it to be a strong displacing ligand on zirconia.[40]

Therefore, carbonate eluent was used herein as it is easily suppressed, it will minimize adsorption of analytes onto ZrO_2 and it is the recommended eluent for the AS12A ion exchange column.[37] Figure 3.6 shows the separation of six organic anions on the latexed sulfonated CCZ using suppressed conductivity detection. The plate heights *H* (mm) are compared in Table 3.3. Efficiencies ranged from 950 plates for formate to 2,550 plates for succinate on the modified CCZ. The plate height (*H*) are comparable or lower than the commercial 200 × 4 mm i.d. AS12A column. The efficiencies are also superior to those achieved on a 50 mm long column packed with quaternized trimethylaminated polystyrene coated zirconia using a 50 mM phosphate/200 mM NaCl eluent and comparable to those using this eluent plus 50 mM fluoride.[41] Further, the peak shape of the carboxylates showed fronting on the quaternized trimethylaminated polystyrene coated zirconia, having asymmetry factors between 0.5-0.8. On the other hand the peaks in Figure 3.6 are tailed. For weakly retained carboxylates the asymmetry factors for the latexed sulfonated CCZ column are higher than those for the commercial IonPac AS12A (Table 3.3), suggesting that extra column band broadening is contributing to the

broadening of early eluting peaks. To further test whether the Lewis acid sites on the underlying zirconia were contributing to band broadening, benzene sulfonate was included in the test mixture. Sulfonic acids show very weak retention on zirconia, whereas dicarboxylates such as succinate show strong adsorption.[39] In Figure 3.6, the efficiencies of succinate (2550 plates) are actually superior to that of benzene sulfonate (1215 plates), indicating that carboxylate adsorption on zirconia is not a significant problem under these operating conditions. Another interesting aspect of the separation in Figure 3.6 is that the selectivity on the latexed sulfonated CCZ column is the same for formate, succinate, oxalate and fumarate as on the commercial Dionex AS12-A column. This indicates that the latex is determining the selectivity rather than the underlying CCZ substrate.

3.3.5 Separation of Inorganic Anions

Figure 3.7 shows the separation of inorganic anions on a latexed CCZ column. The efficiency is 1970 plates for nitrite (H = 0.026 mm). This compares well with the 0.034 mm on the commercial AS12A column. Under these eluent conditions, there is a broad gap between nitrate and sulfate (>10 min gap), which is typical of low capacity ion exchange columns when operated with a low ionic strength eluent.[42] The sulfate peak is well defined on latex coated sulfonated CCZ and yields efficiencies comparable to the commercial column. Fluoride and phosphate are not included in Figure 3.7. Fluoride elutes as an early peak with

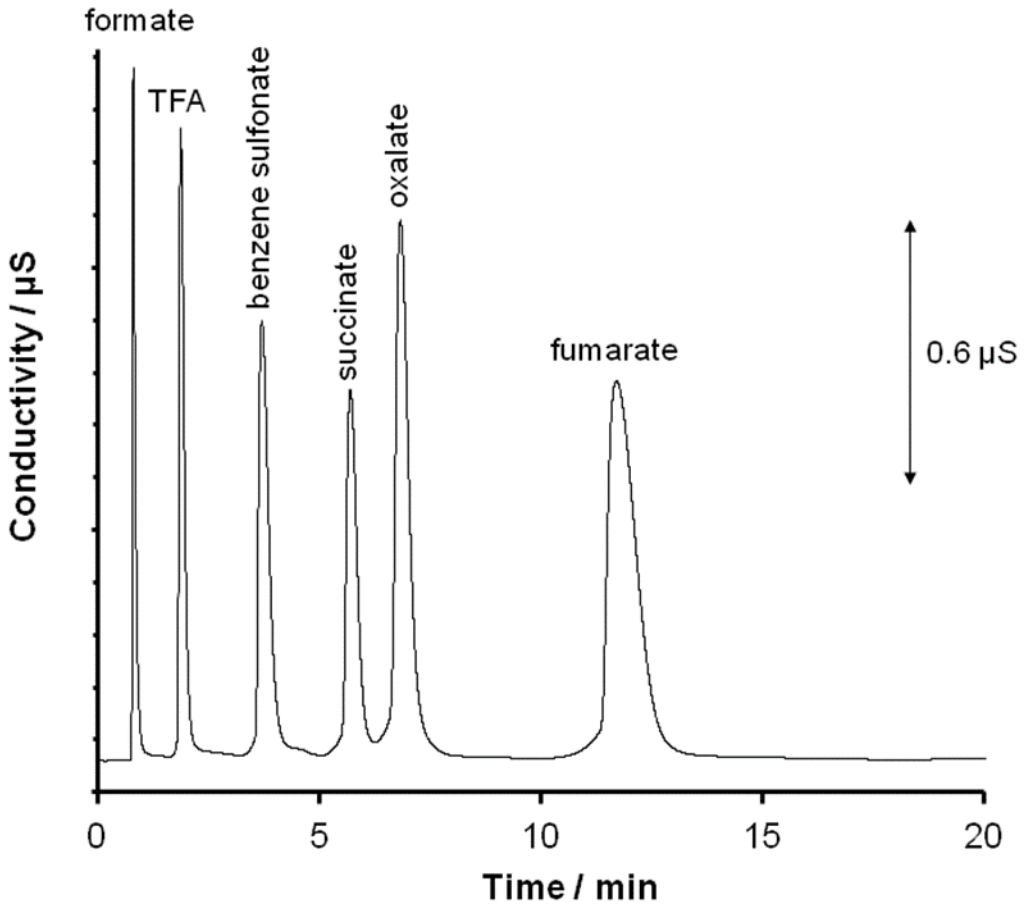

Figure 3.6. Separation of six organic ions on functionalized latex coated sulfonated carbon clad zirconia. Column: 50 x 4 mm i.d. latex coated 3 µm sulfonated carbon clad zirconia, 10 µL injection, Eluent concentration 1.0 mM K_2CO_3-0.1 mM $KHCO_3$ at 0.80 mL/min. Pressure 2170 psi. Formate 0.1 mM, trifluoroacetate 0.15 mM, benzene sulfonate 0.23 mM, succinate 0.25 mM, oxalate 0.18 mM and fumarate 0.30 mM were injected in water.

Table 3.3. Comparison of plate height *H* and peak asymmetry A_s data on organic acids on carbon clad zirconia substrate and the corresponding commercial column having the same type of latex

Anion	IonPac AS12A[a] *H* (mm)	A_s	CCZ[b] *H* (mm)	A_s
Formate	0.0526	1.23	0.0526	2.44
Succinate	0.0444	1.05	0.0196	1.46
Oxalate	0.0408	1.21	0.0198	1.34
Fumarate	0.0526	1.52	0.0322	1.55
Trifluoroacetate	-	-	0.0381	2.05
Benzene sulfonate	-	-	0.0411	1.98

[a] Virtual column™ data, under optimum conditions (200 x 4 mm i.d.) 140 nm latex, 9 µm resin.
[b] 50 x 4 mm i.d., 72 nm latex, 3 µm latex coated sulfonated CCZ. Efficiency (EP) and peak asymmetry (EP) was measured by Chromeleon *6.8.*

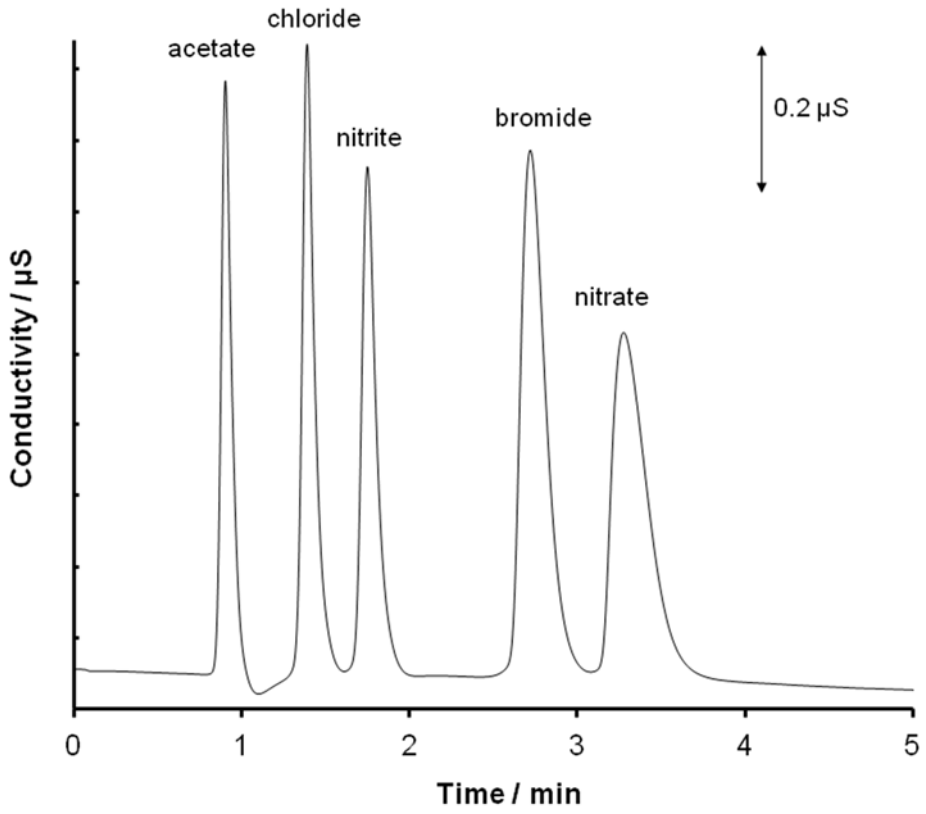

Figure 3.7. Separation of acetate, chloride, nitrite, bromide, and nitrate using 0.2 mM K_2CO_3-0.02 mM $KHCO_3$ at 0.80 mL/min on 50 x 4 mm i.d. on latex coated 3 µm sulfonated carbon clad zirconia.

carbonate eluent on the latexed sulfonated CCZ columns. However its efficiency was very low (~150 plates and A_s = 2). Phosphate ion did not elute from the CCZ columns, due to its strong interaction with Lewis acid sites on zirconia based columns. Both of these ions are very high on the eluotropic series for zirconia.[39] Thus while the latexing and use of carbonate eluent reduced adsorption on the Lewis acid sites on zirconia, these measures were not sufficient to completely eliminate adsorption of phosphate.

3.3.6 Column Stability

One of the motives for using carbon clad zirconia was its superior pH stability to other high efficiency media such as silica. Figure 3.8 shows the overlaid chromatograms of acetate, oxalate and fumarate over 4 h using a strong eluent conditions. Greater than 1000 column volumes of 5.0 mM carbonate-0.5 mM bicarbonate resulted in 4.3% loss in *k* for fumarate, the last eluting peak. Although there is a slow decrease in capacity with usage, baseline separation could be achieved by lowering the eluent concentration. The absence of split peaks or a significant decrease in peak efficiency (2,800 plates for fumarate) leads to the conclusion that the column substrate does not dissolve with aqueous carbonate eluent unlike silica. To accelerate the capacity loss on a re-coated column with latex nanoparticles, we tried relatively high ionic strength salt solution to remove the coating. However, after washing with 1600 column volumes of 0.1 M NaCl, no decrease in retention time was observed (data not shown). However, exposure to more than 100 mL of 50 mM KOH (measured pH = 12.4, ~ 8 h contact time)

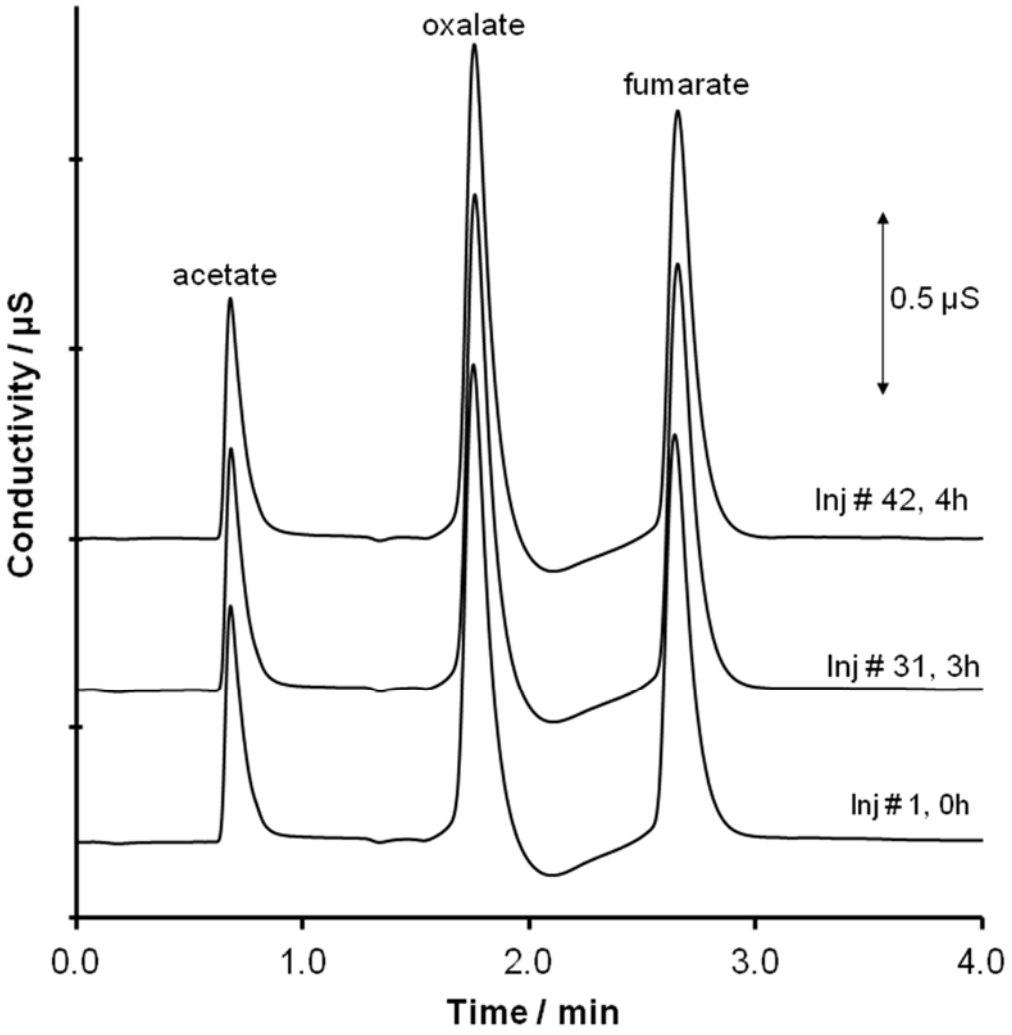

Figure 3.8. Overlaid chromatograms of test analytes, acetate 0.2 mM, oxalate 0.08 mM, and fumarate 0.09 mM, under strong eluent conditions 5 mM K_2CO_3-0.5 mM $KHCO_3$ at 0.80 mL/min, 10 µL injection. Column: 50 x 4 mm i.d. latex coated 3µm sulfonated carbon clad zirconia.

of the same re-coated column resulted in a 5.7% decrease in the retention time for fumarate. This is similar to the decrease in retention observed for carboxylate ions on a cross-linked polystyrene and quaternized with trimethylquaternary groups on bare zirconia upon successive treatment with 0.1 M NaOH. We also observed a similar behaviour when the column is stored in carbonate eluent for several days. That decrease was attributed to the constant surface modification of the underlying zirconia by the base treatment.[41]

3.4 Conclusions

This work explored creating agglomerated ion chromatography particles based on a carbon supports. Different strategies were first explored to modify 3 μm carbon clad zirconia by grafting sulfonic acid *via* diazonium chemistry. Next 72 nanometer-sized latexes were electrostatically adsorbed on the anionic particles. The resultant plate heights were half those of a commercial polymeric column for organic anions, while maintaining the selectivity of the latex. The low plate heights clearly show the feasibility of using small particles in ion chromatography. The Chapter 4 will explore a small polymeric substrate for high efficiency separations. This work shows a facile way of functionalizing carbon surfaces, which are equally, applicable to graphitic stationary phases such as carbon coated silica and alumina and porous graphitic carbon. The grafting reaction also lays the foundation for Chapter 5, where we use a similar chemistry on porous graphitic carbon to achieve novel selectivity without latex coating for superior stability.

3.5 References

1. J. Weiss, *Handbook of Ion Chromatography*, Vol. I, 3rd ed., Wiley VCH, Weinheim, **2004**.

2. P. R. Haddad, *Analytical Bioanalytical Chemistry*, **2004**, *379*, 341-343.

3. P. Zakaria, J. P. Hutchinson, N. Avdalovic, Y. Liu, P. R. Haddad, *Analytical Chemistry*, **2005,** *77*, 417-423.

4. J. P. Hutchinson, E. F. Hilder, R. A. Shellie, J. A. Smith, P. R. Haddad, *Analyst*, **2006**, *131*, 215-221.

5. B. Paull, P. N. Nesterenko, *TrAC, Trends Analytical Chemistry*, **2005**, *24*, 295-303.

6. C. A. Pohl, *LC-GC North America*, **2006**, *24*, 32-37.

7. E. F. Hilder, F. Svec, J. M. J. Fréchet, *Journal of Chromatography A*, **2004**, *1053*, 101-106.

8. R. W. Slingsby, C. A. Pohl, *Journal of Chromatography*, **1988**, *458*, 241–253.

9. X. D. Liu, C. A. Pohl, J. H. Chen, L. A. Woodruff, *US Patent* US 2009/0 277 838 A1, **2009**.

10. H. Small, T. S. Stevens, *US Patent,* 4 101 460, **1978**.

11. C. D. Liang, S. Dai, G. Guiochon, *Analytical Chemistry*, **2003**, *75*, 4904-4912.

12. J. Nawrocki, M. Rigney, A. McCormick, P. W. Carr, *Journal of Chromatography A*, **1993**, *657*, 229-282.

13. D. Connolly, B. Paull, *Journal of Chromatography A*, **2002**, *953*, 299-303.

14. S. Pelletier, C. A. Lucy, *Journal of Chromatography A*, **2006**, *1125*, 189-194.

15. T. P. Weber, P. T. Jackson, P. W. Carr, *Analytical Chemistry*, **1995**, *67*, 3042-3050.
16. R. L. McCreery, *Chemical Reviews*, **2008**, *108*, 2646-2687.

17. S. R. Reznek, J. A. Belmont, A. Kyrlidis, P. W. Carr, C. McNeff, *US Patent* 27 060, **2002**.

18. F. Mirkhalaf, J. Paprotny, D. J. Schiffrin, *Journal of the American Chemical Society*, **2006**, *128*, 7400-7401.

19. T. Severin, R. Schmitz, J. Loske, J. Hufnugel, *Chemische Berichte*, **1969**, *102*, 4152-4156.

20. M. Shibukawa, H. Terashima, H. Nakajima, K. Saitoh, *Analyst*, **2004**, *129*, 623-628.

21. J. A. Harnisch, D. B. Gazda, J. W. Anderegg, M. D. Porter, *Analytical Chemistry*, **2001**, *73*, 3954-3959.

22. S. D. Chambers, C. A. Lucy, *Journal of Chromatography A*, **2007**, *1176*, 178-184.

23. S. D. Chambers, M. T. McDermott, C. A. Lucy, *Analyst*, **2009**, *134*, 2273-2280.

24. S. D. Chambers, C. A. Pohl, C. A. Lucy, *Journal of Chromatography A*, **2011**, *1218*, 263-269.

25. E. Sugrue, P. N. Nesterenko, B. Paull, *Journal of Chromatography A*, **2005**, *1075*, 167-175.

26. K. M. Glenn, C. A. Lucy, P. R. Haddad, *Journal of Chromatography A*, **2007**, *1155*, 8-14.

27. K. H. Saunders, *Aromatic Diazo-Compounds and Their Technical Applications*, Edward Arnold & Co., London, **1936**.

28. *CRC Handbook of Chemistry and Physics*, 76th ed., CRC Press, Taylor & Francis Group, Boca Raton, FL, **1995**.

29. P. Abiman, G. G. Wildgoose, R. G. Compton, *International Journal of Electrochemical Science*, **2008**, *3*, 104-117.

30. M. Toupin, D. Bélanger, *Langmuir*, **2008**, *24*, 1910-1917.

31. V. Mévellec, S. Roussel, L. Tessier, J. Chancolon, M. Mayne-L'Hermite, G. Deniau, P. Viel, S. Palacin, *Chemistry of Materials*, **2007**, *19*, 6323-6330.

32. D. Bélanger, Personal communication (26-5-2010).

33. S. Baranton, D. Bélanger, *Journal of Physical Chemistry B*, **2005**, *109*, 24401-24410.

34. J. S. Fritz, D. T. Gjerde, *Ion Chromatography*, 4th ed., Wiley-VCH, Weinheim, **2009**.

35. D. M. Shewchuk, M. T. McDermott, *Langmuir*, **2009**, *25*, 4556-4563.

36. U. D. Neue, *HPLC Columns: Theory, Technology, and Practice*, Wiley-VCH, USA, **1997**.

37. Column manual www.dionex.com/en-us/webdocs/4460-34975-06_AS12A_V17.pdf (*accessed February 2011*).

38. Zirchrom method development www.zirchrom.com/pdf/RPMDG.pdf (*accessed February 2011*).

39. J. A. Blackwell, P. W. Carr, *Analytical Chemistry*, **1992**, *64*, 863-873.

40. T. Zhou, C. A. Lucy, *Journal of Chromatography A*, **2008**, *1213*, 8-13.

41. J. H. Zhao, P. W. Carr, *Analytical Chemistry*, **2000**, *72*, 4413-4419.

42. C. A. Lucy, P. Hatsis in Chapter 4, "*Chromatography. Part A: Fundamentals and Techniques*", 6th ed., E. Heftmann, Ed., Elsevier, Amsterdam, **2004**.

CHAPTER FOUR. Colloidal Aspects and Packing Behaviour of Charged Microparticulates in High Efficiency Ion Chromatography*

4.1 Introduction

Whenever new chromatographic stationary phases are developed, the next question is: how to best pack the particles? Even with properly tailored surface chemistry for a particular separation, a "poorly" packed HPLC column will yield asymmetrical, broad or split peaks, all degrading resolution. Lately, regulatory agencies such as the United States Food and Drug Administration (FDA) have recommended studying the scientific principles underlying the column packing process.[1]

A review of the current status of packing silica phases is available.[2] Nevertheless, in Guiochon's opinion, the major problem with columns based on modern fine particles is their packing procedure.[3] The harsh eluents used in ion chromatography (IC) are not compatible with conventional silica phases. Therefore IC separations require chemically and mechanically robust polymeric supports. Unfortunately, the packing behaviour of small polymeric particles (< 5 μm) is almost absent in the column packing literature.[2, 4-8] We employ 4.4 μm non-porous charged polymeric particles as a model material and discuss the challenges associated with packing charged microparticulates. The understanding

* A version of this chapter has been published. M. Farooq Wahab, Christopher A. Pohl and Charles A. Lucy, Colloidal Aspects and Packing Behaviour of Charged Microparticulates in High Efficiency Ion Chromatography, *Journal of Chromatography A*, **2012**, *1270*, 139-146. (HPLC 2012 Special Issue)

of packing phenomena described herein is based on packing about 60 such columns. Such polymeric substrates serve as a support for latex coated (nanometer sized particles) phases in IC. At least 16 commercial IC columns are based on this chemistry.

Slurry packing of microparticulates is commonly used in the manufacture of commercial HPLC columns. However as the particle size becomes smaller, approaching colloidal sizes of 1 nm to 1 μm, it becomes more difficult to pack efficient columns.[4] For instance, Jorgenson and co-workers found it necessary to apply 60,000 psi to pack 1.5 μm silica particles in capillaries.[9] Although the IC supports are not in the true colloidal range, their behaviour is expected to be similar to that of colloids.

In the slurry method (Figure 4.1), a suspension of particles is placed in a reservoir which is connected to an empty column. The reservoir is then pressurized to force the slurry into the column, resulting in a packed particulate bed. The column packing process is controlled by: (a) the colloidal behaviour of the particles in a given medium; (b) the rheology of the suspension; and (c) formation of the packed bed at constant pressure or constant flow (Figure 4.1). Following is the background from the fields of colloidal suspensions,[10] rheology,[11] and soil mechanics,[12, 13] as they relate to the processes involved in the packing of charged microparticulates.

4.1.1 Colloidal Properties of Slurries

Extensive studies on packing silica phases have established that the choice of slurry medium is critical – although no theoretical rules exist for choosing one.[2]

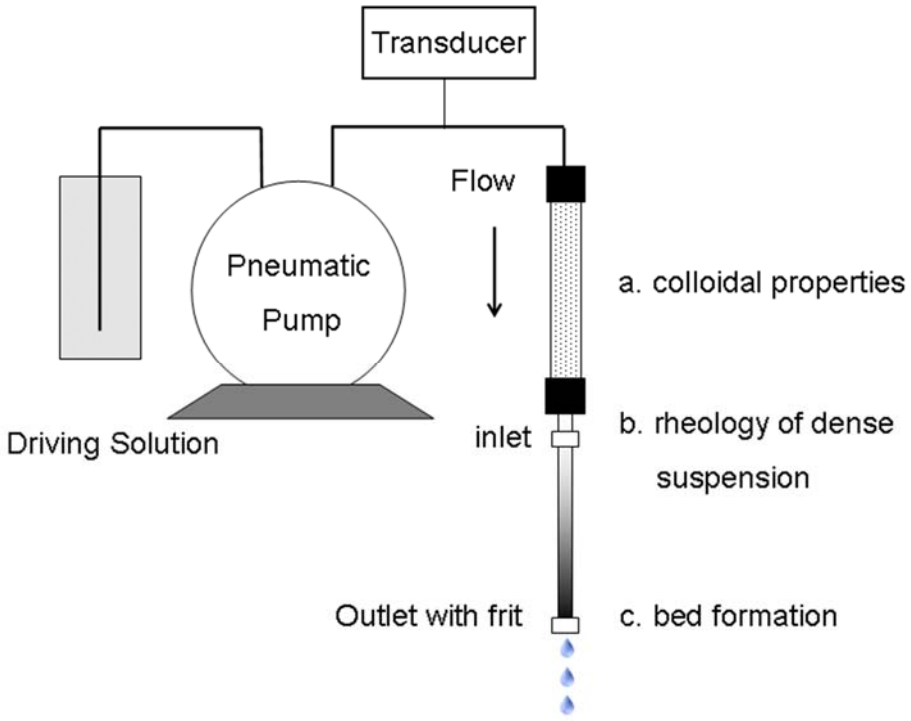

Figure 4.1. A schematic set-up of the downward slurry packing system; packing process relies on: (a) colloidal properties of the dilute starting suspension; (b) rheological properties of the dense suspension; and (c) filter bed formation under constant pressure or constant flow. The tubing that connects the slurry reservoir with the column is the pre-column.

The packing slurries can be classified as non-agglomerating, weakly flocculating or flocculating slurries depending on the state of particle aggregation within the given medium. In a *non-agglomerating* slurry particles exist individually, whereas in a flocculating medium particle clusters are visible (under a microscope). In reversed phase packing some workers prefer the balanced density approach,[14, 15] high or low viscosity solvents; or surfactants in their slurry media.[15-17] Unfortunately, most of these options are not applicable to IC phases due to solvent compatibility. Both classic[18] and recent works[19] discussing the packing of ion exchange particles do not divulge all of the slurry packing conditions.

Guidance for the choice of a slurry medium for IC phases can come from the Schulze-Hardy rule. It states that the valence of the counter-ion of the colloidal particle controls the stability of a colloidal suspension.[20] The critical flocculation concentration, CFC, of an electrolyte is given by:

$$CFC \approx \frac{49.6}{z^6 l^3_b}\left(\frac{k_b T}{A}\right)^2 \qquad \text{(equation 4.1)}$$

where z is the charge on the counter-ion, k_bT is the product of the Boltzmann constant and temperature (in K), l_b is the Bjerrum length (~ 0.714 nm in water), and A is the Hamaker constant.[11] The inverse 6th power dependence on z in equation 4.1 shows the profound influence of the counter-ion charge on particle coagulation. A lower CFC would result in flocculating slurries. Conversely, a higher CFC, favoured by low charge and dilute electrolyte solutions, would yield a non-agglomerating slurry. Thus, it is important to consider the concentration and charge of the counter-ion when selecting the slurry medium.

4.1.2 Rheology of Suspensions

The rheology of the suspension comes into play when the slurry is driven from the slurry reservoir into the empty column blank (Figure 4.1). Under shear, the particles in the suspension experience two dominant forces:[21] (a) chemical forces including electrostatic repulsion and van der Waals attractions; and (b) hydrodynamic forces originating from the viscous drag of the particles in the suspending medium and particle-particle interaction induced by the flowing medium. Thus under certain circumstances, the viscosity of a suspension can increase (shear thickening) or decrease (shear thinning) with increasing shear rate. If the shear rate is high enough, the particles form *hydrocluster*s.[22] This disruption in flow results in an increase of viscosity.[23] It has not been explored how shear thinning or thickening behaviour affects column packing.

4.1.3 High Pressure Filtration

Once the suspension reaches the outlet frit of the column, formation of the chromatographic bed results in an increase in the volume fraction (Φ) of the solid at the outlet. The upper theoretical bound on Φ (densest possible packing of equal spheres) is 0.74. However theoretical simulations and packing experiments have shown that Φ rarely exceeds 0.64 (random close packing).[24] With reference to Section 4.1.2, suspensions typically begin to show their "variable" viscosities when Φ exceeds 0.40-0.50.[25] These shear rate dependent viscosity (non-Newtonian) effects have not been reported in the column packing literature with

the exception of Shelly and Edkins.[7] As will be shown below, these effects are highly relevant in the packing of charged microparticulates.

4.2 Experimental

4.2.1 Materials

The non-porous 4.4 μm ethylvinylbenzene-divinylbenzene (EVB-DVB) particles were synthesized by Dionex Corporation (Sunnyvale, CA, USA) with a 55% DVB crosslink. Elemental analysis gave a wt/wt composition: C (90.1 %), H (8.2 %), and S (0.04%). Deionized water (≥17.7 MΩ) was from either a Milli-Q Plus (EMD Millipore, Billerica, MA, USA) or a Nanopure (Barnstead, Dubuque, Iowa USA) system. The following (reagent grade or better) were purchased from Sigma Aldrich (St. Louis, MO, USA): sulfuric acid (95-98%), ammonium chloride, aluminium sulfate octadecahydrate, sodium bromide, sodium nitrate and sodium nitrite. Lithium chloride and 30% hydrogen peroxide were from Fisher Scientific (Fair Lawn, NJ, USA). Magnesium chloride hexahydrate was from EM Science (Gibbstown, NJ, USA), sodium and potassium chlorides were from EMD (Gibbstown, NJ, USA). Anhydrous sodium carbonate was from Caledon Laboratories (Georgetown, ON, Canada). The 72 nm micro-AS4A anion exchange latex (Dionex Corporation) was synthesized from a dialkylalkanol amine.

4.2.2 Sulfonic Acid Functionalization of the Beads

Batches of 2-5 g of the non-porous 4.4 μm particles were diluted in the weight ratio of 1 part raw material to 20 parts conc. sulfuric acid and heated with stirring at 85 ^{o}C for 1 hour. This temperature was below the glass transition temperature of the particles (130-150 ^{o}C) as determined using a Pyris1 DSC (Perkin Elmer, Shelton, CT, USA) to ensure that the sulfonation was restricted to the outer layers of the particles. The reaction was then quenched on ice and diluted slowly with ~ 150 mL deionized water (*Caution*: *mixture becomes boiling hot during this process*). During sulfonation the resin changed from white to deep red, most likely due to the formation of trace sulfinates.[26] Portions of 10% hydrogen peroxide were added till the colour of the particles changed to brown. The suspension was allowed to stand for a few minutes and then diluted with ~ 1 L of water and filtered over a 0.2 μm glass fiber filter (Millipore Glass Fibre, Ireland) under vacuum (Note: *Glass fibre is recommended for filtration due to the corrosive nature of the solution. However, it is very fragile when wet.*). The particles were re-suspended in water and filtered on a 0.2 μm nylon filter paper (Magna nylon, Krackeler Scientific Inc., Albany, NY, USA). The particles were washed with 5-6 L of deionised water, and stored as a damp cake in a vial to avoid complete drying which may lead to irreversible dehydration of the resin.

Particles were dried in air overnight on a vacuum suction flask and placed overnight under vacuum at room temperature in a vial. The moisture content of the overnight air dried sulfonated resin was 4.8% as determined by thermogravimetry at 100 ^{o}C (Pyris1TGA, Shelton, CT, USA). After sulfonation

the CHS composition was C (77.2 %), H (7.2 %), and S (4.4 %). Batch to batch sulfur content was identical. This is equivalent to 1.4 milliequivalent $–SO_3H$ /g in the air dried resin. The zeta potential of the sulfonated particles was -52 mV in pure water.

4.2.3 Colloidal Characterization of the Resin

A Zeiss EVO MA 15 LaB6 filament scanning electron microscope was used to observe the surface morphology and measure the particle size. The particles were 4.2 ± 0.5 μm with a pore free surface area of 1.3 m^2/g as shown in Figure 4.2(A) and 4.2(B). Zeta potential of sulfonated resin suspension (2.2 mg/ 10 mL) was measured in deionized water in a dip cell using a Zetasizer Nano-ZS (Malvern, Worcestershire, UK) controlled by Malvern 6.20 software. The particles were sonicated for 2 min before transferring to the dip cell. The cell was equilibrated to 25 ^oC for 2 min prior to electrophoretic mobility measurements. The mobilities were calculated from the Smoluchowski model built into the software. Duplicate samples were measured.

Sedimentation experiments, in duplicate, were done in 100 mm long Wintrobe tubes (Fisher brand or Pfeiffer glass USA, ~ 1 mL volume) supported on a levelled Wintrobe tubes rack (Clay-Adams Co. Inc., NY, USA). 80 mg of the sulfonated resin was slurried in 2 mL of the desired slurry medium and sonicated for 2 min to remove dissolved air (presence of air bubbles can give an incorrect sediment height). The Wintrobe tube was filled with the slurry to the 100 mm mark. The sedimentation heights were recorded after 12 - 24 hours.

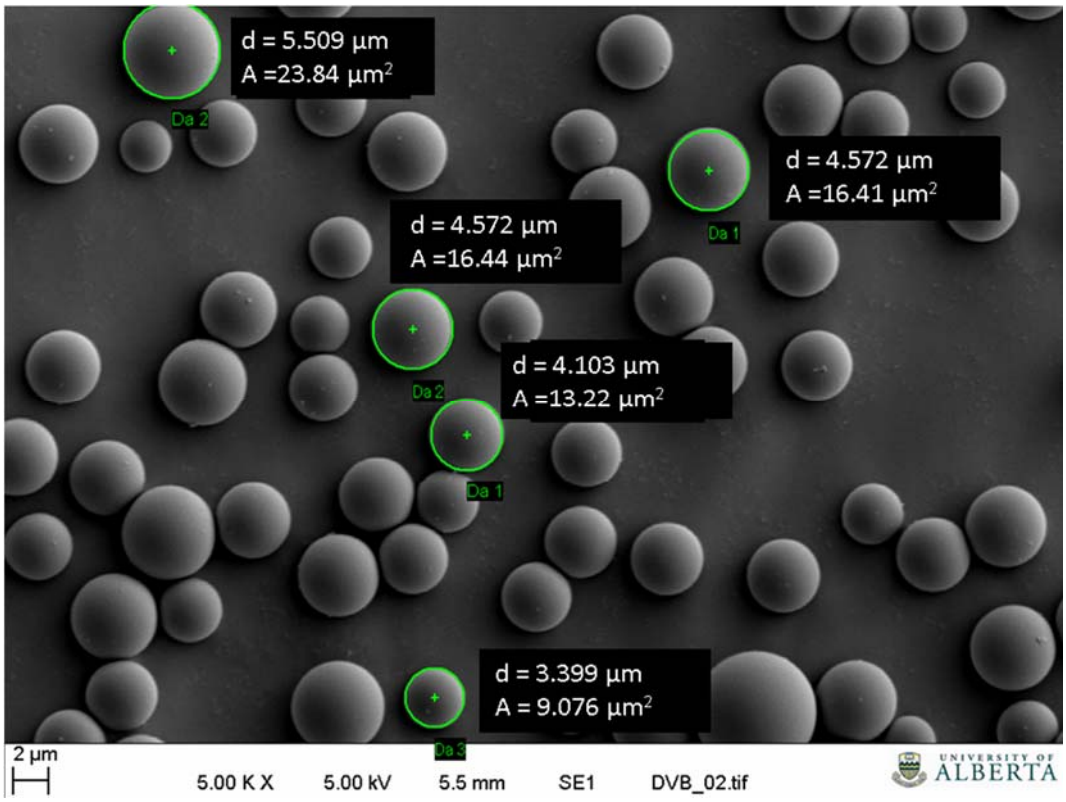

Figure 4.2 (A). SEM image of the 55% DVB-45% EVB particles showing the size distribution of the particle. Note the absence of fines and the smooth surface. No changes were observed with SEM after sulfonation of the particles and repacking twice at 4000 psi.

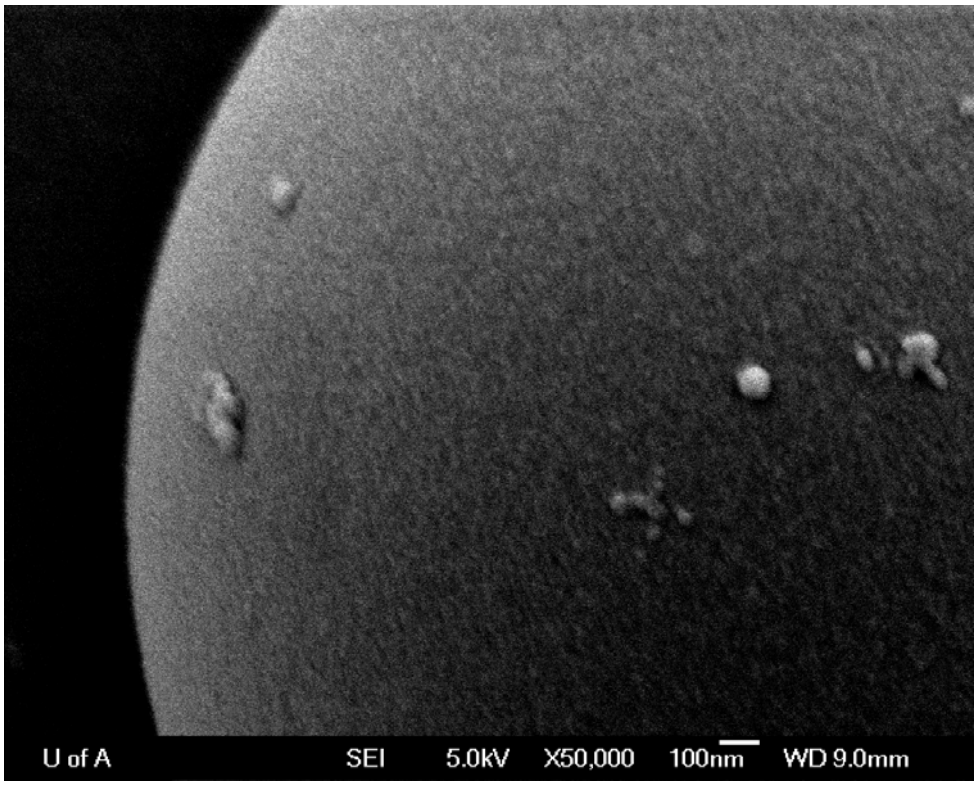

Figure 4.2 (B). A 50,000 times magnification of the surface of a typical particle, showing the absence of macropores in the particles.

A Leitz optical microscope (Wetzlar, Germany) with 25:1 or 45:1 objective magnification was used to monitor the colloidal behaviour on glass slides with a coverslip. A 0.1 mm deep hemocytometer cell counting slide (Hausser Scientific Partnership, Horsham, PA, USA) was occasionally used to monitor the slurry under a microscope. In order to see how the particles would move in the slurry, we looked at the edges of the cover slip on the slide, where the liquid is evaporating and drawing the solution by surface tension or by gently moving the coverslip sideways. Observational tests for non-Newtonian suspensions are described in detail in Section 4.3.3.

4.2.4 Apparatus

In constant pressure packing experiments, a Haskel pump (DSF-122-87153, Burbank, CA, USA), driven with N_2 gas (Praxair Inc., Edmonton, AB, Canada), was used. Most experiments used a cylindrical (14 mm i.d.) 40 mL slurry reservoir from Lab Alliance (State College, PA, USA) connected to a 50 x 4 mm i.d. stainless steel pre-column and then to the empty column. Empty polyether ether ketone (PEEK) columns (100 x 4 mm i.d. Dionex) fitted with 2 μm stainless steel or Ti outlet frits (Dionex) were used during packing.

In experiments where the slurry temperature was varied, a cylindrical stainless steel slurry reservoir (~ 27 mL, 660 mm long) surrounded by a stainless steel water jacket was used. The jacket was connected to a circulating water bath (IsoTemp 1006S, Fisher, Pittsburgh, PA, USA). For constant flow packing, an LC Varian Pro Star HPLC pump (Varian, Australia) was used with a 10 mL slurry

reservoir (made by machine shop of the Department of Chemistry, University of Alberta, 14 mm i.d.) with same pre-column as used in constant pressure packing. For the constant flow experiments the desired initial flow rate was set for 1 h, followed by compaction at 2.5 mL/min setting for 30 min (>6000 psi, ~2.26 mL/min measured when collected in a cylinder).

The chromatography system was a Dionex ICS-3000 equipped with either an electrolytic RFIC™ methane sulfonic acid or potassium carbonate eluent generation system. With the 10 μL injector loop, connecting tubing were the Dionex supplied tubings (0.010 inch i.d., part no. 045877). For the 2 μL injection loop, 1561 PEEK tubing (0.004 inch i.d., S.P.E. Ltd. North York, ON, Canada) was used. All tubing connections were kept short to minimize extra column effects. Unsuppressed conductivity detection was used for efficiency testing by injecting 2 or 10 μL of deionized water at ambient temperature. Virtual Column Separation Simulator (Dionex) provided the (EP) efficiency/ asymmetry data for the IonPac® series of commercial columns.

4.2.5 Packing Procedure

Prior to packing, the Haskel pump was rinsed with a few hundred mL of the driving solution. Sulfonated resin was washed with 0.1 M HCl and then with 5-6 L of deionised water, and then dried for 30 min under vacuum filtration. Three grams of damp resin were sonicated for 10 min in the desired volume of the slurry medium and transferred to the slurry reservoir. The column blank was empty prior to pressurization. No settling of the slurry into the empty column was

observed within the 5-6 min loading of slurry and commencing packing. Columns were packed at 4000 psi for 1.5 h with the same slurry and driving solution unless otherwise stated. The column was detached from the pre-column when the pressure decreased below 100 psi. No extrusion of bed was observed upon removing the column from the packing assembly. The outlet frit was replaced with a Ultrahigh Molecular Weight Polyethylene frit (UHMWPE, Dionex) and Zitex membrane (G-108, Dionex).[27] A polyethylene frit with no Zitex membrane was used for the column inlet. After testing of the column, the packing was recovered from the column by extruding the packed particles and re-used after washing with 0.1 M HCl and copious amounts of water.

4.2.6 Column Efficiency Testing

The efficiency (width at half height) of our columns and IonPac® AS9 HC, AS11 HC, AS 16, AS18, AS19 and AS22-Fast columns were measured for the water dip using 1.5 mM or 10 mM MSA at 1.0 mL/min using a 2 or 10 μL injection loop. Extra column peak variance was subtracted.[28] Column pressure of constant flow packed columns was measured directly by connecting the column to the pump and bypassing the injector and the detector.

4.2.7 Anion Exchange Separations

The experimental considerations for coating particles with latex nanoparticles are detailed in Chapter 3 and in our published work.[27] A column that was packed with 3 g resin in a 27 mL heated reservoir at 50 ^{o}C was coated

with AS4A suspension. A 5% (v/v) suspension of AS4A latex (72 nm particles suspension) diluted in water was flushed through a 100 x 4 mm i.d. packed column at 1 mL/min using a Metrohm-709 IC pump (Herisau, Switzerland). The latex suspension was pumped through the column until the turbidity and color of the effluent matched that of the original latex suspension (~ 33 mL). The coated column was washed with 0.1 M sodium carbonate followed by Nanopure water equilibrated with eluent. The IC instrument used to perform anion exchange separations was as described in Section 4.2.4 except that a 2 mm ASRS 300 suppressor (Dionex) preceded the detector.

4.3 Results and Discussion

The objective of this work was to identify the colloidal and hydrodynamic factors that govern the packing of small polymeric ion-exchange particles. We first identify a measure for the quality of packing, and then detail the colloidal and the hydrodynamic factors that govern the quality of the polymeric packing.

4.3.1 Preliminary Packing Considerations

Commonly unretained probes are used to judge the quality of gas chromatography,[29] LC, electrochromatography,[30, 31] and ion chromatography[32] columns. Herein pure water is used as the unretained probe. Extra-column effects are particularly significant when monitoring an unretained marker.[28] Therefore we used unsuppressed conductivity to eliminate the extra-column band broadening associated with a suppressor. Table 4.1 compares our measured efficiencies with

Table 4.1. **Validation of the water dip efficiency test in commercial Dionex columns.**

IonPac® Column	Nature of the Packed Resin[a]	Column size / mm	*N* Empirical	*h*[b]	*N* (Water dip) Virtual Column®
AS22 Fast	6.5 µm, grafted	150 x 4	5275 ± 25	4.4	Not available
AS19	7.5 µm, grafted	250 x 4	8217 ± 48	4.1	6000
AS18	7.5 µm, agglomerated	250 x 4	8486 ± 201	3.9	7700
AS16	9 µm, agglomerated	250 x 4	8726 ± 50	3.2	6000
AS11 HC	9 µm, agglomerated	250 x 4	5488 ± 64	5.1	5200
AS9 HC	9 µm, agglomerated	250 x 4	6946 ± 23	4.0	6000

[a] All resins are supermacroporous (2000 Å). No extra-column corrections were made.
[b] Reduced plate height h = Plate height (H, µm) / particle diameter (d_p, µm).

Virtual Column database efficiencies for the void peak. Our measured efficiencies are consistently higher, indicating the importance of extra-column effects. However, the *N* in Table 4.1 are still compromised by broadening due to injection, connecting tubing and the detector flow cell. For instance, subtracting the extra column effects from the efficiency of the 150 mm AS22-Fast column results in a corrected efficiency (N_{corr}) of 6700 *vs.* 5275. The quoted efficiencies in this work are those for which all extra column effects have been removed (N_{corr}).

With regard to packing a column, the packing pressure is an important parameter.[33] To prevent bed collapse during column operation, the columns are typically packed at 2-3 the expected working pressure (~1500 psi for IC). Highly cross linked particles can tolerate 10,000 psi without mechanical damage. A 21% improvement in column efficiency was observed for 6000 psi packing as compared to 4000 psi. A packing pressure of 4000 psi was chosen for further studies based on the work of Haddad and coworkers.[19]

4.3.2 Colloidal Properties of Slurry

4.3.2.1 Effect of Monovalent Cation Slurry Medium

The height of a sediment bed is a useful test in colloid chemistry to examine the nature of the suspending medium. Sedimentation behaviour has been studied for packing octadecyl silica (ODS) particles,[7] but has not been reported for IC phases. Table 4.2 summarizes the sediment quotients for the resin suspension in pure water and in electrolyte solutions. A lower sedimentation

Table 4.2. Sedimentation Quotients of the Sulfonated Resin in Various Electrolyte Solutions

A) Ions/ 100 mM	Sedimentation Quotient [a]
Li^+	100
Na^+	100
K^+	100
NH_4^+	100
Mg^{2+}	198
Al^{3+}	223
B) Effect of Al^{3+} concentration /mM	
Deionized water	100
0.01	100
0.1	100
1	130

[a] Sedimentation quotient w.r.t. water = [100*(sediment height in soln.)/(suspension height)]/ [(sediment height in water)/(height of water suspension)]

quotient indicates a more compact bed which should yield a better packed column. In Table 4.2(A) the sedimentation height is the same for all monovalent ions, confirming that the specific nature of the M^+ ion has no effect on the sedimentation as predicted by the Schulze-Hardy rule (equation 4.1). Although the sedimentation heights are the same, optical microscopy further reveals that the particles in pure water were independent and repulsion was apparent when the particles approached each other, as seen in a snapshot of a microscope movie in Figure 4.3(A). This is as would be expected for a charged particle with an uncompressed electrical double layer.[34] Due to the larger size of the particles than the true colloids, the motion was not as frantic as typical Brownian motion, but rather was more subdued. In contrast, in 0.1 M Na^+, the particles were motionless. When motion was induced by perturbing the coverslip, the particles travelled as agglomerates, which are highlighted with the ellipses in Figure 4.3(B).

In Chapter 3, we had developed a "vial test" to assess the quality of a suspending medium.[27] In this test, the resin is allowed to settle in a vial. The vial is then gently rotated, with a slight tilt, to disturb the bed. The sediment from pure water was difficult to disturb by gentle rotation, whereas that settled from 0.1 M Na^+ was much looser. This difference results from the rate at which the particles settled. For water, the resin did not completely settle in 12 h, whereas the resin settled in 1 h in 0.1 M Na^+. The slower settling rate allows more time for each independent particle to glide over the bed until they reach a closed packed structure.[35]

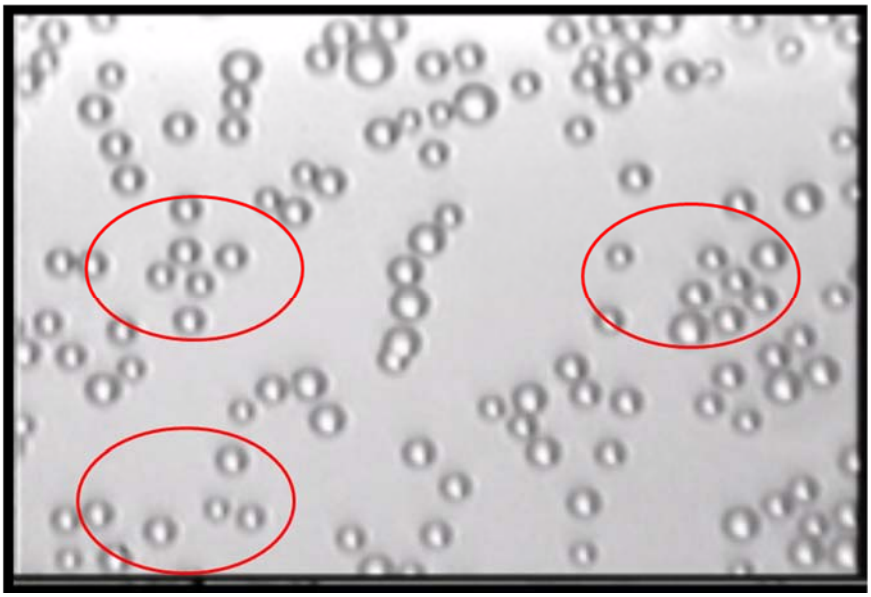

Figure 4.3(A). A snapshot from an optical microscope movie showing the slurry behaviour of sulfonated particles in water. The particles are in constant motion and free to move.

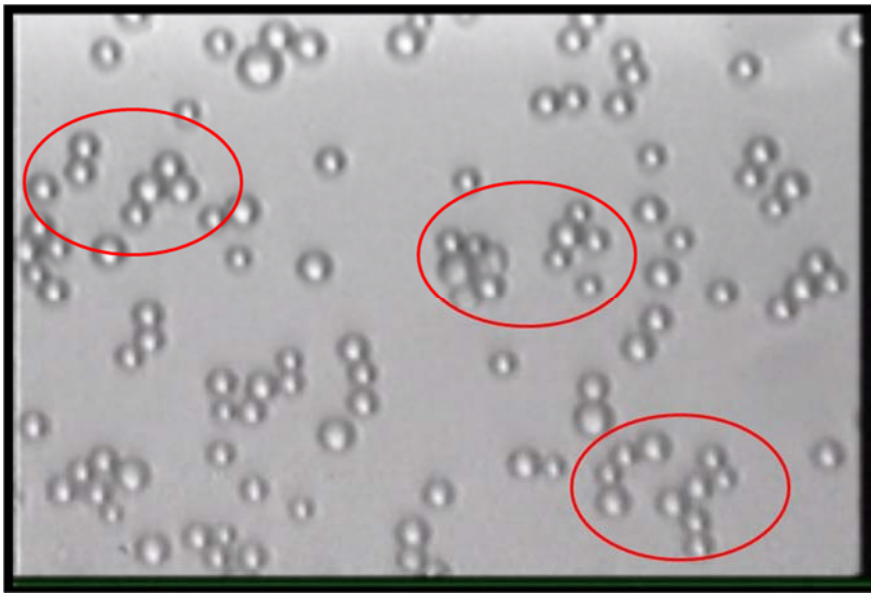

Figure 4.3(B). A snapshot from an optical microscope movie showing the slurry behaviour of sulfonated particles in 0.1 M Na^{+}. The particles exist as clusters which re-form upon disturbance of the coverslip. The clusters remain motionless. Agglomerated particles are highlighted within the ellipses.

The slow settling observed for water and Na^+ slurries is advantageous for packing. In packing, it is desired that the individual particles are forced into chromatographic bed by the motion of the slurry solvent, rather than by settling. Given the slow settling rates observed above, insignificant settling is expected in the ~ 5 min between loading the slurry reservoir and pressurization of the packer. To determine the predictive nature of the three tests above, columns were packed in water and 0.1 M Na^+, and their efficiencies determined (Figure 4.4). The efficiency for a column packed in pure water was much greater than that packed in 0.1 M Na^+. This is consistent with the observations based on optical microscopy and the vial test, suggesting that these tests are effective predictors of packing quality in the case even when sedimentation heights are equal.

4.3.2.2 Effect of Multivalent Cation Slurry Medium

Sedimentation of particles from slurries prepared in 0.1 M divalent (Mg^{2+}) and trivalent (Al^{3+}) ions, as shown in Table 4.2(B), showed greater sedimentation heights than water, indicating that particles were aggregating under these conditions. This is consistent with the strong charge dependence on colloidal stability predicted by the Schulze-Hardy rule (Section 4.1.2). Similarly, rapid sedimentation of particles takes place in Mg^{2+} and Al^{3+} slurries (15-20 min *vs*. 12 h for water and 1 h for Na^+).

Optical microscopy revealed, as shown in Figure 4.5(A) and 4.5(B), that particles in these electrolytes agglomerated instantly after disturbing the suspension, and the vial test showed very loose bed structure. Visually one could

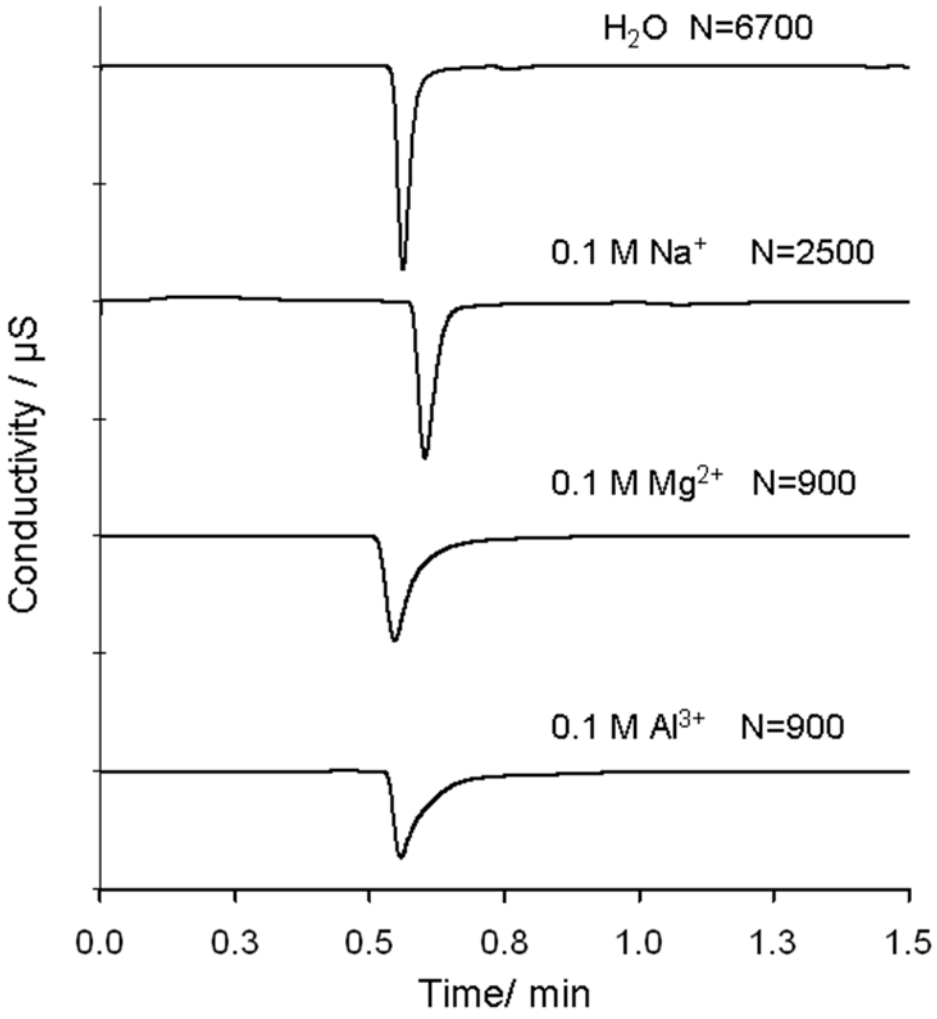

Figure 4.4. Effect of ionic charge on the slurry medium (3 g resin/40 mL) and same driving solution on a 100 x 4 mm i.d. column packed with 4.4 µm sulfonated resin. The efficiency of the water dip decreases drastically as the ionic charge in the slurry medium increases – after column collapse; packing pressure was 4000 psi in each case for 1.5 h.

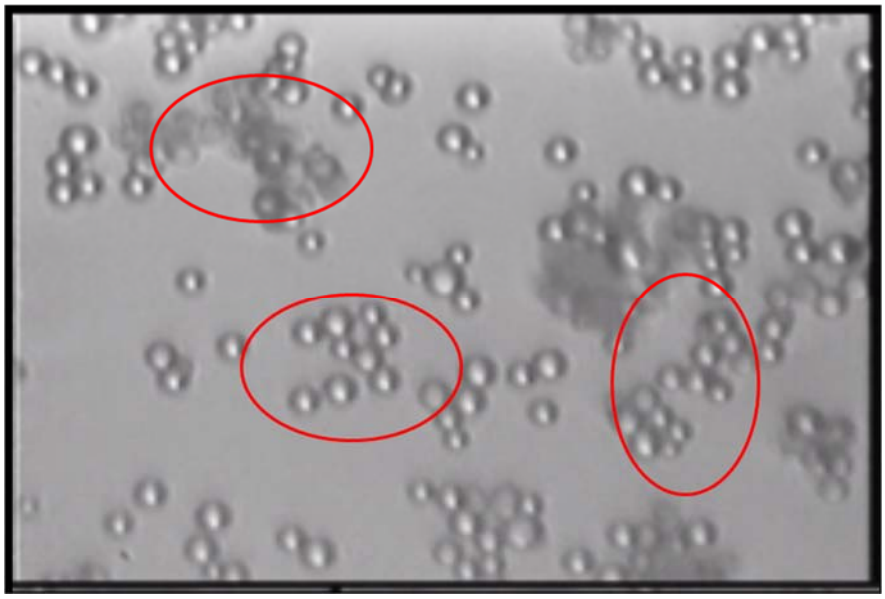

Figure 4.5 (A). A snapshot of an optical microscope movie showing the slurry behaviour of sulfonated particles in 0.1 M Mg^{2+}. The particles exist as clusters which re-form upon disturbance of the coverslip. The clusters, highlighted in ellipses, remain motionless.

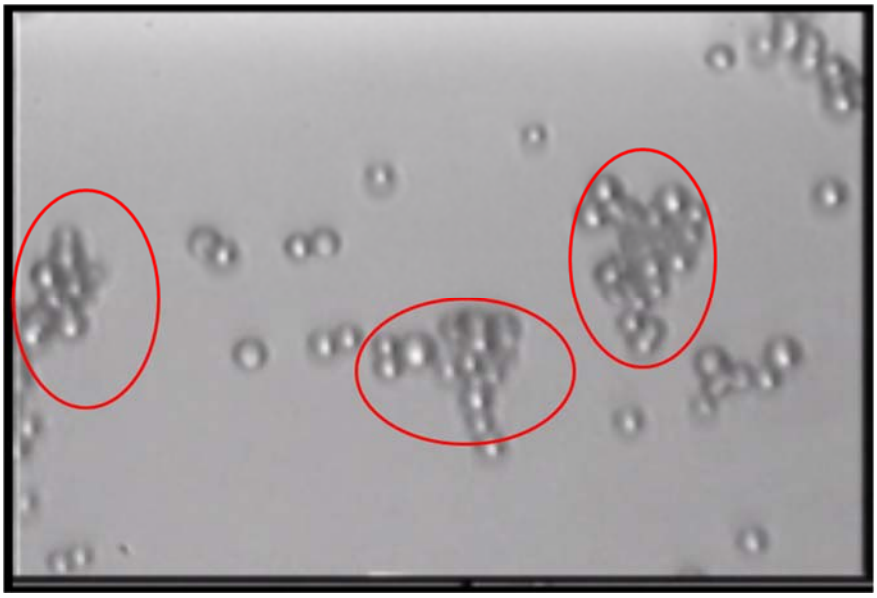

Figure 4.5 (B). A snapshot of an optical microscope movie showing the slurry behaviour of sulfonated particles in 0.1 M Al^{3+}. The particles exist as clusters which re-form upon disturbance of the coverslip. The clusters (highlighted by the ellipses) remain motionless.

see clear agglomerates within 30 s in the Mg^{2+} and Al^{3+} suspensions in Wintrobe tubes. Initially, columns packed using Mg^{2+} and Al^{3+} showed similar efficiency to columns packed with pure water, but soon exhibited a surge in back pressure (300-400 psi increase from the initial operating pressure) and a dramatic drop in efficiency to that shown in Figure 4.4. These changes occurred as the methanesulfonic acid eluent displaced the Mg^{2+} or Al^{3+} from the packing. This increased the inter-particle repulsion, causing the loose aggregate structure to break (as indicated by the sedimentation test in Table 4.2 (B)) resulting in compaction of the bed. The resultant voids significantly impact efficiency. The compaction of the bed is also be related to the rapid settling of the agglomerating particles in Mg^{2+} and Al^{3+} slurries in the reservoir.

Previous studies of reversed phase packing have demonstrated that agglomerating slurries result in lower efficiency columns.[2, 4] Similarly herein, sedimentation, optical microscopy and the vial test all indicate that 0.1 M multiple charged electrolytes result in agglomerating slurries that yield loosely packed columns.

4.3.2.3 Effect of Ionic Strength of a Monovalent Ion

Section 4.3.2.2 represents an extreme case where all particles exist as agglomerates. To test the effect of weakly flocculating conditions we studied the effect of low ionic strength Na^+ slurries. Sedimentation tests with 0.001 to 0.1 M Na^+ showed identical bed heights as water (sedimentation quotient of 100 independent of $[Na^+]$). However, in the vial test settled beds formed in < 0.02 M

Na^+ were similar to water (i.e. difficult to disturb), whereas those settled from higher Na^+ concentration (≥ 0.05 M) were distinctly loose. Optical microscopy showed that particles in 0.01 to 0.02 M NaCl were weakly agglomerating (*i.e.*, free particles as well as agglomerates were seen undergoing oscillatory motion). While, with 0.05 and 0.1 M NaCl the suspension was agglomerated and the motion of the particles came to a halt. Efficiency values for columns packed with slurries in dilute Na^+ are similar to that of pure water (Figure 4.6), but decrease rapidly when more concentrated Na^+ was used. This is consistent with the Schulze-Hardy rule (equation. 4.1) that states that a critical flocculation concentration will exist for an electrolyte.[36] The void time also increased with the electrolyte concentration, indicating formation of a more porous bed.

4.3.2.4 Using Different Slurry and Driving Solutions

The flocculating behaviour of highly charged ions can be used to eliminate electrostatic repulsion *after* packing in a non-agglomerating slurry. This approach of *in situ* elimination of repulsive forces was desirable for our negatively charged microparticulates. In the reverse phase packing for silica, a clever approach was pioneered[37, 38] by using a non-agglomerating slurry and a highly flocculating driving solution to consolidate the bed. For that purpose, sedimentation experiments with a trivalent cation (Al^{3+}) were chosen to help select the concentration of highly agglomerating solutions while closely matching the density of water (e.g. 1 mM Al^{3+}). From Table 4.2(B), it is clear that 1 mM Al^{3+} is

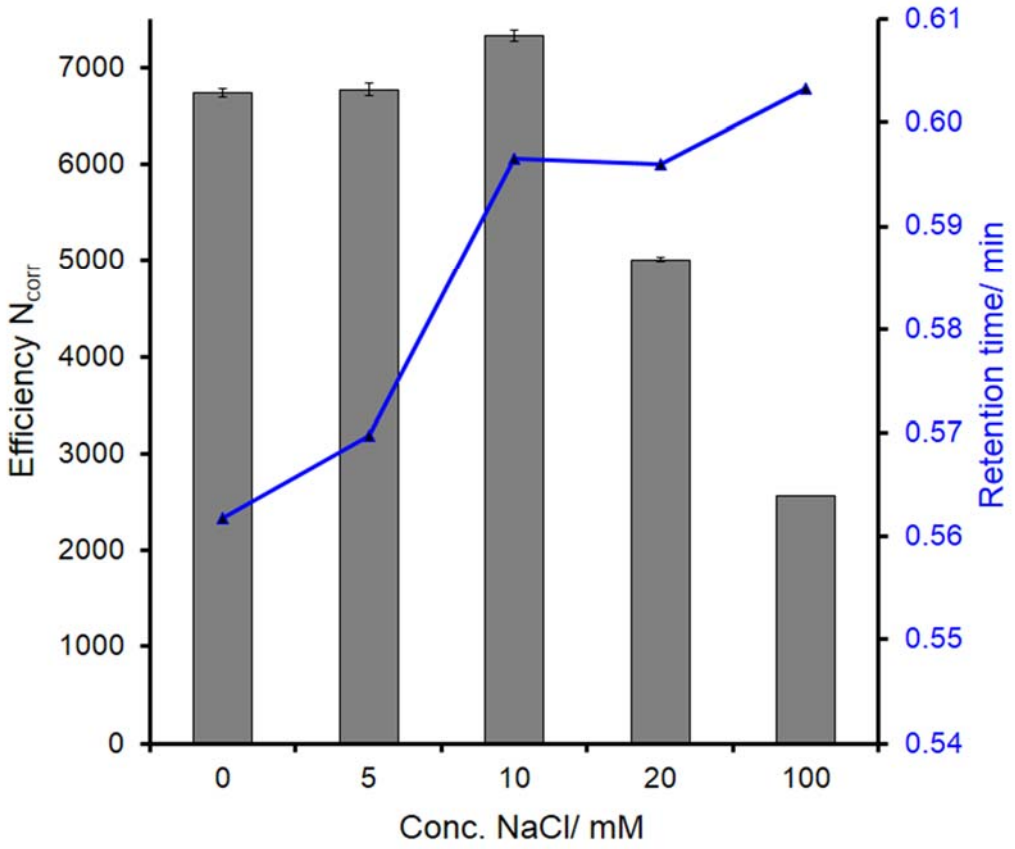

Figure 4.6. Unretained marker (water dip) efficiency of a column (100 × 4 mm i.d.) packed with 4.4 µm sulfonated resin as a function of ionic strength of NaCl. The slurry (3 g resin/40 mL) and the driving solvent were made in the same solution of the salt (triangles represent retention time). Eluent: 1.5 mM MSA at 1.0 mL/min with unsuppressed conductivity detection. Packing pressure 4000 psi for 1.5 h.

still a powerful flocculating agent for these particles, yet it is dilute enough to have similar density as water. Using 1 mM Al^{3+} slurry and water as a driving solution we obtained N_{corr} = 4600. Whereas, using water as a slurry and 1 mM Al^{3+} as a driving solution, the N_{corr} = 6700 was obtained. This is an improvement of 45% in N. Thus our results agree with the observations of other authors who packed silica based columns. Therefore, we agree that a properly chosen flocculating agent in packing is beneficial, but the slurry liquid is critical as well as it should be highly non-agglomerating if such an approach is to be adopted.

4.3.3 Non-Newtonian Behaviour of the Resin Suspension

The initial particle slurry is sufficiently dilute that it exhibits Newtonian viscosity behaviour. However, during the packing process, the suspension becomes more concentrated (Sections 4.1.2 and 4.1.3), and may exhibit non-Newtonian behaviour. As Sec. 4.3.2 established that only a non-agglomerating medium will yield efficient columns, pure water slurries are used in these studies.

The shear thickening behaviour of the sulfonated particles in a non-agglomerating medium can be observed simply by vacuum filtering the slurry. Upon filtering to dryness, the filter cake appeared dry so long as the vacuum was applied. However upon removing the vacuum, the filter cake became a wet "flowing" liquid (Figure 4.7). Agitation of the slurry with a spatula re-solidified the suspension. This process was reversible – indicating that the concentrated suspension will show reversible shear thickening. Structurally, shear thickening

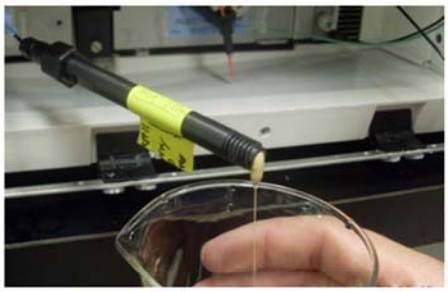

Example of an extruded material

Figure 4.7. Observational tests on non-Newtonian behaviour of the resin on a filtration assembly (vacuum on (bottom) and off (top)). Similar reversible behaviour of becoming a wet paste and a dry cracked solid is seen while doing the Reynold's dilatancy test using a hand palm.

can be considered as a transition from an ordered state to a disordered arrangement of particles leading to a jammed state.[22] Some suspensions expand their volume (dilatancy) under shear forces.[6] All dilatant suspensions are shear thickening but not *vice versa*. The *Reynold's dilatancy test* from soil mechanics can be used to test for dilatancy.[12] A pat of damp sulfonated particles was placed in the palm of a hand and a few drops of water were added to make a moist paste. The resin pat appeared glossy and flowed when the palm was tilted. However as the palm was stretched (sheared) the suspension lost its gloss and actually cracked. The loss in gloss or surface drying is an indicator of volumetric dilatancy.[39] As the suspension expands, the imbibed liquid is sucked in like a sponge making the suspension appear dry. The pat becomes wet again as the shearing force (stretching movement of the palm) is stopped. This established that our particle's suspension is not only shear thickening but also dilatant. Based on the Reynold's test classifications, a dense sulfonated resin suspension in water exhibits "quick dilatancy" (*vs*. "slow dilatancy" or no dilatancy).[12]

A characteristic of shear thickening behaviour is the critical shear rate, *i.e.*, the minimum shear rate at which the viscosity begins to rise quickly. As the movement of a spatula or flexing of a palm are sufficient to shear thickening a dense sulfonated resin suspension, its critical shear rate is low. This is consistent with the critical onset of shear thickening being related to the particle diameter d_p by $\frac{1}{d_p^{\,2}}$.[40] In true colloids (0.1-1 μm) very high shear rates are required (~ 10,000 s^{-1}) to induce shear thickening. But for larger particles, (e.g. < 5 μm used herein),

the onset occurs even at shear rates of 10 to 100 s^{-1}.[40] The constant pressure packing system provides an initial shear rate of ~700 s^{-1} at the column wall. The high shear rate "solidifies" the dense slurry. Subsequently when the pressure is released, the "solid" becomes thin again. Extrusion of the packed bed indicates whether shear thickening occurred during the packing process. Ideally, the packed bed should appear as much like toothpaste. However, if the shear thickening occurred during packing, the bed appears as a thin liquid upon extrusion (Figure 4.7).

4.3.3.1 Hydrodynamic Control of the Suspension Rheology

The most convenient way to slurry pack columns is to use a constant pressure pneumatic pump. This leads to variation in the shear rate during the packing process, from ~ 700 s^{-1} initially, to near zero at the end of packing. Even with RPLC phases, this leads to axially heterogeneous packed beds.[41, 42] Significant density variations are observed along the packed column length. This variation in density is even more critical for short columns.[19] Guiochon and co-workers[43] reported that if short columns are made by sectioning from a longer column, leaving behind the inlet and outlet sections from the longer length, then the axial packing density across the shorter sections is very uniform. However, the variation in packing density across a short column, made without sectioning from a longer column portion is in fact large.[41] We observed a similar behaviour in our columns, where under some conditions the inlet and outlet appeared loose and wet rather than tightly packed. To mitigate these undesirable features of the constant

pressure packing system, we adopted a counterintuitive approach of using a very low initial flow rate (0.15 to 1.5 mL/min) and then consolidating the bed by applying high pressure (~ 6000 psi, 2.5 mL/min setting). Numerical simulations show that slow packing will produce a denser bed.[44] Figure 4.8 shows the dramatic effect of packing flow rate on packing on bed morphology. Columns packed at low flow rates (<0.25 mL/min) extruded as a solid rod. As the packing flow rate increased, the extruded column appears thinner and thinner. This effect was independent of the slurry density. Figure 4.9 shows the effect of packing flow rate on the column backpressure, dead volume and water dip efficiency. Increasing the packing flow rate resulted in a larger dead volume (right axis) and lower backpressure (left axis). These are both consistent with a less dense bed being formed by a higher packing flow rate. The effect of packing flow rate on efficiency is more complex, with an optimum efficiency being observed at a packing flow of 0.75-1.5 mL/min.

4.3.3.2 Changing the Slurry Temperature and Onset of Shear Thickening

The well-known effect of temperature is to reduce the viscosity of solvents. For dense suspensions increased temperature also has the effect of increasing the critical onset of shear thickening.[45] By heating the suspension one can delay the onset of shear thickening or even eliminate it.[40] Thus we explored the effect of controlling the temperature of the slurry reservoir from 5 ^{o}C to 80 ^{o}C under constant pressure mode. Figure 4.10 shows 34% improvement was observed for packing at 50^{o}C relative to packing at room temperature.

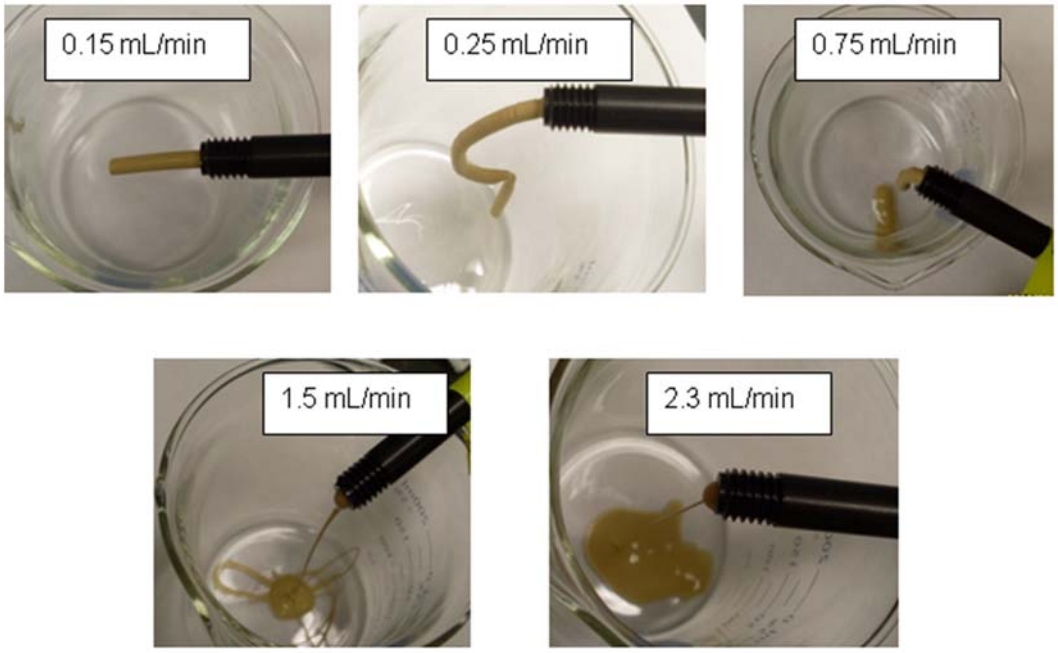

Figure 4.8. Column bed morphology as a function of initial flow rate setting during packing; at low flow rates the extruded material is in the form of a rod and as the flow rate is increased the extruded material is a "wet" paste. The packed columns were extruded at the same flow rate (extrusion method detailed in Section 4.2).

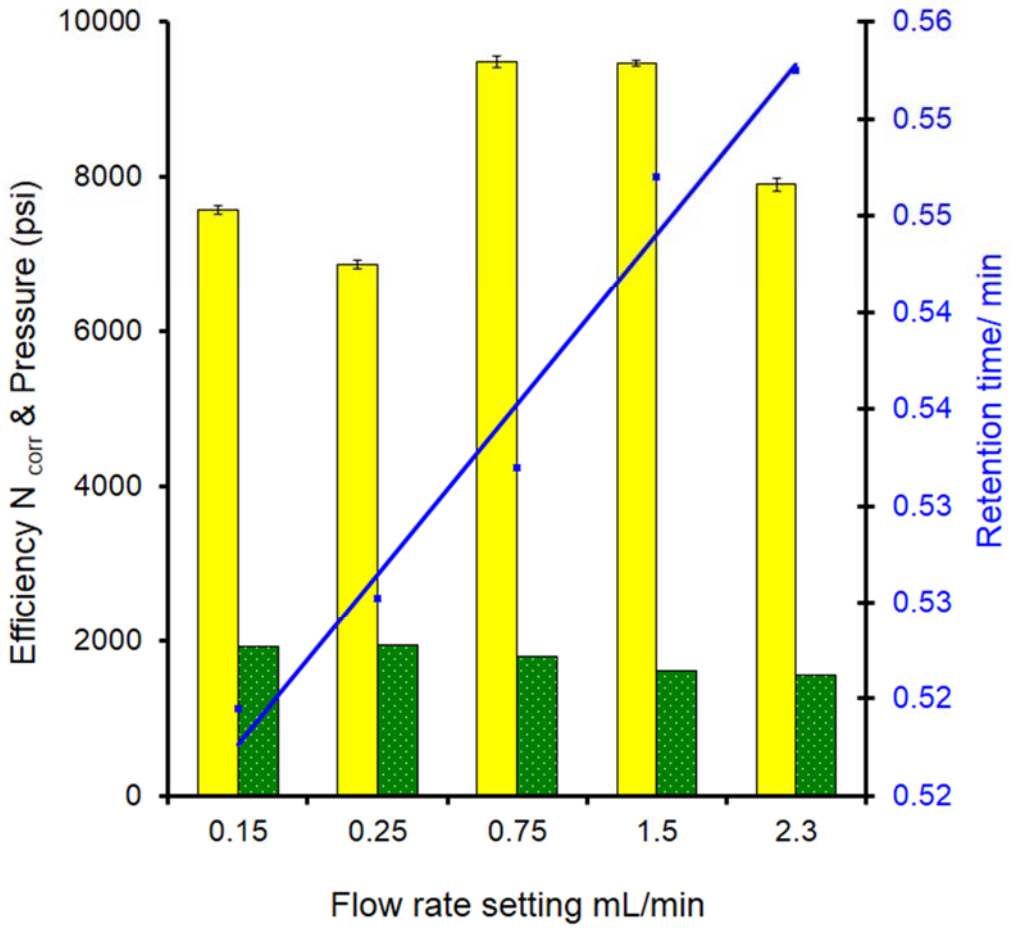

Figure 4.9. Water dip efficiency of a column (100 × 4 mm i.d.) packed with 4.4 µm sulfonated resin as a function of pump flow rate setting followed by compaction at ~ 6000 psi for 30 min. Column backpressure (green-dotted bars) decreases with the flow rate and retention time increases (in blue squares). The slurry density was 3 g/10 mL using water as slurry and as driving solvent. Eluent: 1.5 mM MSA at 1.0 mL/min with unsuppressed conductivity detection.

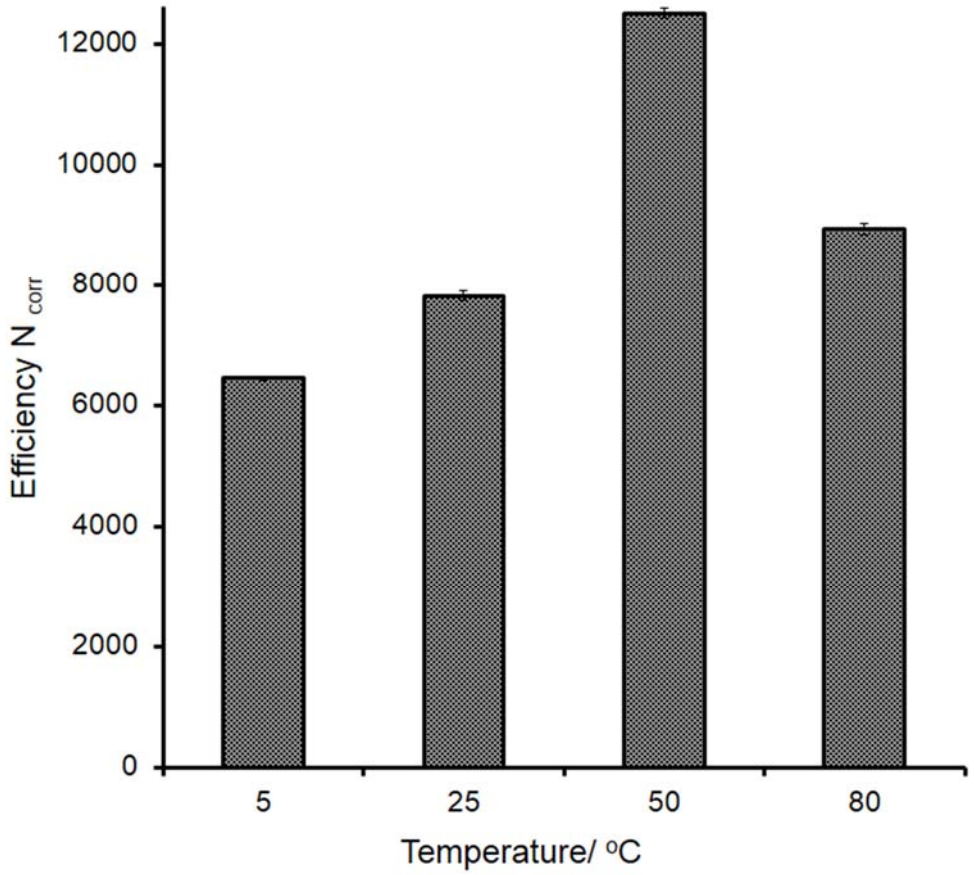

Figure 4.10. Unretained marker (water dip) efficiency of a column (100 × 4 mm i.d.) packed with 4.4 µm sulfonated resin as a function of slurry reservoir temperature. The columns were packed for 1.5 h at 4000 psi. The driving solvent and the slurry medium was water (3 g resin/25 mL). Eluent: 1.5 mM MSA at 1.0 mL/min with unsuppressed conductivity detection.

4.3.4 Chromatographic Performance of the Latex Coated Columns

To perform anion separations, the sulfonated resin was packed using H_2O slurry–H_2O driving solvent at 50 ^oC and then coated with 72 nm AS4A latex nanoparticles. This latex is designed for low surface area and non-porous resins. Figure 4.11 shows the separation of 5 common anions in 5 minutes. The efficiency of fluoride is lowest ~ 2700 with highest asymmetry ~ 1.6. Later eluting ions show an asymmetry between 1.04 to 1.16 and 7200 to 10936 plates. The 4.4 micron substrate in 100 x 4 mm i.d. column in Figure 4.11 shows 49 % improvement in peak efficiency as compared to a commercial 250 mm AS4A-SC column. Table 4.3 compares the reduced plate heights of the commercial columns employed in 250 x 4 mm i.d. format with the performance of the column packed at high slurry temperature under optimum eluent conditions. It is clear that small particles in short columns can provide superior efficiency as reduced plate heights of 1.9 can be easily achieved with peak asymmetry close to unity. Unfortunately, typical polymeric substrates in chromatography are notorious for lower efficiency than silica phases but it is clear that latex coated columns on a polymeric substrate can be equivalent or even superior to silica based phases in terms of efficiency and pH stability.

4.4 Conclusions

This chapter provides an understanding of the column packing processes for small charged polymeric phases. We explored the colloidal and rheological factors that influence the packing of polymeric particles bearing permanently

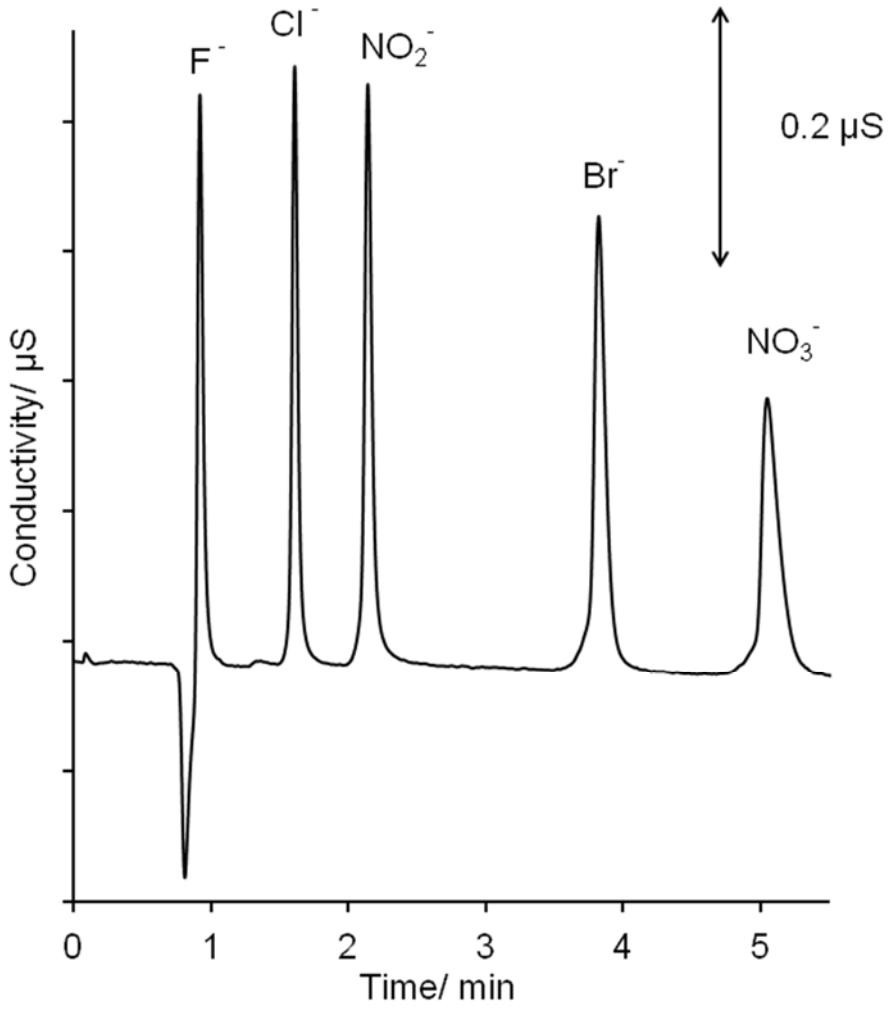

Figure 4.11. Chromatograms showing the separation of 5 common anions using 2.0 mM K_2CO_3–0.2 mM $KHCO_3$ at 1 mL/min with suppressed conductivity detection on 72 nm AS4A latex coated column. The column (100 x 4 mm i.d.) was packed in 3 g resin in a heated slurry reservoir at 50 ◦C at 4000 psi in water slurry and water driving solvent. Injection volume: 2 µL; concentration of anions: fluoride (50 µM), chloride (40 µM), nitrite, bromide, and nitrate (60 µM).

Table 4.3. **Reduced plate heights *(h)* on commercial agglomerated columns under optimized conditions[a]**

IonPac Series (Particle size)	Fluoride	Chloride	Nitrite	Bromide	Nitrate
AS4A-SC (13 μm)	4.5	3.0	2.8	2.6	3.0
AS11-HC (9.0 μm)	4.7	4.3	3.9	3.6	3.8
AS9-HC (9.0 μm)	4.4	3.3	3.5	3.2	3.4
AS12A (9.0 μm)[a]	4.3	3.6	3.8	3.8	3.8
AS10 (8.5 μm)	4.1	3.3	3.7	4.1	5.5
AS18 (7.5 μm)	3.3	2.5	2.9	2.5	2.9
AS4A (4.4 μm)[b] *packed at 50 °C in water*	7.5	2.5	2.0	1.9	2.7

[a] Column dimensions are 250 x 4 mm i.d., except for the AS12A which is 200 x 4 mm i.d. and the AS4A (4.4 μm) which is 100 x 4 mm i.d.

[b] Conditions: Optimum eluents conditions have been used for each column in the Virtual Column software. Eluent for AS4A (4.4 μm): 1.0 mM K_2CO_3-0.1 mM $KHCO_3$ at 1.0 mL/min (2 μL injection). Separation time: 7 min. Plate heights uncorrected for extra column effects.

ionized functional groups. The phenomena involved in the column packing process are very complex. However the knowledge from the established fields of colloid chemistry and suspension rheology is immensely helpful in explaining the behaviour of the packed column. The quality of packed column can be controlled by manipulating the colloidal properties or hydrodynamic properties of the slurries of the particles. Simple tests using optical microscopy, sedimentation height, sedimentation bed intactness, settling rate, were devised to predict column efficiency of packed ion-exchange resins. Their utility was shown as a time saving effort for the column packer without resorting to actual column preparation. It can be concluded that aspects of packing of charged microparticulates in columns is different, especially the shear thickening effects, from what is known from the column packing studies on silica based phases. However, the common ground between silica and functionalized polymer is that slurry conditions must be adjusted to prevent agglomerating slurries since such agglomerating can also settle in the slurry reservoir. Very high efficiencies corresponding to the reduced plate heights of 2 can be readily achieved once a well packed column is coated with latex nanoparticles bearing quaternary ammonium functional groups on polymer substrates.

4.5 References

1. A. S. Rathore, R. M. Kennedy, J. K. O'Donnell, I. Bemberis, O. Kaltenbrunner, *Biopharm International-the Applied Technologies of Biopharmaceutical Development* **2003**, *16*, 30-40.

2. J. J. Kirkland, J. J. DeStefano, *Journal of Chromatography A* **2006**, *1126*, 50-57.

3. L. Bush, *LC GC North America* **2012**, *30*, 664.

4. M. Verzele, C. Dewaele, D. Duquet, *Journal of Chromatography A* **1987**, *391*, 111-118.

5. J. H. Knox, G. Vaswari, *Journal of Chromatography* **1973**, *83*, 181-194.

6. S. C. Dennis, T. J. Edkins, *Journal of Chromatography* **1987**, *411*, 185-199.

7. D. C. Shelly, V. L. Antonucci, T. J. Edkins, T. J. Dalton, *Journal of Chromatography* **1989**, *458*, 261-279.

8. J. C. Liao, J. L. Ponzo, *Journal of Chromatographic Science* **1982**, *20*, 14-18.

9. J. E. MacNair, K. C. Lewis, J. W. Jorgenson, *Analytical Chemistry* **1997**, *69*, 983-989.

10. E. J. W. Verwey, J. T. G. Overbeek, *Theory of the Stability of Lyophobic Colloids*; Courier Dover Publications: Toronto, 1999.

11. J. Mewis, N. J. Wagner, *Colloidal Suspension Rheology*; Cambridge University Press: New York, 2012.

12. D. L. Shah, A. V. Shroff, *Soil Mechanics and Geotechnical Engineering*; Taylor and Francis, 2003, p 547.

13. J. T. Germaine, A. V. Germaine, *Geotechnical Laboratory Measurements for Engineers*; John Wiley & Sons Inc.: Hoboken, NJ, 2009, p 351.

14. Engelhar.H, J. Asshauer, U. Neue, N. Weigand, *Analytical Chemistry* **1974**, *46*, 336-340.

15. J. Asshauer, I. Halasz, *Journal of Chromatographic Science* **1974**, *12*, 139-147.

16. M. Verzele, *Journal of Chromatography* **1984**, *295*, 81-87.

17. J. P. McCall, *A Twist on Packing Columns for Reversed Phase Liquid Chromatography*. PhD Thesis, The Florida State University2004.

18. C. D. Scott, N. E. Lee, *Journal of Chromatography A* **1969**, *42*, 263-265.

19. É. Tyrrell, E. F. Hilder, R. A. Shalliker, G. W. Dicinoski, R. A. Shellie, M. C. Breadmore, C. A. Pohl, P. R. Haddad, *Journal of Chromatography A* **2008**, *1208*, 95-100.

20. J. H. Masliyah, S. Bhattacharjee, *Electrokinetic and Colloid Transport Phenomena*; John Wiley & Sons: New Jersey, 2006.

21. R. Kaji, Y. Muranaka, H. Miyadera, Y. Hishinuma, *AIChe Journal* **1987**, *33*, 11-18.

22. E. Brown, N. A. Forman, C. S. Orellana, Hanjun Zhang, BenjaminW. Maynor, Douglas E. Betts, J. M. D. and, H. M. Jaeger, *Nature Materials* **2010**, *9*, 220-224.

23. H. A. Barnes, J. F. Hutton, K. Walters, *An Introduction to Rheology*, 3rd ed.; Elsevier Science Publications: Amsterdam, 1993.

24. S. Torquato, T. M. Truskett, P. G. Debenedetti, *Physical Review Letters* **2000**, *84*, 2064-2067.

25. J. Mewis, G. Biebaut, *Journal of Rheology* **2001**, *45*, 799.

26. M. Y. Kariduraganavar, R. K. Nagarale, A. A. Kittur, S. S. Kulkarni, *Desalination* **2006**, *197*, 225-246.

27. M. F. Wahab, C. A. Pohl, C. A. Lucy, *Analyst* **2011**, *136*, 3113-3120.

28. K. M. Usher, C. R. Simmons, J. G. Dorsey, *Journal of Chromatography A* **2008**, *1200*, 122-128.

29. J. C. Sternberg, R. E. Poulson, *Analytical Chemistry* **1964**, *36*, 1492-1502.

30. J. H. Knox, I. H. Grant, *Chromatographia* **1991**, *32*, 317-328.

31. Eric C. Peters, Miroslav Petro, a. Frantisek Svec, J. M. J. Fre´chet, *Analytical Chemistry* **1998**, *70*, 2288-2295.

32. T. Hanai, H. F. Walton, J. D. Navratil, D. Warren, *Journal of Chromatography* **1978**, *155*, 261-271.

33. R. F. Meyer, R. A. Hartwick, *Analytical Chemistry* **1984**, *56*, 2211-2214.

34. A. J. Bard, L. R. Faulkner, *Electrochemical Methods: Fundamental and Applications*, 2nd ed.; Wiley: New York, 2001.

35. H. Freundlich, A. D. Jones, *Journal of Physical Chemistry* **1936**, *40*, 1217-1236.

36. M. Sano, J. Okamura, S. Shinkai, *Langmuir* **2001**, *17*, 7172-7173.

37. T. Wang, R. A. Hartwick, N. T. Miller, D. C. Shelly, *Journal of Chromatography* **1990**, *523*, 23-34.

38. H. Johannes P. C. Vissers, H. A. Claessens, J. Lven, C. A. Cramers, *Analytical Chemistry* **1995**, *67*, 2103-2109.

39. A. B. Metzner, M. Whitlock, *Transactions of the Society of Rheology* **1958**, *2*, 239-253.

40. H. A. Barnes, *Journal of Rheology* **1989**, *33*, 329-366.

41. V. Wong, R. A. Shalliker, G. Guiochon, *Analytical Chemistry* **2004**, *76*, 2601-2608.

42. R. A. Shalliker, V. Wong, B. S. Broyles, G. Guiochon, *Journal of Chromatography A* **2002**, *977*, 213-223.

43. G. Guiochon, T. Farkas, H. GuanSajonz, J. H. Koh, M. Sarker, B. J. Stanley, T. Yun, *Journal of Chromatography A* **1997**, *762*, 83-88.

44. J. P. C. Vissers, M. A. Hoeben, J. Laven, H. A. Claessens, C. A. Cramers, *Journal of Chromatography A* **2000**, *883*, 11-25.

45. I. F. Efremov, G. M. Lukashenko, E. A. Terenteva, *Colloid Journal of the USSR* **1980**, *42*, 728-733.

CHAPTER FIVE: Carboxylate Modified Porous Graphitic Carbon – A New Class of Hydrophilic Interaction Liquid Chromatography Phases*

5.1 Introduction

Hydrophilic interaction liquid chromatography (HILIC) can often retain and resolve hydrophilic analytes such as pharmaceuticals that are difficult to separate by reversed phase liquid chromatography (RPLC).[1, 2] In HILIC, a hydrophilic stationary phase and an organic rich (*e.g.*, > 60 % ACN) aqueous eluent are used. Polar stationary phases (mainly ion exchangers) have been used with organic rich aqueous eluents for the separation of hydrophilic analytes since the early chromatographic literature.[3, 4] But it was not until 1990 that the term "HILIC" was coined by Alpert.[1] In HILIC, a stagnant water layer forms on the surface of the hydrophilic stationary phase. Analytes partition between the stagnant water rich solvent layer and the moving organic rich eluent.[1] The primary mechanism of retention is postulated to be partitioning of the analyte into this water rich layer. However, adsorption, ion-exchange, dipole-dipole interaction, hydrogen bonding,[5-7] π-π, and n-π interactions[8] also contribute to retention on HILIC stationary phases.

The majority of the stationary phases employed in HILIC are based on silica, polymers or pure inorganic oxides such as TiO_2 and ZrO_2. Surface

* A version of this chapter has been published. M. Farooq Wahab, Mohammad E.A. Ibrahim, and Charles A. Lucy, *Analytical Chemistry* **2013**, *85*, 5684-91. I conceived the idea, synthesized and characterized the carboxylate-PGC phase, and M. E. A. Ibrahim performed the chromatographic characterization.

modification can alter the selectivity of silica and polymer HILIC phases. Neutral HILIC phases include diol, amide and cyanopropyl. Zwitterionic phases are mainly based on sulfoalkylbetaine chemistry. Positively charged phases include those containing aminoalkyl groups. Negatively charged HILIC phases may be underivatized silica or polysuccinimide derivatized silica.[3, 7]

Hence, a variety of selectivities is available with silica and polymer based HILIC phases. However, silica has limited chemical and temperature stability, especially at high and low pH. This fragility is a liability for biological samples since highly acidic or alkaline washing steps (100 mM acid or base) are often required to elute any irreversibly bound matrix.[9] Polymeric particles overcame the pH stability issue associated with silica, but earlier polymer phases had limitations associated with swelling-deswelling in organic solvents.[10] More recent commercial polymeric HILIC phases such as ZIC-pHILIC®, apHera-NH_2®, and Frulic-N® are stable in common HILIC solvents.[7]

Porous graphitic carbon (PGC) was introduced by Knox *et al*.[11] as a chemically robust reversed phase – an alternative to overcome the drawbacks of bonded silica phases. PGC is pH stable from 0-14, shows very low bleed in mass spectrometry, and can be used at temperatures up to 200 ^{o}C.[12] Some chromatographers refer to PGC as a "super reversed phase"[13] since 20-40% higher organic modifier is needed to yield the same retention as on a conventional reversed phase. Paradoxically, PGC also retains highly polar analytes, such as arsenic species,[14] nucleosides, nucleotides, sugars,[15] and lipid linked oligosaccharides.[16] This *polar retention effect on graphite* (PREG)[17] is due to

induced dipole interactions between the analyte and the graphitic surface.[18, 19] In the presence of organic rich aqueous phases, the unmodified PGC shows only weak polar retention.[20] Thus PGC must be surface modified to behave as a HILIC phase.

The chemical inertness of PGC makes it very difficult to covalently modify the surface.[21] The hydrophilicity of carbon can be increased by using harsh oxidizing agents such as nitric acid,[22] hypochlorite, and permanganate.[12] However this treatment forms multiple types of surface oxides on carbon[23] which lead to poor chromatographic performance. One of the most promising strategies for covalent modification of carbon is on-column electrochemical functionalization by aryl diazonium ions using a packed bed of particles as the electrode.[24, 25] However, the on-column electrografting apparatus is challenging to construct. Alternately, free radical chemistry of diazonium ions without electrochemical reduction can be applied.[26-28] Free radicals generated by peroxides, and alkyl or aromatic halides have also been employed for carbon surface modification.[29] Modified carbonaceous phases have been developed mainly for reversed phase applications[24, 30] and ion chromatography.[27, 28]

In this chapter, we report the first description of HILIC on a covalently modified porous graphitic carbon phase. Benzene carboxylic acid moieties are covalently attached to the carbon surface *via* chemical reduction of diazonium ions pre-adsorbed onto the PGC. Detailed surface and chromatographic characterization of the phase is described. The selectivity and retention characteristics of the new carboxylate-PGC phase differs from that of 35

previously characterized stationary phases (representing different types of chemistries).[31]

5.2 Experimental

5.2.1 Reagents

Porous graphitic carbon (PGC, 5µm, Lot # PGC366C) was a gift from Thermo Fisher Scientific, UK. Deionized water was from a Barnstead E-pure system (Dubuque, IA, USA). Hydrochloric acid (37% wt/wt) and potassium hydroxide were from Caledon Laboratory Chemicals (Georgetown, ON, Canada). Sodium borohydride was purchased from EMD Chemicals (Gibbstown, NJ, USA). Sodium nitrite ReagentPlus™, 4-aminobenzoic acid, and 50% sodium hydroxide Uracil, cytosine, benzylamine, 1-naphthoic acid, acetylsalicylic acid, gentisic acid, α-hydroxyhippuric acid, hippuric acid, salicyluric acid, L-methionine, tryptophan, glycine, L-serine, L-threonine, cytidine monophosphoric acid (CMP), adenosine 5'-monophosphate (AMP) sodium salt, adensoine 5'-diphosphate (ADP) sodium salt, adenosine 5'-triphosphate (ATP) sodium salt, benzoic acid, 1,2,4-benzenetricarboxylic acid, 1,2,4,5-benzene tetracarboxylic acid, resorcinol (99%), isocytosine and aniline (99.5%) were from Sigma Aldrich (St. Louis, MO, USA). HPLC grade acetonitrile (ACN), salicylic acid and toluene were from Fisher Scientific (Fairlawn, NJ, USA). Ammonium acetate was from Anachemia (Lachine, QC, Canada) or Fisher Scientific (Fair Lawn, NJ, USA). Benzyltrimethylammonium chloride (BTMA) was from ACROS Organics (Fair Lawn, NJ, USA). Phenol (ACS reagent, 99%) was purchased from ACP

(Montreal, QC, Canada) and phloroglucinol (> 99 %) was from Fluka (Buchs, Switzerland).

5.2.2 Apparatus

The packing apparatus consisted of a Haskel pump (DSF-122-87153, Burbank, CA, USA) driven with N_2 gas (Praxair Inc., Edmonton, AB, Canada). The column packing process used the following supplies from Thermo Fisher, Dionex (Sunnyvale, CA, USA): an empty polyether ether ketone (PEEK) column (150 × 3 mm i.d.), PEEK screw caps, 2 μm Ti and stainless steel frit, Zitex membrane, and ultrahigh molecular weight polyethylene (UHMWPE) frits. A cylindrical (14 mm i.d.) 40 mL slurry reservoir from Lab Alliance (State College, PA, USA) was connected to a 50 × 4 mm i.d. stainless steel pre-column and then to the empty column. The other end of the column was capped with a PEEK screw cap by a 2 μm frit. The whole system was pressurized by the pneumatic Haskel pump.

Chromatographic studies were performed using a model 709 dual-piston pump (Metrohm, Herisau, Switzerland) operating at 0.8 or 1.0 mL/min. A 6-port Rheodyne 8125 injection valve (Cotati, CA, USA) with a 2 μL injection loop was used. A Lambda-Max Model 481 UV detector was used at 215, 254 and 268 nm (Waters, Milford, MA, USA). Separations were performed at ambient temperature (~25 ºC).

5.2.3 Methods

5.2.3.1 Synthesis of the Stationary Phase (Carboxylate-PGC)

The synthetic approach using diazonium chemistry is based on Chapter 3.[27] 1.7 g of porous graphitic carbon (PGC) were mixed with 40 mmol of 4-aminobenzoic acid in 50 mL deionized water, and stirred over ice using a magnetic stir bar until the PGC particles were well dispersed (*unreacted PGC is highly hydrophobic and floats in water*). The stirring did not cause fracturing of the particles as confirmed by scanning electron microscopy. To the suspension, 40 mmol of $NaNO_2$ in 50 mL water was added quickly. The solution was allowed to stir very well before the addition of 33 mL conc. HCl. The mixture was stirred for 30 min to allow adsorption of the diazonium salt onto the PGC. Sodium borohydride (100 mmol in 50 mL water) was added in small portions over 30 min with vigorous stirring over ice. (CAUTION: *the reaction is vigorous due to the evolution of both hydrogen and nitrogen. An open 1 L beaker was used for the reaction)*. The suspension was filtered using a 0.22 μm nylon filter, and then successively washed with deionized water, 1% KOH, ACN, and then > 3 L of deionized water. The modified particles were de-fined by sedimentation (12-18 h) in deionized water. De-fining is achieved by letting the particles settle in water (or in a given solvent). The supernatant5 liquid (containing the fines) is discarded. The grafting reaction was repeated a second time on the de-fined material. Repetition of the grafting reaction gave similar atomic O content by XPS as a single grafting reaction. In contrast, surface loading improvements were observed in our previous study on repeated grafting reaction sulfonic acid moiety on carbon

by the same borohydride reaction (Chapter 3).[27] After the second modification, the particles were de-fined once more, washed and vacuum dried in air for 90 min. Three different batches of carboxylate-PGC were synthesized from the same PGC lot to assess the chromatographic reproducibility of the surface modification.

5.2.3.2 Packing of the Stationary Phase (Carboxylate-PGC)

The modified PGC was slurried in deionized water and packed at constant pressure (5000 psi) with a Haskel pneumatic pump into a 150 x 3 mm i.d. PEEK column. Pressure was maintained for 1.5 h using deionized water as the driving solvent. The column was then detached from the packing assembly and subjected to washing step as discussed below. Finally, PEEK screw caps with UHMWPE and Zitex membranes were installed on both ends. The column washing step consisted of mixtures of ACN-NaOH (0.1 to 0.2 M) till the baseline became stable at 254 nm. Before any separation, a final wash of 0.2 M aqueous NaOH at 40 ^{o}C (at least 60 mL) was used to ensure complete removal of any adsorbed species on the column. Further nuances of packing charged particles are detailed in Chapter 4.[32]

5.2.3.3 Mobile Phase Preparation

The mobile phase consists of a mixture of ACN, ammonium acetate and water. The pH was adjusted with NaOH or HCl. The aqueous stock ammonium acetate solutions (2 M) at the desired pH were made and refrigerated. The reported buffer concentration is the final concentration in the eluent after mixing with ACN and the reported pH of the buffer is the final pH of aqueous diluted

buffer of the same volume. The percentage of ACN in this work represents the volume of the ACN relative to the total volume of the solvents including buffer and ACN.

5.2.4 Characterization of PGC Phases

X-ray Photoelectron Spectroscopy (XPS) was performed on an AXIS 165 spectrometer (Kratos Analytical, NY, USA). XPS spectra of the unmodified PGC were collected on the raw material as received. The modified particles were thoroughly soaked and washed with 1% KOH, deionized water and ACN, and then allowed to vacuum dry for 2 days prior to XPS analysis. The zeta potential was measured using a Malvern Zetasizer (Worcestershire, UK). Two 23 mg portions of the modified material were suspended in 15 mL of deionized water and 0.1 M NaOH, respectively, sonicated, and then transferred to the Zetasizer dip cell. The electrophoretic mobilities of the particles were converted into zeta potentials using the Smoluchowski equation within the Zetasizer software (version 6.2). Methods to determine the water layer thickness under HILIC conditions by Karl Fisher titration and Bicker *et al*.[33] were inappropriate for the carboxylate-PGC phase. Measurement of water adsorption is the most direct measure of relative hydrophilic character of a stationary phase. Direct method (Karl Fisher titration) was attempted to measure the water adsorption on carboxylate-PGC and silica various ACN-water compositions. However, both of these phases showed statistically negligible difference in water adsorption. The only exception to the method[34] is that we did not vacuum dry material in an oven

for 3 days at 90 ^{o}C, since carbon spontaneously forms surface oxides and oxidizes itself. Instead, the stationary phase was dried with acetone and kept in vacuum dessicator at room temperature for 24 hours. An indirect chromatographic measurement of the water layer, by Bicker's method[33] was not successful due to the lack of a suitable unretained marker on carboxylate-PGC.

5.3 Results and Discussion

Our aim is to design a hydrophilic graphitic carbon column for HILIC separations. To be useful as a HILIC phase, the carbon surface must be "wettable" by water in order to form a surface water layer. In this chapter, benzene carboxylate groups are attached onto porous graphitic carbon (PGC) to convert the hydrophobic PGC surface into a hydrophilic surface suitable for HILIC.

Numerous approaches have been reported in the literature to introduce bonded functionalities onto carbon for reversed phase and ion chromatography.[24, 27, 30, 35] Such bonded PGC phases have shown improved peak shape or decreased retention, but no selectivity changes. Figure 5.1 shows our synthetic route for introducing benzene carboxylate functionality onto PGC. This synthesis mimics the electrografting process in which the diazonium ions are reduced by a working electrode and the aryl radicals are formed adjacent to the carbon surface. Here, the *in-situ* formed diazonium salt of 4-aminobenzoic acid is pre-adsorbed directly onto the PGC surface (Figure 5.1). Due to the pre-adsorption, the aryl radicals generated by borohydride reduction are formed close to the surface.[26,36]

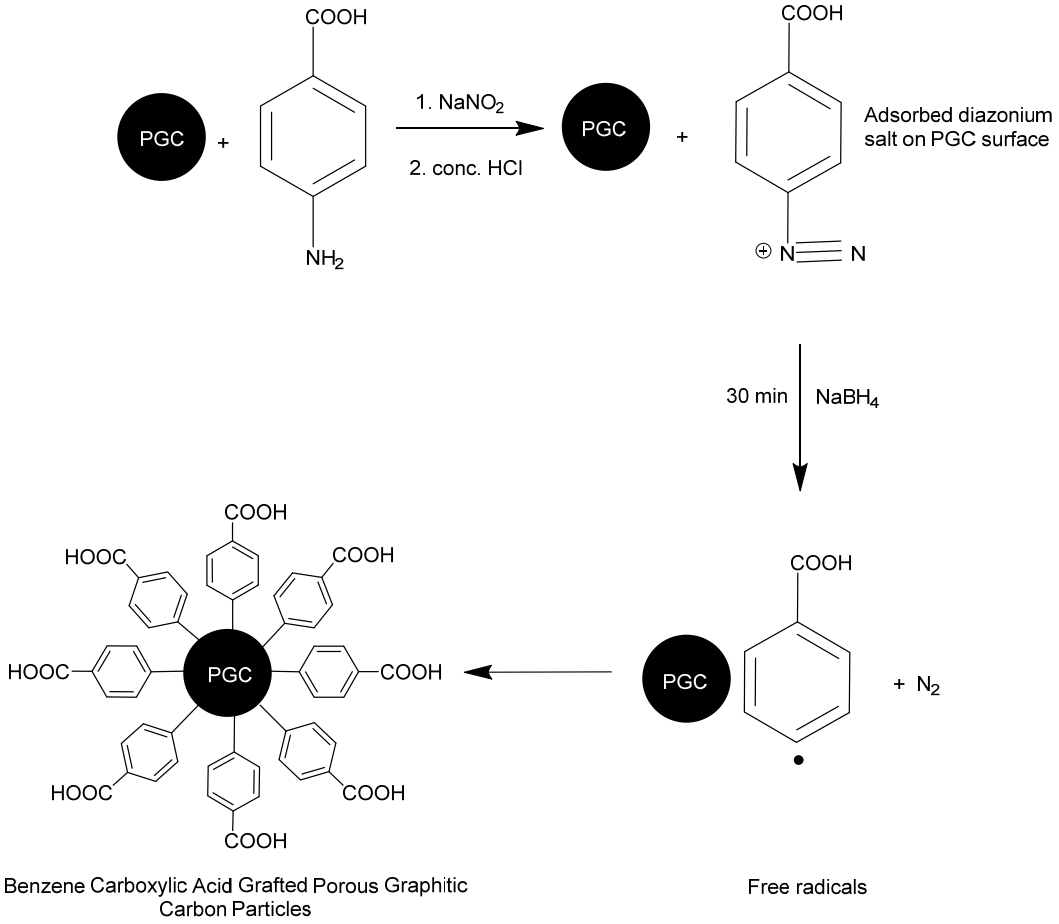

Figure 5.1. Scheme for creating carboxylate functionality on porous graphitic carbon (PGC) using *in situ* generated benzene carboxylic acid diazonium salt.

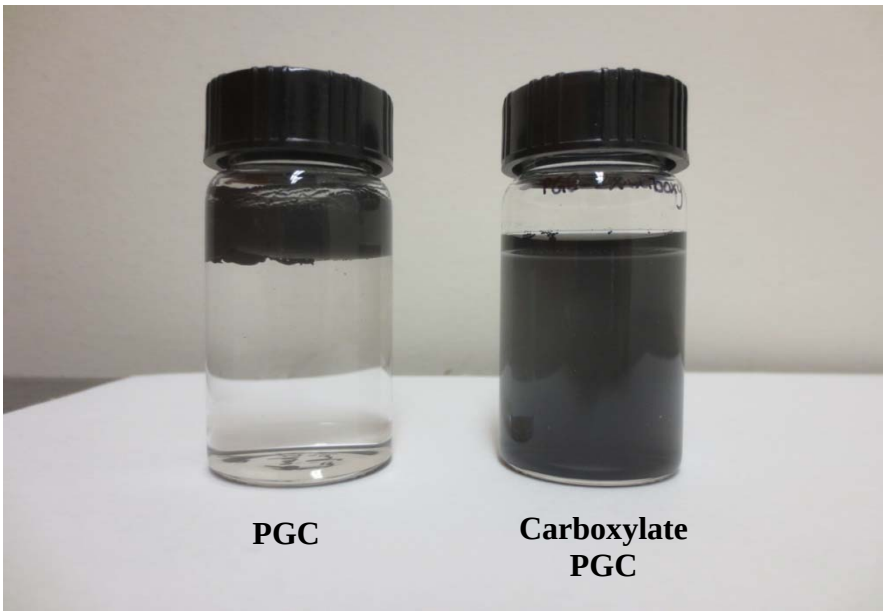

Figure 5.2. Difference in wettability between PGC and carboxylate-PGC in deionized water. The hydrophobic PGC particles do not disperse in water but hydrophilic carboxylate-PGC particles disperse uniformly. Unmodified PGC continues to float even after a month of standing showing their extremely hydrophobic character.

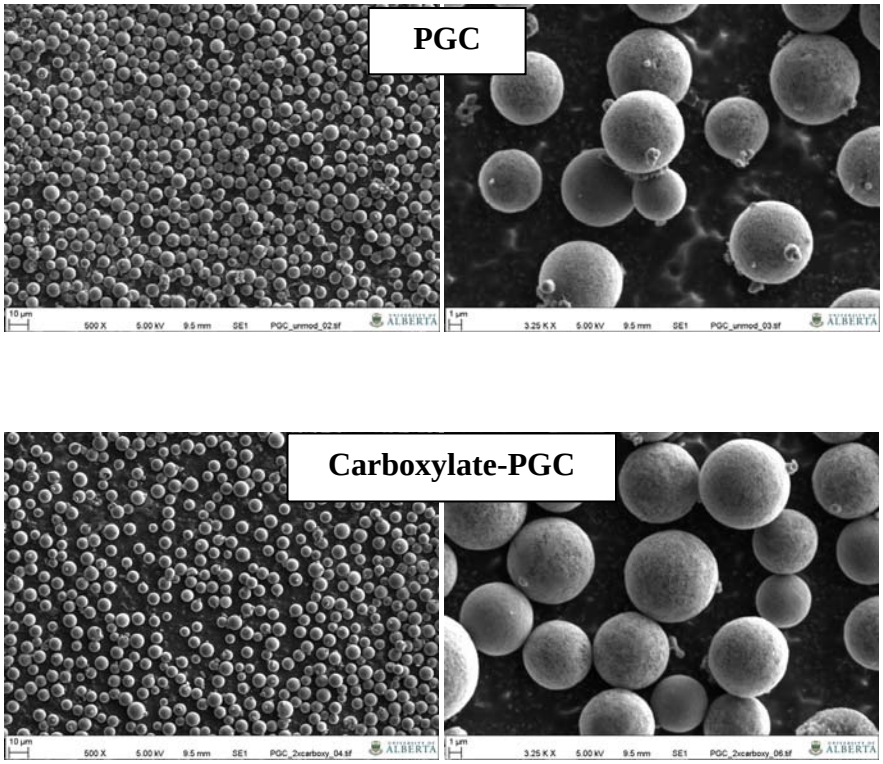

Figure 5.3. Scanning electron microscopy (SEM) images of both unmodified PGC (top) and carboxylate-PGC (bottom). The porous structure at higher magnification is clear (right) showing that the grafted layer does not clog the pores. The mechanical strength of the graphitic particles is also evident as the particles were subjected to stirring via magnetic bar, sonication, and 5000 psi. The modified particles were extruded from a slurry reservoir (1.5 h) and they still remain intact without any breakage.

Borohydride does not attack the carboxylate group.[37] After modification, the particles become highly hydrophilic as shown in Figure 5.2. Additionally no physical damage to the particles was evident, in contrast to that observed when diazonium salts are reduced with sodium metal in non-aqueous medium.[38]

Scanning electron microscopy (SEM) of the modified and unmodified PGC particles (Figure 5.3) showed no changes in surface morphology or pore structure. The SEM also confirms the robustness and mechanical strength of the carboxylate-PGC particles, as no fragments were observed even after vigorous magnetic bar stirring, sonication, and exposure to 5000 psi for 1.5 h.

5.3.1 Characterization of the Carboxylate-PGC

Based on elemental analysis the bulk unmodified porous graphitic carbon particles were 99.3% C with very low (0.2%) oxygen content. Synthesis as per Figure 5.1 decreased the carbon content to 97.7% and increased the bulk oxygen to 1.2%. Assuming all oxygen atoms exist in the carboxylate moiety, the bulk oxygen content is equivalent to 320 μeq -COOH/g dry weight of the stationary phase (moisture free particles). Thermogravimetric analysis (under nitrogen) showed a negligible weight loss (0.3% decrease) up to 200 ^{o}C, indicating an absence of moisture and other volatile matter. This also confirms the thermal stability of the carboxylate-PGC phase.

The zeta potential of carboxylate-PGC in deionized water was -33 ± 3 mV, indicating that anionic surface functional groups are present. The zeta potential increased to -38 ± 3 mV in 0.1 M NaOH due to further ionization of the

carboxylic acid groups. For comparison, a sulfonated divinylbenzene-ethylvinylbenzene resin has a zeta potential of ~ -50 mV in deionized water and in 0.1 M NaOH,[39] a sulfobetaine type zwitterionic silica exhibited a zeta potential of -16 mV in 20 mM ammonium formate buffer (pH 7),[40] and methylacrylate based particles have a zeta potential of −30 to −10 mV at pH > 1.5.[41] Unmodified PGC particles do not disperse in water, and therefore their zeta potential could not be determined. These results indicate that the carboxylate-PGC particles should behave as an anionic HILIC phase whose surface charge can be controlled by pH.

Surface composition analysis is also critical to rationalize the behavior of the stationary phases. The XPS survey scans (Figure 5.4) show that the PGC surface is composed predominantly of carbon, with 2 atom % oxygen. The surface oxygen content on bare PGC (Table 5.1) is comparable to the previously reported ~ 2.7 atom % oxygen.[30] "Surface oxides" form spontaneously along the edges of the graphene sheets on graphitic carbon when exposed to air.[42] However, these surface oxides are non-specific and are composed of carbonyls, phenols, lactones, carboxylates and quinones.[23, 43] Grafting benzene carboxylate groups on PGC results in a 167 % increase in atomic oxygen. The high resolution XPS of oxygen (Figure 5.5) shows the presence of both doubly bound (532.2 eV, C=O) and singly bound (533.8 eV, C-O) oxygen,[43] supporting the presence of carboxylate groups on the modified PGC. Assuming that the population of carbon atoms is 7.3 $x10^{-9}$ mol/cm^2 (*i.e.*, equal to that of the flat surface of the basal plane graphite),[44]

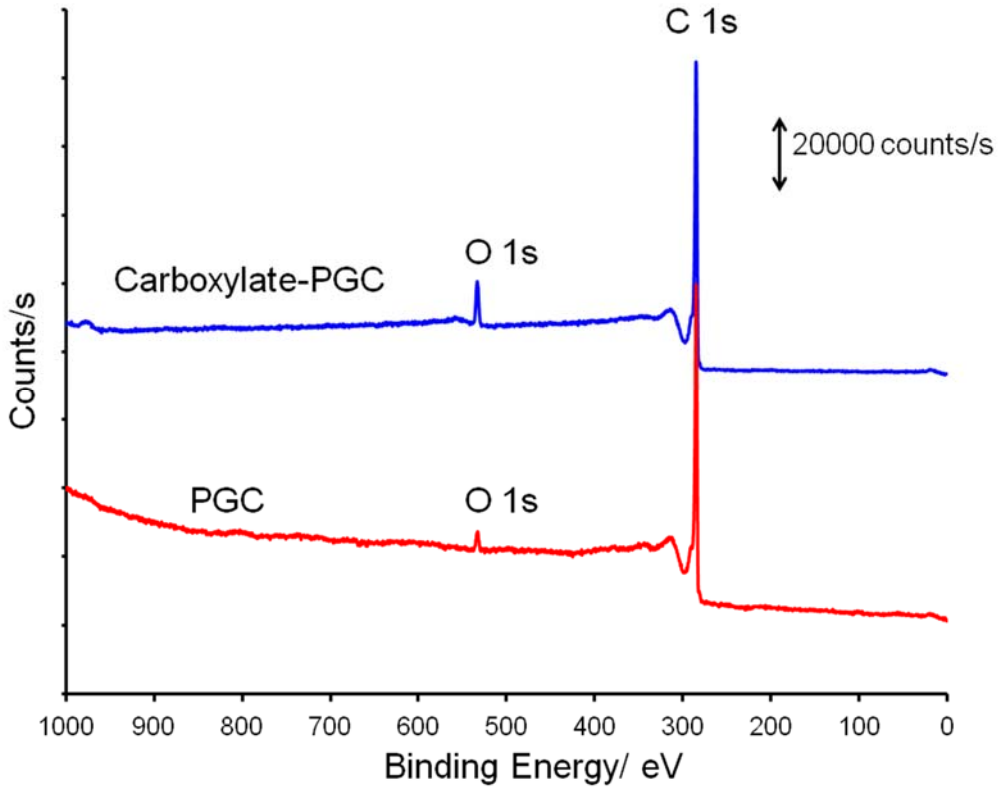

Figure 5.4. Survey XPS scans of PGC (as received) and carboxylate-PGC. XPS measurements were performed on an AXIS 165 spectrometer. The general XPS conditions are as follows: The base pressure in the analytical chamber was lower than 3 x 10^{-8} Pa. A monochromatic Al Kα source (hν = 1486.6 eV) was used at a power of 210 W. The analysis spot was 400 x 700 μm. Survey scans were collected for binding energy from 1100 eV to 0 with an analyzer pass energy of 160 eV and a step of 0.35 eV. The small peak in the carboxylate-PGC survey scan at 980 eV is the oxygen Auger peak.

Table 5.1. Surface composition from XPS survey scans of unmodified PGC and carboxylate-PGC

Element	Peak, eV	% Atomic concentration (PGC) [a]	% Atomic concentration (carboxylate-PGC)[b]	O/C Peak area ratio[c]
Carbon	1s, 285.0	98.0	94.6	0.053
Oxygen	1s, 533.4	2.00	5.35	0.147
Nitrogen	1s, 393.7	0	0[d]	

[a.] The composition was calculated from the peak areas in the spectra using the CasaXPS (version 2.3) with Scofield values of relative sensitivity factors (RSF). A linear background was used. The oxygen peak position was found in the range from 531.8 eV to 533.4 eV in XPS survey scans in the preliminary work.

[b.] The second grafting reaction gave similar surface oxygen content as the first grafting reaction. The data reported in the table refers to two times grafted reaction.

[c.] The surface coverage of -COOH on carboxylate-PGC was estimated by subtracting the O_{1s} / C_{1s} ratios of both the modified and unmodified PGC, and then multiplying by the carbon atom density on basal plane graphite. This calculation assumes a flat sheet of basal plane carbon.

[d.] Nitrogen was not found in high resolution scans indicating the absence of diazo-linkages or other adsorbed reaction by-products.

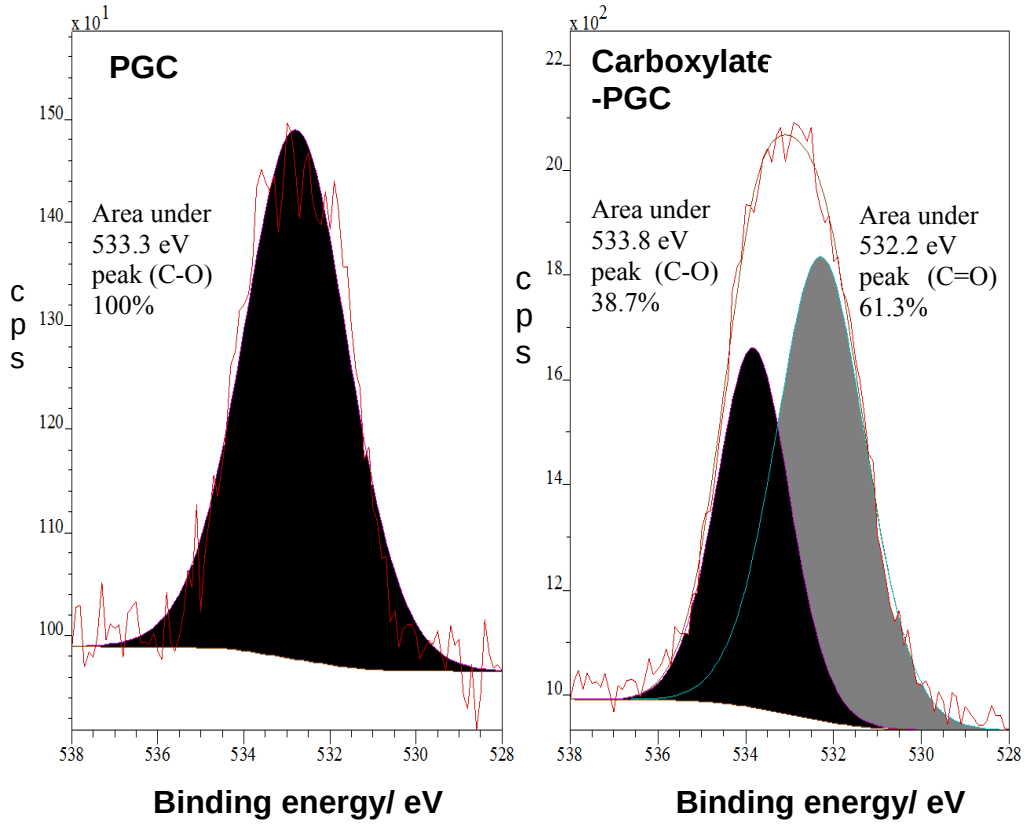

Figure 5.5. High resolution deconvoluted XPS spectrum of the oxygen 1s band. Fitting the spectrum shows the presence of both doubly bound (532.2 eV, C=O) and singly bound (533.8 eV, C-O) oxygen on the carbon surface of carboxylate-PGC. Fits were generated in the CasaXPS software. Both one component and two component fits were attempted for each spectra. The curves above are the optimized fits that yield the chemically most realistic results. The full widths half maximum of PGC and carboxylate-PGC are 3.351 eV and 3.366 eV respectively.

we conservatively estimate the oxygen surface coverage of carboxylate-PGC to be $6.8x10^{-10}$ mol/cm^2. However it should be noted that XPS cannot explore the level of grafting inside the pores of the particles. This oxygen coverage is near that expected for a complete monolayer coverage on the outer surface of the particles.[44] Moreover, this grafting makes the particles sufficiently hydrophilic to be dispersed in water (Figure 5.2) whereas unmodified PGC floats on water. This hydrophilic character was also observed for sulfonated carbon clad zirconia (Chapter 3).[27] No residual –N=N– signal is observed at 405 eV by XPS signal, whereas residual diazonium has been observed on carbon electrochemically modified by diazonium chemistry.[26, 45, 46] On the other hand, nitric acid oxidized carbons show oxygen as well as nitrogen species in XPS.[43] Thus the carboxylate-PGC particles are free of side products which might lead to undesired chromatographic interactions.

5.3.2 Approaches for Packing Carboxylate-PGC

Colloidal properties of charged particles are highly critical during the packing process. The aspects of chromatographic particles bearing charged functional groups have been examined in detail and involve non-Newtonian rheological properties as discussed in Chapter 4.[32] Mild shear thickening was observed with carboxylate-PGC. Water was chosen as the slurry and driving solvent because the carboxylate-PGC gave a stable non-agglomerating suspension in water which should yield a tightly packed bed.[32] The early eluting peaks indicate the quality of the packed bed, whereas the late eluting peaks convolute

the properties of the packed bed along with multiple interactions. The water packed column with modified particles produced ~ 5000 plates/m for 2,5-dihydroxybenzoic acid (early eluting peak). This efficiency is better than the 3400 plates/m efficiency for early eluting peaks on di-tert-amylperoxide modified PGC (packed by Thermo Fisher)[30] but lower than that of 11,000 plates/m reported for unmodified PGC (Hypercarb^{TM}) capillaries with ACN.[47] Unfortunately, further details and optimized conditions for packing for any carbon phase are not disclosed in the literature. Attempts to pack our carboxylate-PGC material using ACN as the slurry/driving solvent resulted in agglomeration of the particles, indicating that ACN is not an optimum medium for packing. Thus, the carboxylate-PGC particles have a different packing behavior than Hypercarb^{TM}.

5.3.3 HILIC Behaviour of Unmodified and Carboxylate-PGC

Unmodified PGC (Hypercarb^{TM}) shows a reversed phase behavior.[18] Figure 5.6 shows the effect of % ACN on the retention of uracil (neutral) and 1-naphthoic acid (anionic) on unmodified PGC and carboxylate-PGC. Uracil and 1-naphthoic acid are weakly retained on unmodified PGC ($k < 0.5$ and 4 respectively for 90% ACN). This minor increase in retention of uracil and 1-naphthoic acid on unmodified PGC is most likely due to small amounts of "hydrophilic" surface oxide functionalities, most likely phenolics (singly bonded oxygen) as supported by XPS (Figure 5.5). PGC can retain polar analytes by PREG, *i.e.*, by induced dipoles.[17] However PREG would decrease retention of polar analytes with increasing ACN. In Figure 5.6 retention increases with %ACN

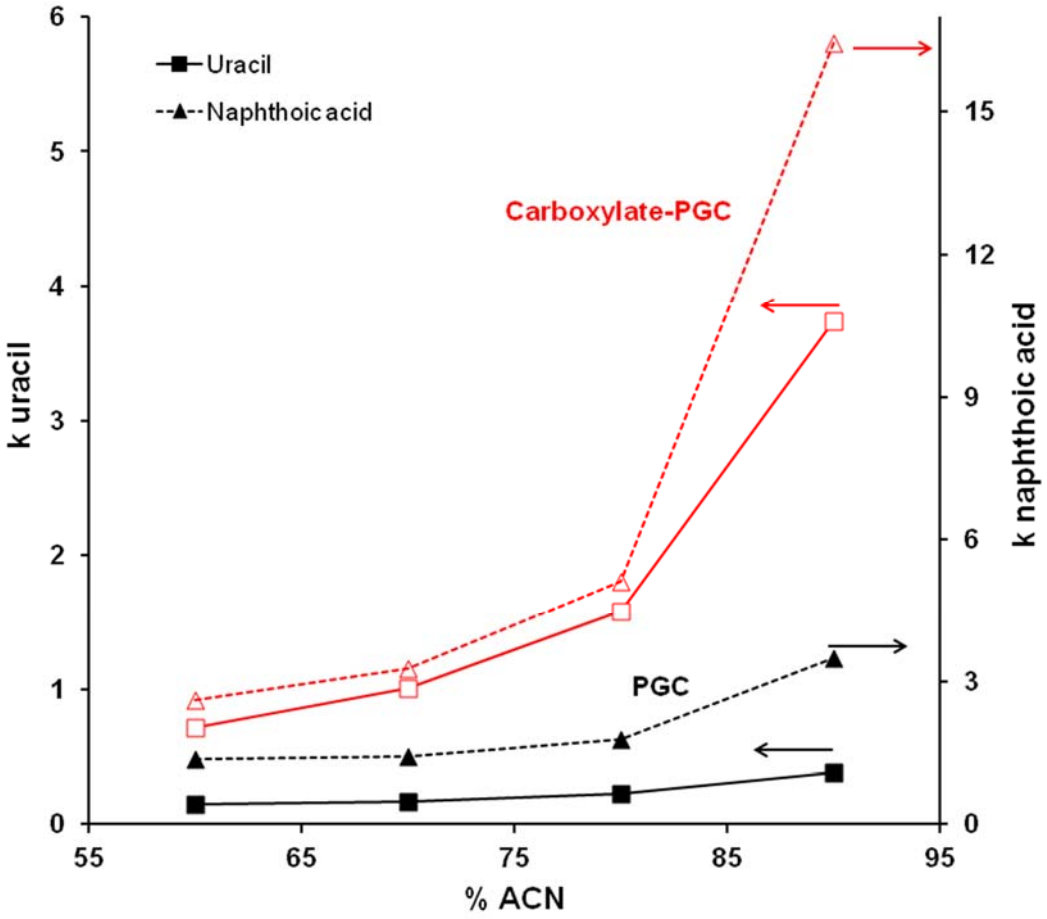

Figure 5.6. Retention behavior of uracil and 1-naphthoic acid on carboxylate-PGC (red) and Hypercarb (black) as a function of % ACN in the eluent. Experimental conditions: columns, carboxylate-PGC (150 × 3 mm i.d.); Hypercarb (100 × 4.6 mm i.d.); flow rate, 0.8 mL/min; eluent, 10 mM ammonium acetate (pH = 8.3) in 60–90% ACN; analytes, 0.2 mM uracil and 1-naphthoic acid in the same % ACN as the mobile phase; UV detection at 254 nm with a 2 µL loop.

supporting the speculation that the increased retention seen here reflects a low level of hydrophilic interaction.[20]

In contrast, in Figure 5.6 carboxylate-PGC shows significantly greater retention for both polar analytes. Further retention increases significantly at high %ACN, consistent with HILIC behavior.[1, 48] 1-Naphthoic acid has a k of ~ 16 with 90% ACN despite being deprotonated at the mobile phase pH (8.3) – given that both carboxylate-PGC and the acid are negatively charged at this pH. Further, retention increases significantly at high %ACN, consistent with HILIC behavior.[1, 48] With 60% ACN, benzylamine (pK_a = 9.35) eluted with a k of 2.3, but did not elute within 40 min *i.e.* $k > 43$ with 70% ACN. This behavior parallels the strong retention of cationic benzyltrimethylammonium (BTMA as chloride) on bare silica columns under HILIC conditions.[31]

5.3.4 HILIC Selectivity of Carboxylate-PGC

One of the most important parameters in optimizing separation resolution is the selectivity factor.[49] My collaborator Mohammed Ibrahim had previously devised a graphical visualization for the selectivity of HPLC columns to reflect the hydrophilic and electrostatic character of the column.[31] Figure 5.7 illustrates the selectivity of 35 different stationary phases in addition to the carboxylate-PGC phase. In the selectivity chart (Figure 5.7), the retention factor ratio k_{BTMA}/k_{uracil} is plotted against the retention ratio $k_{cytosine}/ k_{uracil}$. The use of relative retention eliminates the influence of factors such as surface area. For example in Figure 5.7, columns no. 2 and 3 are both 3.5 μm ZIC-HILIC phases with different surface

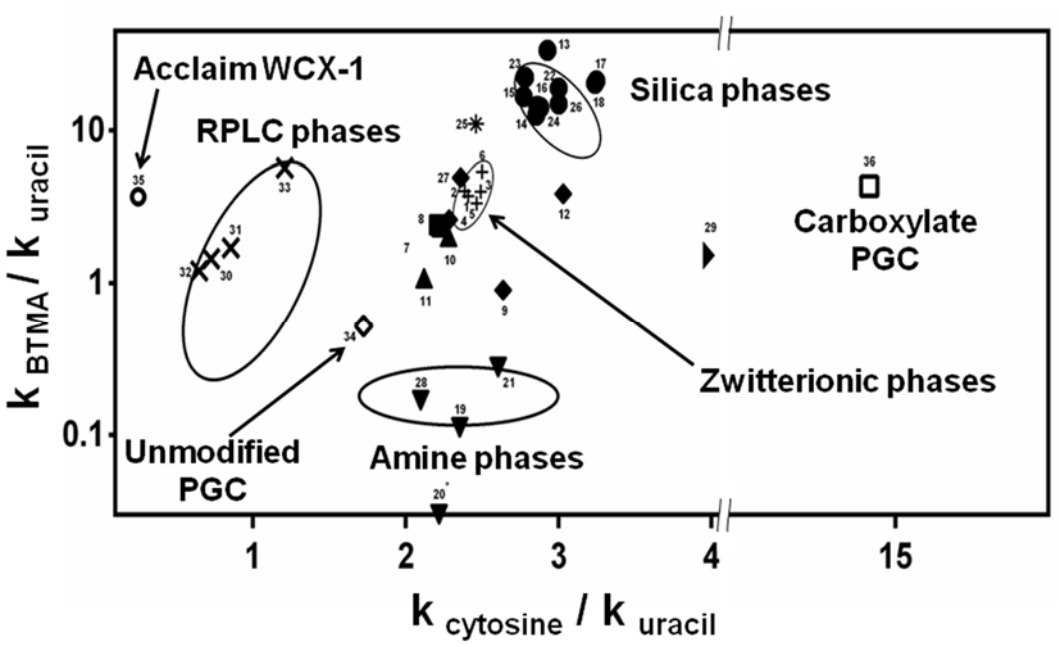

Figure 5.7. Selectivity plot of Carboxylate-PGC (no. 36) and PGC (Hypercarb^{TM}, no. 34) with respect to 35 commercial columns (see Table 5.2 for commercial column data). Legend: bare silica (•), amide (■), diol (▲), amine and/or triazole (▼), polymer substrate and/or polymer coated silica (♦), zwitterionic (+), RPLC (×), latex coated silica (*), proprietary polar phase (►), unmodified PGC (Hypercarb^{TM}) (◊, 34), carboxylate-PGC (□, 36), Acclaim WCX-1 (○, 35). Conditions: eluent, 5 mM ammonium acetate, pH 6.8, in 80% ACN; test analytes, 0.044–0.44 mM BTMA, cytosine, and uracil in 80% ACN; UV detection at 254 nm. 20 µL loop injection for all columns except PGC, Acclaim-WCX-1, and carboxylate-PGC, where a 2 µL loop was used. Data adapted from reference 31

Table 5.2. Characteristics of the commercial stationary phases in Figure 5.7. Data from reference 31. (*S* = Surface area, Dimensions: Length x diameter)

#	Name (Company)	Particle Diameter (Support)	Functional Group	Pore size (Å)	*S* (m^2/g)	Column Dimensions (mm x mm)
1	ZIC-HILIC (Merck)	5 µm (Silica)	Polymeric sulfoalkylbetaine zwitterionic	200	135	100 x 4.6
2	ZIC-HILIC (Merck)	3.5 µm (Silica)	Polymeric sulfoalkylbetaine zwitterionic	200	135	150 x 4.6
3	ZIC-HILIC (Merck)	3.5 µm (Silica)	Polymeric sulfoalkylbetaine zwitterionic	100	180	150 x 4.6
4	ZIC-pHILIC (Merck)	5 µm (Porous polymer)	Polymeric sulfoalkylbetaine zwitterionic	-	-	50 x 4.6
5	Nucleodur HILIC (Macherey-Nagel)	5 µm (Silica)	Sulfoalkylbetaine zwitterionic	110	340	100 x 4.6
6	PC HILIC (Shiseido)	5 µm (Silica)	Phosphorylcholine zwitterionic	100	450	100 x 4.6
7	TSKgel Amide 80 (Tosoh Bioscience)	5 µm (Silica)	Amide (polymeric carbamoyl)	80	450	100 x 4.6
8	TSKgel Amide 80 (Tosoh Bioscience)	3 µm (Silica)	Amide (polymeric carbamoyl)	80	450	50 x 4.6
9	PolyHydro-xyethyl A (PolyLC)	5 µm (Silica)	Poly(2-hydroxy-ethyl aspartamide)	200	188	100 x 4.6
10	LiChrospher 100 Diol (Merck)	5 µm (Silica)	2,3-Dihydroxypropyl	100	350	125 x 4.0
11	Luna HILIC (Phenomenex)	5 µm (Silica)	Cross-linked diol	200	185	100 x 4.6
12	PolySulfoethyl -A (PolyLC)	5 µm (Silica)	Poly(2-sulfoethyl aspartamide)	200	188	100 x 4.6
13	Chromolith Si (Merck)	Silica monolith	Underivatized	130	300	100 x 4.6
14	Atlantis HILIC Si (Waters)	5 µm (Silica)	Underivatized	100	330	100 x 4.6
15	Purospher STAR Si (Merck)	5µm (Silica)	Underivatized	120	330	125 x 4.0

#	Name (Company)	Particle Diameter (Support)	Functional Group	Pore size (Å)	*S* (m^2/g)	Column Dimensions (mm x mm)
16	LiChrospher Si 100 (Merck)	5 µm (Silica)	Underivatized	100	400	125 x 4.0
17	LiChrospher Si 60 (Merck)	5 µm (Silica)	Underivatized	60	700	125 x 4.0
18	Cogent Type C Silica (Microsolv)	4 µm (Silica)	Silica hydride ("Type C" silica)	100	350	100 x 4.6
19	LiChrospher 100 NH_2 (Merck)	5 µm (Silica)	3-Aminopropyl	100	350	125 x 4.0
20	Purospher STAR NH_2 (Merck)	5 µm (Silica)	3-Aminopropyl	120	330	125 x 4.0
21	TSKgel NH_2-100 (Tosoh Bioscience	3 µm (Silica)	Aminoalkyl	100	450	50 x 4.6
22	Atlantis HILIC (Waters)	3 µm (Silica)	Underivatized	100	330	50 x 1.0
23	Onyx silica monolith (Phenomenex)	Silica monolith	Underivatized	130	300	100 x 4.6
24	Zorbax HILIC plus (Agilent)	3.5 µm (Silica)	Underivatized	95	160	100 x 4.6
25	Silica monolith coated with AS9-SC (Homemade)	Silica monolith	Silica – cationic nanoparticle	130	300	80 x 4.6
26	Zorbax RRHD HILIC plus (Agilent)	1.8 µm (Silica)	Underivatized	95	160	100 x 3.0
27	Acclaim Trinity P1 (Dionex)	3 µm (Silica)	Silica-cationic nanoparticle	-	-	150 x 3.0
28	Cosmosil HILIC (Nacalai)	5 µm (Silica)	Triazole	120	300	150 x 4.6
29	Acclaim HILIC-10 (Dionex Thermo Scientific)	3 µm (Silica)	Proprietary neutral polar functionality	120	300	150 x 4.6

#	Name (Company)	Particle Diameter (Support)	Functional Group	Pore size (Å)	*S* (m^2/g)	Column Dimensions (mm x mm)
30	Zorbax Eclipse XDB-C18 (Agilent)	5 µm (Silica)	Octadecyl	80	180	150 x 4.6
31	XBridge C18 (Waters)	5 µm (Silica BEH)	Octadecyl	130	185	150 x 4.6
32	YMC Pro C18 (YMC)	3 µm (Silica)	Octadecyl	120	340	150 x 2.0
33	Zorbax SB-aq (Agilent)	3.5 µm (Silica)	Octadecyl	80	180	150 x 2.1
34	Hypercarb™ (Thermo Fisher)	5 µm (Carbon)	Underivatized	250	120	100 x 4.6
35	Acclaim-WCX-1 (Dionex)	5 µm (Silica)	Carboxylic acid	120	300	150 x 4.6

areas (135 and 180 m^2/g, respectively). As the surface chemistry of these columns is the same, identical HILIC selectivity would be expected. Indeed, columns 2 and 3 are very closely clustered in Figure 5.7. Similarly LiChrospher Si 100 and LiChrospher Si 60 pair (columns no. 16 and 17) which differ only in surface area are adjacent in Figure 5.7.[31]

Irgum and co-workers [6] used the relative retention of cytosine/uracil as a generic measure of the "hydrophilic" character of HILIC columns. Cytosine and uracil are both highly hydrophilic (octanol/water partition coefficients at pH 7 of $10^{-1.97}$ and $10^{-1.05}$, respectively), and so both show strong HILIC retention. A higher $k_{cytosine}/k_{uracil}$ ratio indicates a more hydrophilic column. BTMA is a hydrophilic quaternary amine and it will undergo electrostatic interaction with the stationary phase regardless of the eluent pH. Therefore, the ratio k_{BTMA}/k_{uracil} reflects the electrostatic character (attraction or repulsion) of the stationary phase. Also, on positively charged HILIC phases (*e.g.*, amine), BTMA still exhibits measurable retention, despite experiencing electrostatic repulsion. By using these two parameters, various classes of columns (silica, zwitterionic, diol, RPLC, and amine) can be classified.[31]

Unmodified PGC (column no. 34) is a strong reversed phase material,[11, 24] and so appears to the left of Figure 5.7. It also exhibits weak anion exchange character, consistent with its ability to retain inorganic anions (data not shown). Attaching benzene carboxylate groups to PGC increases the water "wettability" of the phase, consistent with the behavior seen with aryl carboxylate modified glassy carbons.[50] The ratio of k_{BTMA}/k_{uracil} for the Carboxylate-PGC column (no. 36,

k_{BTMA}/k_{uracil} = 4.3) is lower than that of silica, indicating a weaker electrostatic character. The k_{BTMA}/k_{uracil} of Carboxylate-PGC is comparable to that of the Dionex Acclaim WCX-1 phase which consists of alkyl bonded silica phase with a carboxylate terminus. Cytosine shows much stronger retention on carboxylate-PGC ($k_{cytosine}/k_{uracil}$ ~14.9) *vs.* silica ($k_{cytosine}/k_{uracil}$ ~3). This may be due to hydrogen bonding interactions with the carboxylate moiety along with the hydrophilic character of this phase. Crystallographic studies of cytosine-carboxylic acid co-crystals show hydrogen bonds exist between the amino group, the pyrimidine backbone of cytosine and the carboxylate moiety.[51]

To determine whether the high cytosine retention may also be influenced by the underlying graphitic carbon of PGC, the retention of isocytosine, an isomer of cytosine, was studied. If retention were purely hydrophilic in nature, isocytosine would be much less retained due to its higher octanol/water partition coefficient than cytosine ($10^{-0.59}$ vs. $10^{-1.97}$ at pH 7). In contrast, isocytosine is retained even more strongly on carboxylate-PGC phase than cytosine ($k > 70$ *vs.* $k = 19.3$, respectively). This indicates that the shape selective properties of the underlying graphitic planes of PGC[48] are still operative on the carboxylate-PGC phase.

To further examine the selectivity of carboxylate-PGC, Figure 5.8 compares the elution order of six carboxylic acids on the carboxylate-PGC phase to that on nine commercial chemistries.[52, 53] The number in the rows indicate the elution order of the six acids. The elution order on carboxylate-PGC shows different selectivity than the other HILIC phases. Of the nine commercial phases,

Column Chemistry	Retention Times and Selectivity of Analytes
Amide	1 2 3 4 5 6
Polyhydroxyethyl-Aspartamide	1 2 3 4 5 6
Sulfobetaine	1 2 3 4 6 5
Silica	1 3 4 2,6 5
Diol	1 2 3 4 6,5
Cross-linked diol	1 2,3 4 5,6
Polyvinyl alcohol	1 2 3 4 6 5
Bare PGC	(6,3,2,1),5 4
Alkyl silica with -COOH terminus	(1,2 3 4,6),5
Carboxylate-PGC	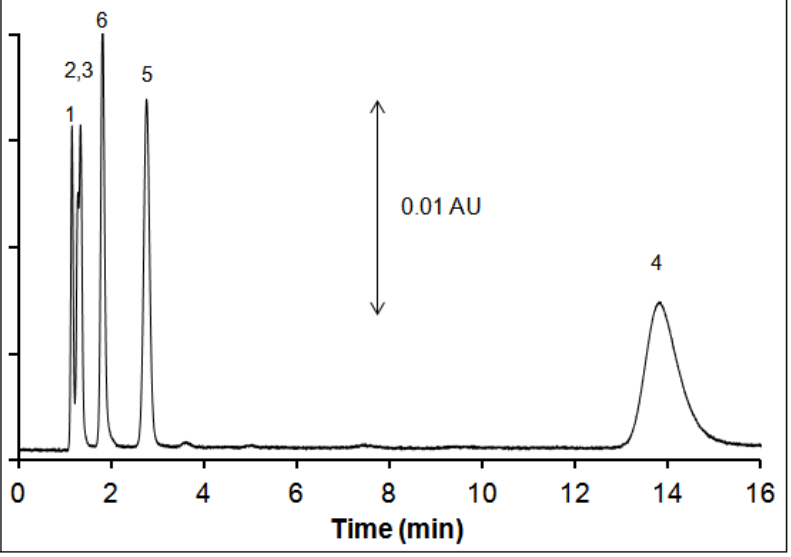

Figure 5.8. Comparison of the selectivity of six aromatic carboxylic acids on nine different column chemistries and carboxylate-PGC under HILIC mode. Analytes separated by commas coelute. The positions of the peak numbers reflect the actual retention time of the analytes. Experimental conditions: column, carboxylate-PGC (150 × 3 mm i.d., 5 μm); flow rate, 1.0 mL/min; eluent, 20 mM ammonium acetate (pH = 6.97) in 85% ACN; analytes, 0.12–0.35 mM of (1) salicylic acid, (2) gentisic acid, (3) acetylsalicylic acid, (4) salicyluric acid, (5) hippuric acid, and (6) α-hydroxyhippuric acid. UV detection at 254 nm with a 2 μL loop. Retention data for the commercial columns is from reference 53.

the elution order of carboxylate-PGC is most similar to that of the diol and PVA phases. In addition, salicyluric acid has an unusually strong retention (k = 13.9) on the carboxylate-PGC phase. On other HILIC phases including the Acclaim WCX-1 phase with terminal carboxylic acid groups - salicyluric acid shows similar retention to its isomer α-hydroxyhippuric acid. These two acids differ in the -OH position from the rest of the acids; -OH is phenolic in salicyluric acid whereas it is a secondary alcohol in α-hydroxyhippuric acid. The selectivity factor α of the two isomers on carboxylate-PGC is 14 with respect to each other, whereas the selectivity factors for the rest of the nine columns range from 0.70 to 0.92. As noted for cytosine above, this may indicate retention contributions from the shape selectivity properties of flat graphitic planes.[54, 55] Indeed, on unmodified PGC salicyluric acid shows much stronger retention (k =1.1) than all of the other acids (k ~0.2). Such a high isomeric selectivity on carboxylate-PGC is an appealing incentive for exploring covalently modified carbon based HILIC phases.

We note that all of the acids in Figure 5.8 are negatively charged (pK_a of 2.9-3.7) under the chromatographic conditions. Similarly the carboxylate-PGC is negatively charged (zeta potential ~ - 33 mV in deionized water). Therefore all the negatively charged acids should undergo electrostatic repulsion and elute before the void volume. However in electrostatic repulsion hydrophilic interaction chromatography (ERLIC) when the organic content increases above 60%, hydrophilic interaction dominates the electrostatic effects.[48]

5.3.5 Switching Retention Mode of Carboxylate-PGC with pH

The carboxylate functionality displays weak acid behavior (pK_a ~ 2.8 - 3.1).[56, 57] At low pH, carboxylate modified glassy carbon was hydrophobic, as measured by contact angle.[50] Adjusting the pH above the pK_a increased the wettability of the modified glassy carbons.[50] A similar change in hydrophobic to hydrophilic character is illustrated in Figure 5.9 for the carboxylate-PGC phase. The hydrophobic toluene is retained due to interaction with the underlying carbon, and shows little change in retention with pH. At pH 9.7, benzoate is repelled by Donnan exclusion and elutes essentially unretained, while the deprotonated aniline shows weak hydrophobic retention. At low pH, benzoic acid retention increases due to protonation of the analyte and phase, while the protonated aniline shows lower reverse phase behavior. A silica column with alkyl carboxylate terminus (Acclaim WCX-1) shows very similar retention behavior with respect to pH.[58]

5.3.6. Chromatographic Separations on Carboxylate-PGC at High pH

To illustrate the applicability of the carboxylate-PGC as a HILIC phase, we performed separations of carboxylates, nucleotides, phenols and amino acids (Figure 5.10). Many of these separations were facilitated by the use of alkaline mobile phases that would damage traditional silica based HILIC phases. Aromatic carboxylic acids can be retained on RPLC columns only by using low organic modifier content. However, the low organic modifier content can cause "phase de-wetting" leading to a drastic decrease in retention.[59]

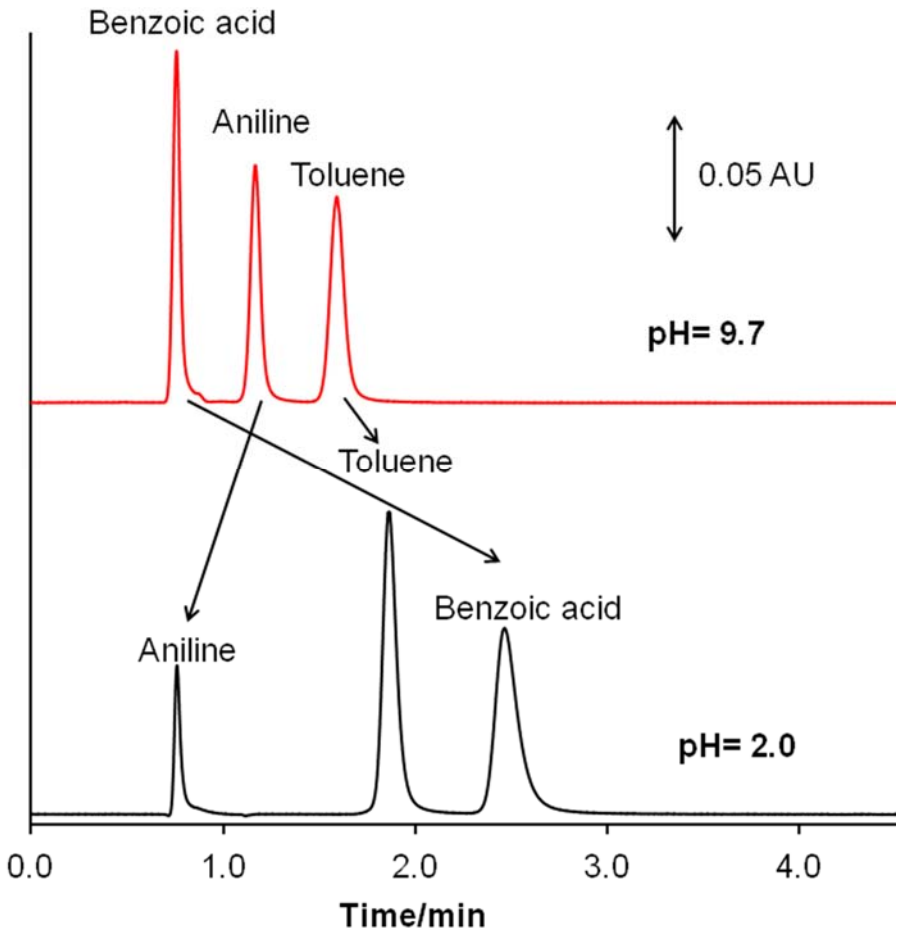

Figure 5.9 Selectivity changes with pH on Carboxylate-PGC for aniline, benzoic acid and toluene. Conditions: Column, 150 x 3 mm i.d., Carboxylate-PGC; eluent, 25 mM ammonium acetate in 65% ACN; desired pH adjusted with HCl or NaOH, 2 μL loop injection, UV detection at 254 nm.

Similarly, ion chromatography phases cannot be used for organic acids due to their low conductivity especially in organic-rich mobile phases. Thus HILIC is an attractive alternative for carboxylic acids separations. Figure 5.10 (A) shows the separation of five fully deprotonated aromatic carboxylic acids (pK_a: 1.9 - 4.7).[59] Retention increased with the number of carboxylic acid groups, *i.e.,* benzoic acid < phthalic acid < 1,2,4-benzenetricarboxylic acid < 1,2,4,5-benzenetetracarboxylic acid. 1-Naphthoic acid is more retained than phthalic acid based on its hydrophobic interaction with the underlying graphitic surface. Retention due to electrostatic attraction can be ruled out since the analytes and the stationary phase bear the same charge under alkaline conditions. All such anionic analytes should be expelled by Donnan exclusion from a negatively charged particle. The presence of a low dielectric medium solvent and high ionic strength ensures retention due to hydrophilic interaction despite the electrostatic repulsion. This parallels the ERLIC behavior of cationic analytes on cation exchangers in the presence of low dielectric medium solvent and high ionic strength buffers.[48]

Analysis of nucleotides and nucleosides is challenging with RPLC.[15, 60] Several silica columns have been designed with polar embedded groups to increase the polarity of the stationary phase. Nonetheless very low retention factors (k < 2) are still observed for nucleotides.[60] Bare PGC can be used for nucleotides, but requires "electronic" modifiers such as diethylamine under gradient conditions to elute the otherwise strongly retained nucleotides.[60] ATP shows poor chromatographic performance on PGC compared to other nucleotides.[15] The nucleotides were irreversibly adsorbed when trifluoroacetic

acid was used on PGC.[15] Thus, many challenges are still observed with the separation of nucleotides by RPLC on either silica bonded phases or bare PGC.

In recent years, HILIC has become a popular separation mode for these hydrophilic nucleotides.[48] Figure 5.10 (B) shows the fast baseline resolution of four nucleotides (CMP, AMP, ADP, and ATP) on carboxylate-PGC under isocratic conditions. In line with the ERLIC behavior seen for the carboxylic acids in Figure 5.8 and 5.10 (A), the negatively charged nucleotides show retention on carboxylate-PGC. The retention order is related to the number of phosphate groups in the nucleotides. ATP, being the most polar analyte is retained most strongly. This is different than the elution order seen on bare PGC.[60]

Figure 5.10(C) shows the separation of phenol, resorcinol and phloroglucinol in 3 min at pH 9.7. As expected, the most polar phloroglucinol (3 - OH) shows the highest retention, followed by resorcinol and phenol. Bare PGC on the other hand, showed co-elution of the tested phenols under the same conditions (data not shown). The retention order on carboxylate-PGC follows the solubility order of the phenols at pH 9 (phenol 109 g/L, resorcinol 222 g/L and phloroglucinol 579 g/L),[59] consistent with HILIC theory. Finally, Figure 5.10(D) shows the separation of four amino acids namely, methionine, threonine, glycine and serine on carboxylate-PGC and elute in the same order as listed. This elution order corresponds with the solubility: methionine has the lowest water solubility (16 g/L) as compared to the rest of the three amino acids (> 80 g/L)[59] at pH 7. Serine shows higher retention than glycine due to its additional hydroxyl group.

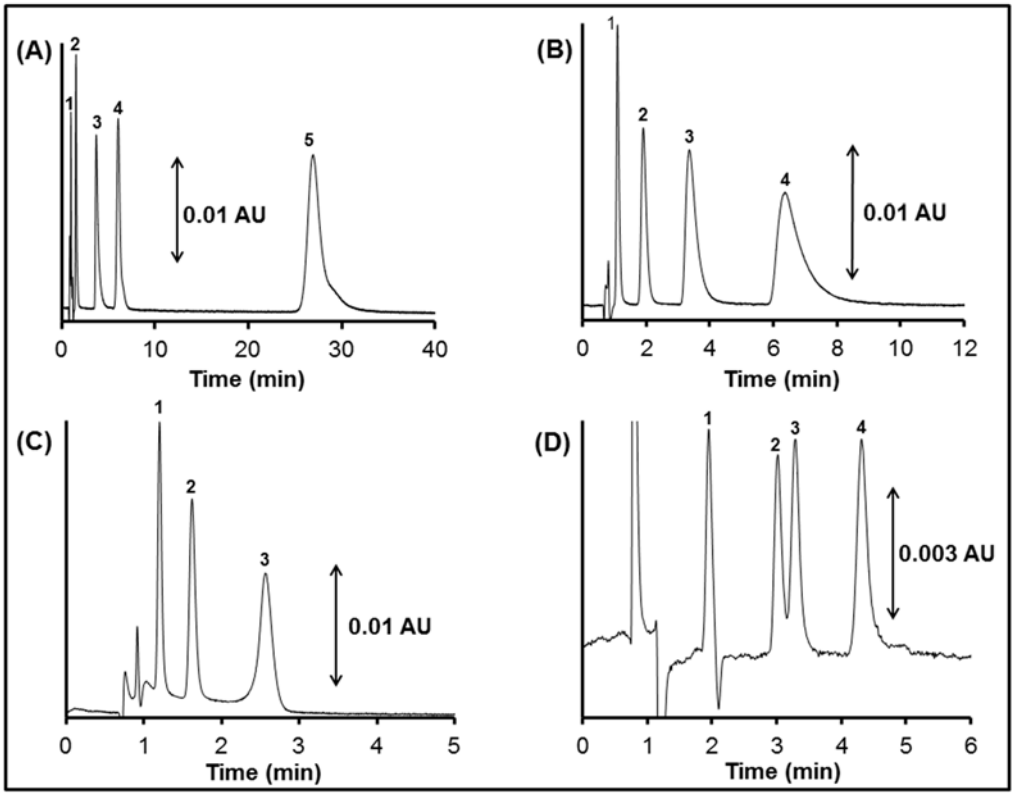

Figure 5.10. Separation of (A) aromatic carboxylic acids, (B) nucleotides, (C) phenols, and (D) amino acids on carboxylate-PGC. All chromatograms were processed by Savitzky-Golay smoothing. Experimental conditions: Column, carboxylate-PGC (150 x 3 mm i.d.), flow rate: 1.0 mL/min; eluent, (A), (D) 20 mM ammonium acetate (pH =7.6) in 80 %ACN, (B) 50 mM ammonium acetate (pH =9.8) in 60 %ACN, (C) 20 mM ammonium acetate (pH =9.7) in 70 %ACN; analytes: (A) 0.18-0.67 mM of (1) benzoic acid, (2) phthalic acid, (3) 1-naphthoic acid, (4) 1,2,4 benzene tricarboxylate, (5) 1,2,4,5 benzene tetracarboxylate; (B) 0.05-0.14 mM of (1) CMP, (2) AMP, (3) ADP, (4) ATP; (C) 0.2-0.75 mM of (1) phenol, (2) resorcinol, (3) phloroglucinol; (D) 0.17-5.31 mM of (1) L-methionine, (2) L-threonine, (3) glycine, (4) L-serine. UV detection at 254 nm for (A) and (B), 268 nm for (C) and 215 nm for (D) with a 2 μL loop.

Amino acids with high pK_a (*e.g.* histidine and lysine) were strongly retained, similarly to benzylamine on carboxylate-PGC.

5.3.7 Column Stability and Retention Time Reproducibility

C_{18} silica columns begins to leach silica (10-30 µg/mL) when exposed to 10 mM NaOH : EtOH (50:50 v/v). Increasing the NaOH to 100 mM, increases the Si concentration in the effluent to 511 µg/mL.[61] Simultaneously retention of the basic analyte amitryptyline increased by 20-31% due to the formation of new silanols and detachment of the bonded phase.[61] Thus, silica based columns are incompatible with high pH eluents.

In contrast, PGC is stable from pH 0-14.[11] Flushing the Carboxylate-PGC column with 100 mM NaOH : ACN (50:50 v/v) for 5 h (262 column volumes) had little impact on retention (t_R decreased by 0.7% for benzylamine and 0.9% for tryptophan, Figure 5.11). High pH eluents maximize the negative charge on the carboxylate PGC. The zeta potential of carboxylate-PGC in 0.1 M NaOH increases from -33 mV in deionized water to -38 mV at pH > 12. This increases the "wettability" of the carbonaceous stationary phase.[50]

Column synthesis reproducibility is also critical from a given lot. In order to assess the reproducibility of the synthesis three batches were synthesized from the same lot. Figure 5.12 shows the overlaid chromatograms from the three columns. Retention time RSD for early and late eluting acid were 2.6 % and 5.0%, respectively for three separate columns of carboxylate-PGC (Figure 5.12). The low relative standard deviations show that the batch to batch column performance is very good.

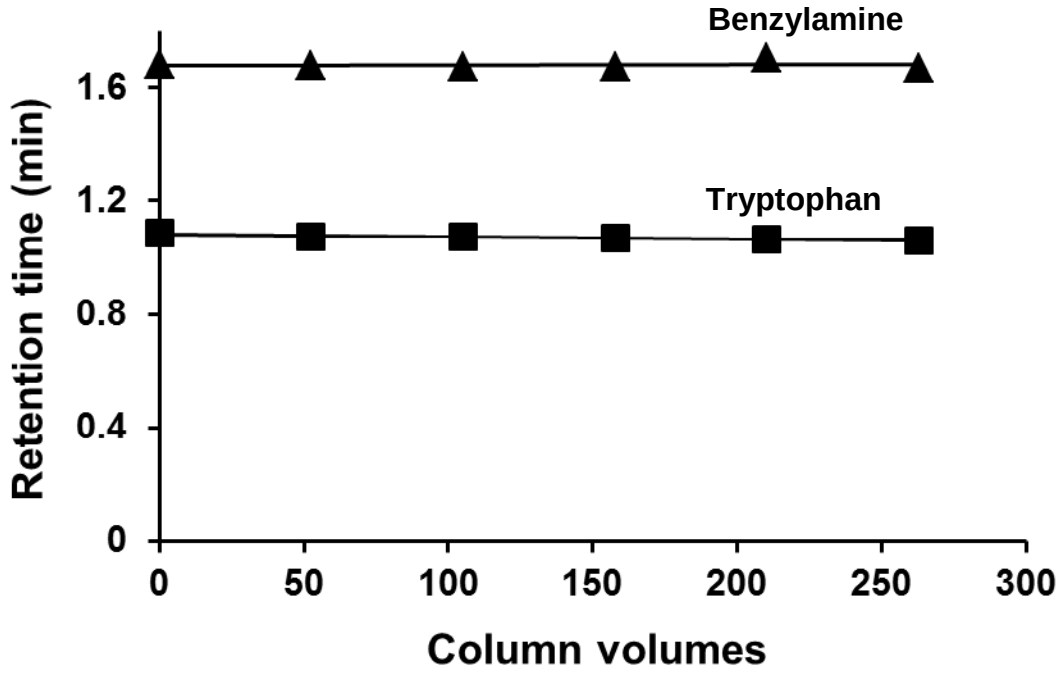

Figure 5.11. Stability of Carboxylate-PGC column under strong alkaline conditions. Experimental conditions: Column, Carboxylate-PGC (150 x 3 mm i.d., 5 µm), flow rate: 0.8 mL/min (dead volume =0.91 mL); eluent, 100 mM sodium, hydroxide (pH =12.6): ACN (50:50, v/v), analytes: 5 mM benzylamine and 0.5 mM tryptophan in the same % ACN as the mobile phase. UV detection at 254 nm with a 2 µL loop. The y-axis error is less than the size of the markers.

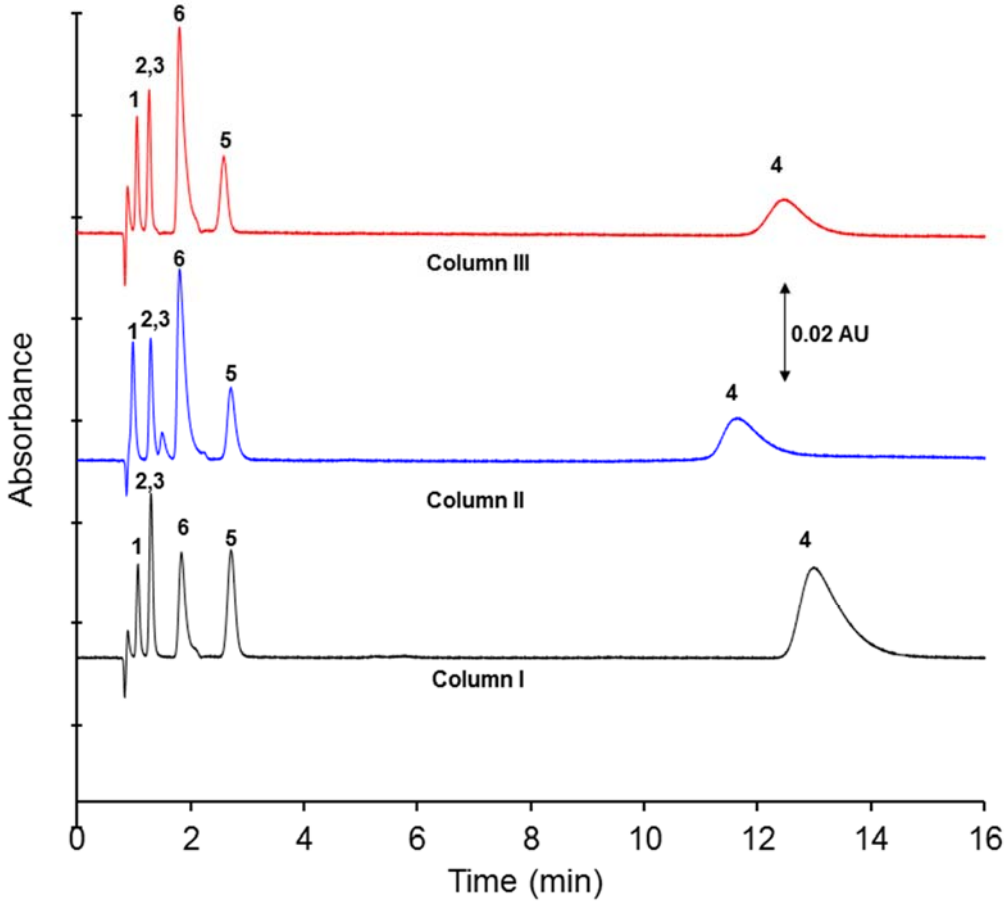

Figure 5.12. Reproducibility of synthesis of Carboxylate-PGC. The three columns were prepared separately from the same lot of PGC, and tested under HILIC conditions. Analytes separated by commas show refer to co-elution. Column II was even exposed to alcoholic KOH during pre-conditioning. Conditions: Columns, Carboxylate-PGC (150 x 3 mm i.d.), flow rate: 1.0 mL/min; eluent, 20 mM ammonium acetate (pH =6.9) in 85 %ACN; analytes 1. salicylic acid, 2. gentisic acid, 3. acetylsalicylic acid, 4. salicyluric acid, 5. hippuric acid and 6. α-hydroxyhippuric acid. UV detection at 254 nm with a 2 µL loop.

5.4 Conclusions

Porous graphitic carbon is a highly attractive substrate for hydrophilic interaction liquid chromatography due to its appealing selectivity, high chemical compatibility, pH stability, temperature resistivity, and mechanical strength. The surface chemistry of highly hydrophobic carbon was modified with a benzene carboxylate moiety using diazonium chemistry. This modification converted the reversed phase PGC into a HILIC phase. The carboxylate-PGC demonstrated a selectivity that is different from that of 35 other columns with an additional advantage of retaining hydrophobic compounds. The effectiveness of the carboxylate-PGC column under high pH conditions was also demonstrated. The diazonium modification approach employing a hydrophilic functional group yielded the first example of HILIC on modified porous graphitic carbon, thus opening a new avenue of selectivity on robust stationary phases.

5.5 References

1. A. J. Alpert, *Journal of Chromatography* **1990**, *499*, 177-196.
2. S. Di Palma, P. J. Boersema, A. J. R. Heck, S. Mohammed, *Analytical Chemistry* **2011**, *83*, 3440-3447.
3. M. E. A. Ibrahim, C. A. Lucy, In *Hydrophilic Interaction Chromatography: A Guide for Practitioners*, B. A. Olsen; B. W. Pack, Eds.; John Wiley & Sons Inc., 2013, pp 43-85.
4. C. Wang, C. Jiang, D. W. Armstrong, *Journal of Separation Science* **2008**, *31*, 1980-1990.
5. D. W. Armstrong, H. L. Jin, *Journal of Chromatography A* **1989**, *462*, 219-232.

6. N. P. Dinh, T. Jonsson, K. Irgum, *Journal of Chromatography A* **2011**, *1218*, 5880-5891.

7. P. Hemström, K. Irgum, *Journal of Separation Science* **2006**, *29*, 1784-1821.

8. H. Qiu, E. Wanigasekara, Y. Zhang, T. Tran, D. W. Armstrong, *Journal of Chromatography A* **2011**, *1218*, 8075-8082.

9. D. Gétaz, M. Gencoglu, N. Forrer, M. Morbidelli, *Journal of Chromatography A* **2010**, *1217*, 3531-3537.

10. B. Ells, Y. Wang, F. F. Cantwell, *Journal of Chromatography A* **1999**, *835*, 3-18.

11. J. H. Knox, B. Kaur, G. R. Millward, *Journal of Chromatography* **1986**, *352*, 3-25.

12. A. Tornkvist, K. E. Markides, L. Nyholm, *Analyst* **2003**, *128*, 844-848.

13. E. Forgács, *Journal of Chromatography A* **2002**, *975*, 229-243.

14. S. Mazan, G. Crétier, N. Gilon, J. M. Mermet, J. L. Rocca, *Analytical Chemistry* **2002**, *74*, 1281-1287.

15. M. Pabst, J. Grass, R. Fischl, R. Léonard, C. Jin, G. Hinterkorner, N. Borth, F. Altmann, *Analytical Chemistry* **2010**, *82*, 9782-9788.

16. C. W. Reid, J. Stupak, C. M. Szymanski, J. Li, *Analytical Chemistry* **2009**, *81*, 8472-8478.

17. J. H. Knox, P. Ross (editors), *Carbon-based packing materials for liquid chromatography—Structure, performance, and retention mechanisms,* Marcel Dekker Inc., New York, **1997**.

18. M. C. Hennion, V. Coquart, S. Guenu, C. Sella, *Journal of Chromatography A* **1995**, *712*, 287-301.

19. C. West, C. Elfakir, M. Lafosse, *Journal of Chromatography A* **2010**, *1217*, 3201-3216.

20. L. Pereira, *LC GC North America* **2011**, *29*, 262-269.

21. J. H. Knox, Q. H. Wan, *Chromatographia* **1996**, *42*, 83-88.

22. N. Zhang, L. Y. Wang, H. Liu, Q. K. Cai, *Surface and Interface Analysis* **2008**, *40*, 1190-1194.

23. H. P. Boehm, W. Heck, R. Sappok, E. Diehl, *Angewandte Chemie, International Edition in English* **1964**, *3*, 669-677.

24. J. A. Harnisch, D. B. Gazda, J. W. Anderegg, M. D. Porter, *Analytical Chemistry* **2001**, *73*, 3954-3959.

25. J. L. Bahr, J. P. Yang, D. V. Kosynkin, M. J. Bronikowski, R. E. Smalley, J. M. Tour, *Journal of the American Chemical Society* **2001**, *123*, 6536-6542.

26. M. Delamar, R. Hitmi, J. Pinson, J. M. Saveant, *Journal of the American Chemical Society* **1992**, *114*, 5883-5884.

27. M. F. Wahab, C. A. Pohl, C. A. Lucy, *Analyst* **2011**, *136*, 3113-3120.

28. S. D. Chambers, M. T. McDermott, C. A. Lucy, *Analyst* **2009**, *134*, 2273-2280.

29. H. Ganegoda, D. S. Jensen, D. Olive, L. Cheng, C. U. Segre, M. R. Linford, J. Terry, *Journal of Applied Physics* **2012**, *111*, 053705.

30. D. S. Jensen, V. Gupta, R. E. Olsen, A. T. Miller, R. C. Davis, D. H. Ess, Z. Zhu, M. A. Vail, A. E. Dadson, M. R. Linford, *Journal of Chromatography A* **2011**, *1218*, 8362-8369.

31. M. E. A. Ibrahim, Y. Liu, C. A. Lucy, *Journal of Chromatography A* **2012**, *1260*, 126-131.

32. M. F. Wahab, C. A. Pohl, C. A. Lucy, *Journal of Chromatography A* **2012**, *1270*, 139-146.

33. W. Bicker, J. Y. Wu, M. Lammerhofer, W. Lindner, *Journal of Separation Science* **2008**, *31*, 2971-2987.

34. F. Mihci, *Water Adsorption Isotherms Among HILIC Phases*. Degree Project in Chemistry, Umea University, Sweden, Umea, 2011.

35. M. R. Linford, D. Jensen, L. Yang, L. Wiest, *USA Patent*, WO2010033903A1, 2010.

36. A. Rieker, *Industrie Chimique Belge-Belgische Chemische Industrie* **1971**, *36*, 1078.

37. J. B. Hendrickson, *Journal of the American Chemical Society* **1961**, *83*, 1251-1251.

38. J. M. Englert, C. Dotzer, G. A. Yang, M. Schmid, C. Papp, J. M. Gottfried, H. P. Steinruck, E. Spiecker, F. Hauke, A. Hirsch, *Nature Chemistry* **2011**, *3*, 279-286.

39. M. F. Wahab, C. A. Pohl, C. A. Lucy, *Journal of Chromatography A* **2012**, *1270*, 139-146.

40. W. Jiang, G. Fischer, Y. Girmay, K. Irgum, *Journal of Chromatography A* **2006**, *1127*, 82-91.

41. A. P. Parker, P. A. Reynolds, A. L. Lewis, L. Kirkwood, L. G. Hughes, *Colloids and Surfaces B: Biointerfaces* **2005**, *46*, 204-217.

42. R. L. McCreery, *Chem. Rev.* **2008**, *108*, 2646-2687.

43. S. Kundu, Y. Wang, W. Xia, M. Muhler, *Journal of Physical Chemistry C* **2008**, *112*, 16869-16878.

44. Y. C. Liu, R. L. McCreery, *Journal of the American Chemical Society* **1995**, *117*, 11254-11259.

45. P. A. Brooksby, A. J. Downard, *Langmuir* **2004**, *20*, 5038-5045.

46. S. Baranton, D. Belanger, *Journal of Physical Chemistry B* **2005**, *109*, 24401-24410.

47. A. Tornkvist, *Aspects of Porous Graphitic Carbon as Packing Material in Capillary Liquid Chromatography*. PhD thesis, University of Uppsala, Uppsala, **2003**.

48. A. J. Alpert, *Analytical Chemistry* **2008**, *80*, 62-76.

49. J. L. Glajch, J. J. Kirkland, *Analytical Chemistry* **1983**, *55*, 319A-336A.

50. D. M. Packwood, P. A. Brooksby, A. D. Abell, A. J. Downard, *Australian Journal of Chemistry* **2011**, *64*, 122-126.

51. B. Sridhar, J. B. Nanubolu, K. Ravikumar, *CrystEngComm* **2012**, *14*, 7065-7074.

52. Y. Guo, S. Gaiki, *Journal of Chromatography A* **2005**, *1074*, 71-80.

53. Y. Guo, In *Hydrophilic Interaction Liquid Chromatography (HILIC) and Advanced Applications*; CRC Press, 2011, pp 401-426.

54. S. Bieri, E. Varesio, O. Munoz, J. L. Veuthey, P. Christen, *Journal of Pharmaceutical and Biomedical Analysis* **2006**, *40*, 545-551.

55. J. C. Reepmeyer, J. F. Brower, H. P. Ye, *Journal of Chromatography A* **2005**, *1083*, 42-51.

56. J. Y. Liu, L. Cheng, B. F. Li, S. J. Dong, *Langmuir* **2000**, *16*, 7471-7476.

57. C. Saby, B. Ortiz, G. Y. Champagne, D. Belanger, *Langmuir* **1997**, *13*, 6805-6813.

58. *http://www.dionex.com/en-us/webdocs/65840-DS_Acclaim_Mixed_Mode_WCX-1_21Feb08_LPN2024.pdf*, (accessed May 2013)

59. v. C. A. S. C. SciFinder Scholar, OH, 2006; RN 50-78-2.

60. J. Xing, A. Apedo, A. Tymiak, N. Zhao, *Rapid Communications in Mass Spectrometry* **2004**, *18*, 1599-1606.

61. S. W. Pettersson, E. Collet, U. Andersson, *Journal of Chromatography A* **2007**, *1142*, 93-97.

CHAPTER 6. Elution Profiles and Overloading Effects on Analytical Ion Chromatography Column*

6.1 Introduction

Ion chromatography (IC) has become a standard analytical technique for the determination of inorganic and organic ions. More than 70 IC columns are commercially available with different selectivities and capacities to deal with a wide range of analytes in various matrices.[1] Modern IC phases consist of macroporous polymeric beads with fixed ion exchange sites. Thus, IC columns are characterized by their exchange capacity.[2, 3] Typical capacities of analytical ion exchangers range from 40 to 2800 μeq/column for conventional diameter columns (> 2 mm i.d.).[4] In suppressed ion chromatography, higher capacity analytical columns are rarely used, as a more concentrated mobile phase would be needed, which would overwhelm the capabilities of the suppressor.

A consequence of using predominantly low capacity anion exchangers is that the analytical columns are prone to overload. In many samples, the ionic concentrations can be disproportionately high,[5] *e.g.*, in the case of seawater the ionic strength can be as high as 500 mM with trace anions of interest present at the micromolar level. In such cases, the trace anion peaks are severely distorted, with the shape and height depending upon the proximity to the overload peak.[6] An example is the analysis of bromate in a highly concentrated matrix.[6] In such cases,

* A version of this chapter has been submitted as M. Farooq Wahab, Jordan K. Anderson, Mohamed Abdelrady, and Charles A. Lucy to *Analytical Chemistry*. Author contributions: The data presented here were equally collected by J. K. Anderson (Chem. 299) and myself. M. Abdelrady performed initial survey experiments in this project as an undergraduate summer student under my supervision.

the bromate peak shifts its retention time and broadens due to the column overloading by the matrix ions, even when the peaks are baseline resolved under analytical conditions. In disinfection by-product analysis using two dimensional IC, this broadening and peaks shift will affect the width and position of the time window used for heart cutting (Figure 2.5).[7]

The objective of this chapter is to explore the impact of overload in ion chromatography, and to develop general rules for prediction of whether the overloaded peaks will be tailed or fronted.

6.1.1 Overloading Effects in Analytical HPLC

Overloading effects in preparative and analytical reversed phase chromatography have been studied in detail.[8-10] Chromatographic overload can be due to: (a) volume overload; or (b) concentration overload.[11, 12] Volume overload is caused by injection of a large sample volume. Such overload is characterized by broad, symmetric and often flat topped peaks, even for low analyte concentrations.[12] Volume overload is easily diagnosed from the symmetric flattened peak profile.

Concentration overload leads to a variety of peak shapes including fronting, tailing, split peaks and peaks which have secondary humps.[13] The specific peak shape observed under concentration overload conditions depends on the shape of the sorption isotherm (*i.e.*, plot of C_S vs. C_M) as shown in Figure 6.1. Figure 6.1(A) represents the ideal *analytical condition* where the analyte

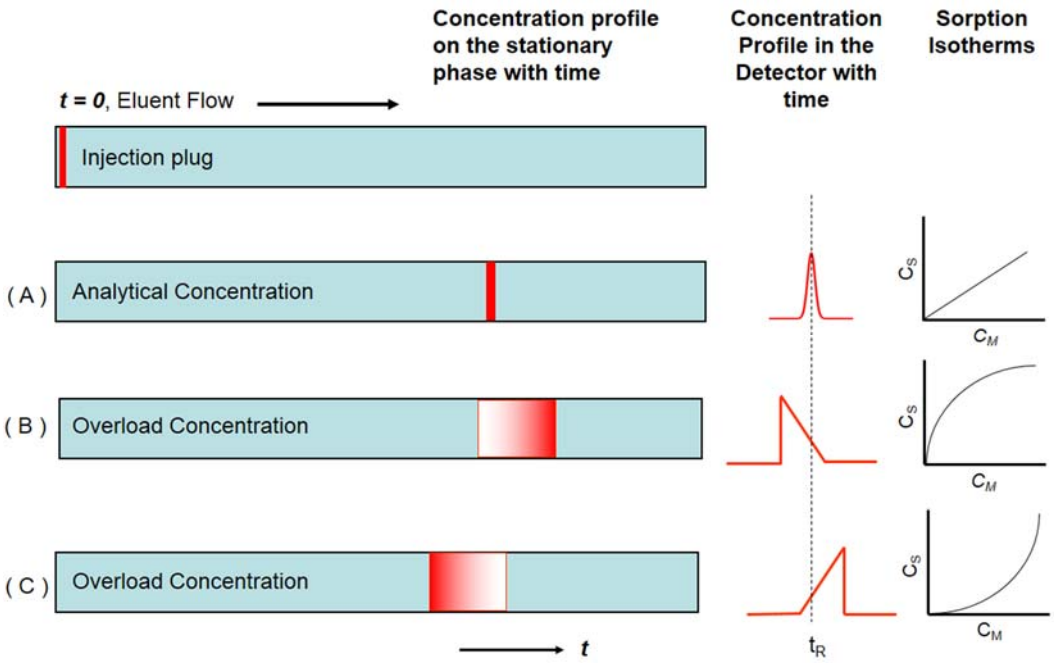

Figure 6.1. Development of elution profiles (A, B and C) under overload condition as seen in the column and the detector. The shades in the column reflect the concentration gradient of the analyte on the stationary phase.

concentration is within the *linear isotherm range* (when the analyte occupies << 1% of the exchange capacity).[14] As a result, sharp Gaussian peaks are observed. Under concentration overload conditions, the isotherm will not be linear but rather can take on a variety of nonlinear profiles. Type I isotherms (Figure 6.1(B)), which include Langmuir isotherms, have convex curvature and give rise to tailing peaks. Type III isotherms (Figure 6.1(C)) have concave curvature and show "anti-Langmuirian" peaks having a diffuse front and a steep rear.[15] However, as will be discussed below, fronting) peaks can also occur when competitive components each follow a type-I isotherm.[16-18] Type II or S-shaped isotherms give rise to very unusual peak shapes.[19, 20]

The determination of sorption isotherms and peak profile prediction requires extensive numerical modeling.[16] In most HPLC separations, the mobile phase contains additional components besides the primary eluent (*e.g.*, organic solvent in RPLC). As a result multiple species (*i.e.* both mobile phase components and analytes) are simultaneously competing for sorption sites on the stationary phase.[19, 20] Assuming Langmuir isotherms, the competitive situation is described by:

$$\frac{q_k}{q_s} = \frac{b_k C_k}{1 + \sum_{k=1}^{n} b_k C_k} \qquad \text{(equation 6.1)}$$

where q_k is the amount of the analyte or mobile phase component in equilibrium with the stationary phase vs. q_s which is the saturation capacity of the given compound. In the right hand side, b_k is the Langmuir coefficient specific to the k^{th} component, and the denominator sums the impact of all species sorbing onto the

surface.[13, 19] On the basis of the competitive Langmuir isotherms (equation 6.1), models have been developed to predict the peak shape under overload conditions in normal phase and reversed phase chromatography.[13, 20] Whether tailing or fronting is observed depends on the relative retention of the strong mobile phase component and the analyte; and the relative retention of mobile phase system peak and the analyte peak. Unfortunately, the rules developed for reversed phase cannot be easily applied in IC given the fact that system peaks in IC are essentially eliminated by suppression. We will use the IC selectivity coefficients $K_{E,A}$ (Section 1.8.2) in our discussion. The fundamental equilibrium in ion exchange chromatography is:[21-23]

$$yA^{x-}_{(mobile)} + xE^{y-}_{(resin)} \rightleftharpoons yA^{x-}_{(resin)} + xE^{y-}_{(mobile)} \qquad \text{(equation 6.2)}$$

where A^{x-} is the analyte ion of charge x and E^{y-} is the eluent ion of charge y. This equilibrium results in the retention law for the analyte retention factor (k):[24]

$$\log k = \frac{1}{y}\log K_{A,E} + \frac{x}{y}\log\left(\frac{Q}{y}\right) + \log\left(\frac{w}{V_M}\right) - \frac{x}{y}\log[E^{y-}] \qquad \text{(equation 6.3)}$$

where k is the retention factor, $K_{A,E}$ is the ion exchange selectivity constant of anion over eluent, Q is the nominal column capacity in mmole, w is the weight of resin in the column, V_M is the dead volume of the column (mL), and $[E^{y-}]$ is the eluent concentration in molarity. For a monovalent eluent and monovalent analyte the corresponding ion exchange selectivity constant $K_{E,A}$ (reciprocal of $K_{A,E}$) is for eluent over anion can be derived:[25]

$$K_{E,A} = \frac{Q}{V_M k[E^-]} \qquad \text{(equation 6.4)}$$

6.2 Experimental

6.2.1 Chemicals and Reagents

Sodium bromide and disodium tetraborate decahydrate were purchased from Sigma-Aldrich (St. Louis, MO, USA); sodium nitrate and sodium chloride were from EMD Chemicals (Gibbstown, NJ, USA); and sodium bicarbonate, anhydrous sodium carbonate and sodium acetate trihydrate were from Caledon (Georgetown, ON, Canada). Deionized water (> 17.7 MΩ) from a Barnstead or MilliQ system was used for solution preparation. Sodium chloride, sodium bromide and sodium nitrate solutions were prepared in deionized water in the range of 0.1 mM to 500 mM for column overloading studies.

6.2.2 Instrumentation

Either a Dionex ICS-2000 or ICS-3000 ion chromatography system (Thermo Scientific, Sunnyvale, CA, USA) was used. A Dionex EluGen III NaOH eluent generator was used for the generation of NaOH eluent for the IC-2000. The carbonate eluent was prepared manually. All connections were made with PEEK tubings. Injections used a 20 μL loop. For overloading studies, samples in the concentration range (0.1 - 500 mM) were injected in duplicate. Three Dionex columns (250 x 4 mm i.d.) were used: IonPac AS23; IonPac AS18; and IonPacAS16. The properties of the columns are summarized in Table 6.1. Studies were at 1.0 mL/min and ambient temperature or 30 ^{o}C, as noted. A 4 mm ASRS-300 suppressor (Dionex) was used in the recycle mode prior to conductivity detector. *Chromeleon* (version 6.80) was used for data collection at 20 Hz.

Table 6.1. Column characteristics

Columns (Capacity)[a]	Eluent Selectivity[b]	Column Chemistry
AS16 (170 μeq)	Hydroxide	Latex coated resin, 9 μm, alkanol quaternary ammonium ion, "ultralow hydrophobicity"
AS18 (285 μeq)	Hydroxide	Latex coated resin, 9 μm, alkanol quaternary ammonium ion, "low hydrophobicity"
AS23 (320 μeq)	Carbonate	Hyperbranched resin, 6 μm, alkanol quaternary ammonium ion, "ultralow hydrophobicity"

[a] nominal capacities as reported by the manufacturer.

[b] manufacturer's recommended eluent.

6.2.3 Calculations

The retention data needed to calculate $K_{E,A}$ from equation 6.4 was obtained from Virtual Column (Dionex Corporation, SP 6.80) when available. The parameters (V_M, k, eluent concentration, [E^-]) used in equation 6.4, were directly obtained from the chromatograms (k) in the case of borate. The dead volume V_M was determined from the dead time based on the water dip and the flow rate. Calculated selectivity coefficients for common monovalent ions have already been listed elsewhere.[25] The data was obtained from the Virtual Column data.[25] The statistical moments were determined by the Chromeleon software (Dionex Corporation, SP 6.80). The second centralized statistical moment (variance) is:

$$\mu_2 = \frac{\int (t - \mu_1)^2 \, f(t) dt}{\mu_0} \qquad \text{(equation 6.5)}$$

in which μ_0 is the zero statistical moment (area), μ_1 is the first statistical moment (*i.e.* center of gravity) and *f(t)* represents the baseline corrected signal over time *t*. The peak skewness *S* is calculated as:

$$S = \frac{(\mu_1 - t_R)}{\sqrt{\mu_2}} \qquad \text{(equation 6.6)}$$

where t_R is the retention time of the peaks. When $S = 0$, the peak is symmetrical; $S < 0$ implies fronting; and $S > 0$ indicating tailing.

6.3. Results and Discussion

The peak elution profile fundamentally gives information about the processes occurring on the stationary phase and within the mobile phase. Modern

IC columns are intentionally designed to be of low capacity to enable use of low concentrations eluents that can be easily suppressed for conductivity detection. Extensive research has gone into improving the efficiency[1] and selectivity[25] of the ion exchange phases to enable fast and high resolution separations. However the chromatographic figures of merit such as retention time, column efficiency and peak asymmetry change with analyte concentration when a column becomes overloaded.[26] This work investigates the peak overload patterns observed in ion chromatography with a variety of common IC analytes and eluents (borate, hydroxide and carbonate). This enables the establishment of guidelines to predict peak shapes under overload conditions in ion chromatography.

6.3.1 Overload Peak Shapes with Borate Eluent

Borate is a commonly employed eluent in suppressed IC separations for high resolution separation of weakly retained inorganic and organic anions.[27] Borate has weak elution power[27] on anion exchangers and is therefore used in high concentration to elute ions in a reasonable time. Figure 6.2 shows the peak shape when 1 to 500 mM bromide is injected into AS16, AS18 and AS23 columns with a 32 mM tetraborate eluent (pH ~ 9.1). All three columns show *tailing* behaviour when overloaded ($S > 0$ for all concentrations), and the skewness (*i.e.*, amount of tailing) increases with the injected concentration. Simultaneously, the efficiency in Figure 6.3 drops from 7000 - 3440 under analytical conditions to <40 plates at 500 mM Br^-. It should be noted that injection of 500 mM Br^- only utilizes 3-5% of the total anion exchange capacity of these columns.

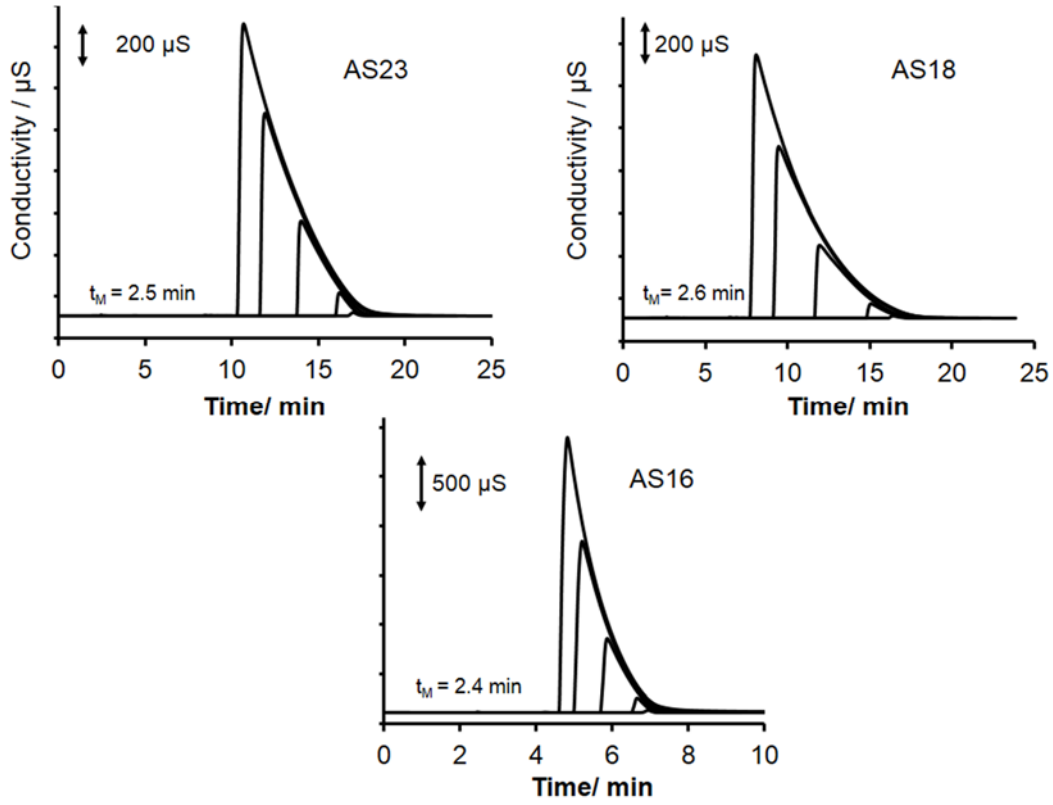

Figure 6.2. Overload profiles of bromide ion on AS16, AS18 and AS23 columns. Conditions: eluent, 32 mM sodium tetraborate (pH ~ 9.1) with a flow rate of 1.0 mL/min, Br^- concentration: 1, 10, 100, 300 and 500 mM, suppressed conductivity detection in recycle mode. All columns are 250 mm x 4 mm i.d. and used with 20 µL injection loop.

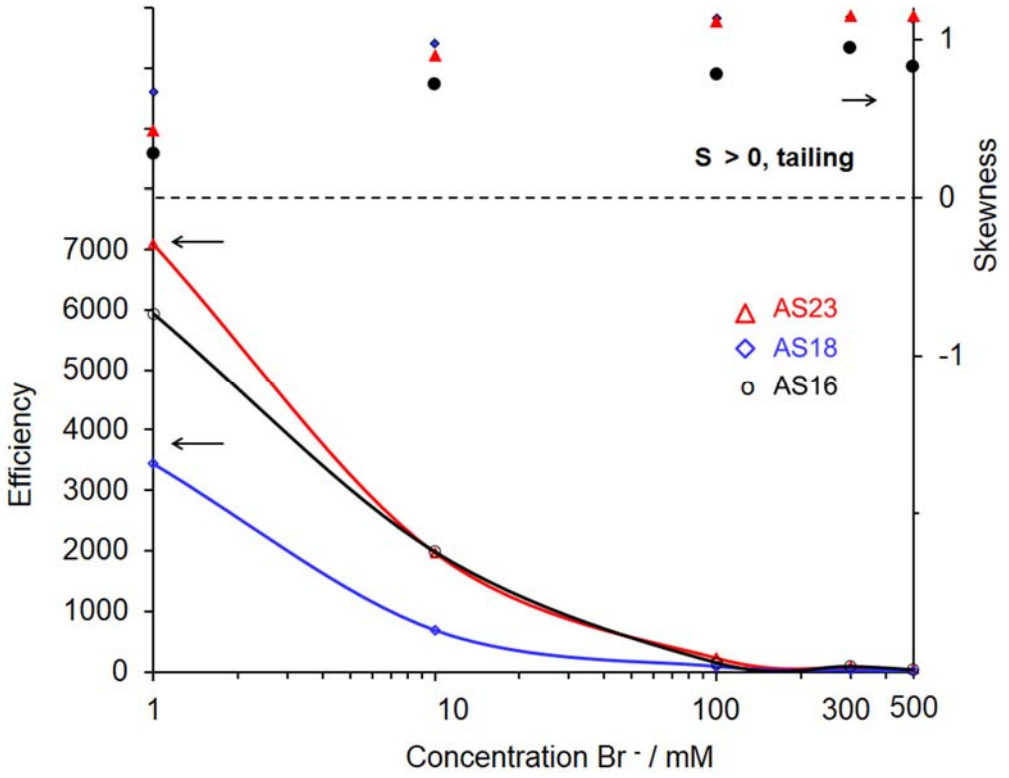

Figure 6.3. Efficiency and skewness trends with borate eluent on analytical columns as function of bromide concentration. Conditions: Columns AS16 (○), AS18 (◊) and AS23 columns (Δ) (250 x 4 mm i.d.); eluent, 32 mM sodium tetraborate at 1.0 mL/min; Br^- concentration: 1, 10, 100, 300 and 500 mM with 20 µL injection; suppressed conductivity detection in recycle mode.

6.3.2. Peak Shapes with Hydroxide Eluent

Hydroxide is an ideal eluent for suppressed IC, as its suppression product is pure water, which yields the lowest conductivity background possible for any aqueous eluent.[28] Fundamentally, hydroxide is a weak eluent for anion exchanger resins, due to its very strong interaction with water. A highly hydrated ion, like hydroxide, prefers the aqueous phase rather than the hydrophobic resin phase where waters of hydration are not readily available.[29] Figure 6.4 shows the bromide overload behaviour on the AS16 column for various NaOH eluent concentrations. Two trends are evident: (a) bromide shows fronting overload behaviour; and (b) the concentration of the hydroxide eluent does not affect the fronting characteristics of the overload peaks. This behaviour is in stark contrast with the tailing behaviour observed on the same column with a borate eluent (Figure 6.2).

As seen previously for borate (Figure 6.3), the efficiency drops from >5000 plates under analytical conditions to < 1000 plates at 100 mM Br^- and ~ 200 plates by 500 mM Br^-. The peak skewness in each case is < 0 (S_{AS16} ~ -1.2 with 500 mM Br^- for all NaOH eluent concentrations).

6.3.3. Prediction of Peak Shape Under Overload IC Conditions

Sections 6.3.1 and 6.3.2 show that simply changing the eluent used with a given IC column (AS16) can alter the type of overload observed. We propose a qualitative and semi-quantitative explanation for the overload elution profiles.

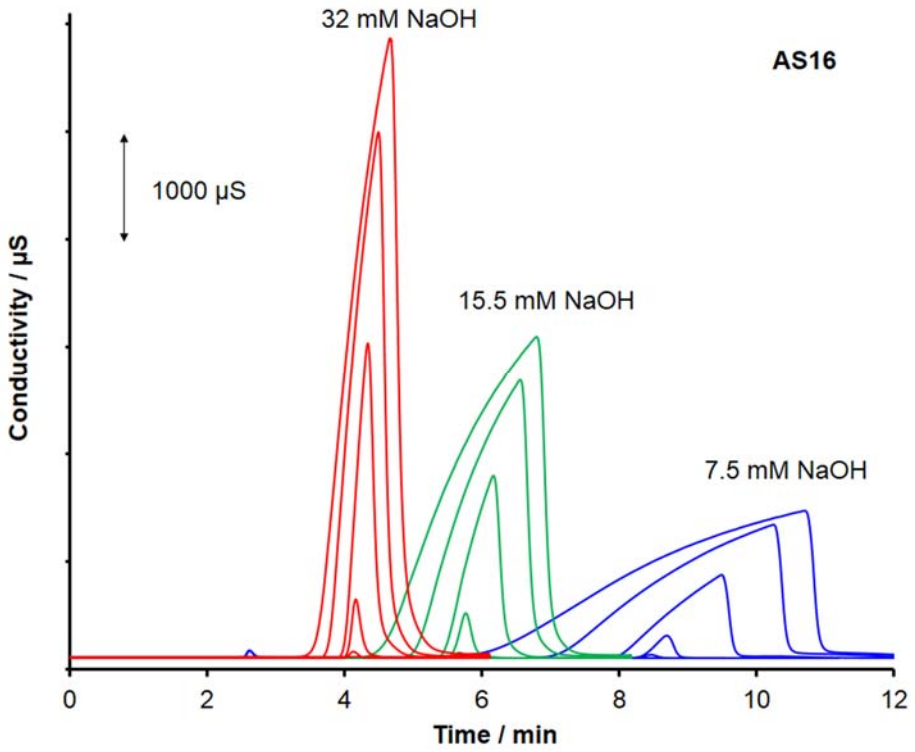

Figure 6.4. Overload profiles of bromide ion on AS16 (250 x 4 mm i.d.) columns with sodium hydroxide eluent at 30 ºC. Conditions: eluent, 7.5 - 32 mM NaOH at 1.0 mL/min; Br^- concentrations of 0.1, 1, 10, 100, 300 and 500 mM; suppressed conductivity detection in recycle mode. Column is used with a 20 µL injection loop.

As discussed in Sec. 6.1.1, overload behaviour cannot simply be viewed in terms solely of the analyte sorption behaviour. Rather, the components in the mobile phase compete with the analyte(s) for the sorption sites on the stationary phase, resulting in the competitive Langmuir isotherm (equation 6.1).

Fundamental studies have shown that in normal and reversed phase chromatography the strength of the adsorption of the strong mobile phase component dictates the analyte peak shape under overload conditions.[10, 15, 17] The comparative adsorption strength of the mobile phase components *vs.* the analyte was determined by injecting the mobile phase component (acetonitrile, or methanol) and the analyte into the RPLC column using pure water as an eluent. If the strong mobile phase component in RPLC (*e.g.*, methanol or acetonitrile) was more weakly adsorbed onto the stationary phase than the analyte, the analyte peaks were always tailed (*i.e.*, Langmuirian) under overload conditions.[20, 30, 31] Alternately, if the strong mobile phase component was more strongly sorbed onto the stationary phase than the analyte, fronting might be observed.[20]

In IC, the eluent consists of water (extremely weak eluent component) and the eluent ion (E^-, strong eluent component). In anion exchangers, the eluent anion competes with the analyte anion for the limited number of available sites on the stationary phase (equation 6.2). The selectivity coefficient $K_{E,A}$ of a monovalent eluent *vs.* a monovalent analyte provides insight into the relative interaction between the charged species and the resin. If $K_{E,A} = 1$, then the analyte anion interacts with the stationary phase similarly to the eluent anion. If $K_{E,A} > 1$ the

eluent anion interacts more strongly than the analyte, and if $K_{E,A} < 1$ then resin retains the analyte anion more strongly than the eluent anion.[32]

The $K_{Borate,\ Br}$ values were determined based on bromide retention on each column and equation 6.4. The $K_{Borate,\ Br}$ for the AS16, AS18 and AS23 columns are 1.2, 0.62, and 0.67 respectively. That is, borate has either comparable or lower affinity for the stationary phase than does the bromide ion. In Figure 6.2, all overloaded bromide peaks were tailed when borate was used as eluent, regardless of the column capacity or chemistry. This is consistent with past fundamental studies[13, 20, 30] which stated that tailed analyte peaks are observed for competitive Langmuir isotherm where the strong eluent component (borate in this case) is more weakly retained than the analyte.

Qualitatively, this tailed peak shape can be explained using Figure 6.1 Under competitive Langmuir isotherm conditions, both the A^- and E^- can act as eluents. Under trace conditions (Figure 6.1A), the analyte concentration is low, such that elution depends only on E^-. Hence, Gaussian peaks are observed at t_R. In Figures 6.1B and 6.1C high analyte concentrations have been injected such that the eluent behaviour of both A^- and E^- must be considered. In Figure 6.1B the E^- is less strongly sorbed than A^-. The highly concentrated analyte plug readily displaces the more weakly retained E^-, and saturates the ion exchange sites. The excess A^- self-displaces the retained analyte, causing the analyte band to move down the column more rapidly. Hence, under such conditions the sharp front of the overloaded band in Figure 6.1B elutes *earlier* than the true retention time observed under analytical conditions (Figure 6.1A). The resultant peak in the

chromatogram shows a sharp front and a gradual tail that extends back to t_R. The larger the concentration of sample injected, the greater the analyte self-displacement and so the earlier the peak maximum is observed.

In the case of NaOH eluent with the AS16 column (Figure 6.4), all overloaded Br^- peaks are fronted. The peak shape is independent of the hydroxide ion concentration. Traditionally, hydroxide is a weak eluent for anion exchanger resins, because of its very strong interaction with water. A highly hydrated ion, like hydroxide, prefers the aqueous phase rather than the hydrophobic anion exchanger resin phase where waters for hydration are not readily available.[29] However, replacing one or more of the alkyl groups on a quaternary amine anion exchanger with a more polar functional groups such as an alkanol greatly increases the affinity of the resin to hydroxide eluent (*i.e.*, increases the hydrophilic character of the resin).[29, 33] On such hydrophilic resins, hydroxide ion becomes a more powerful eluent. For instance, simply changing the ion exchange site from trimethylammonium group to dimethylethanolamine reduced the retention factor k of Br^- from 19.2 to 0.92 when using a 100 mM OH^- eluent.[29] While the exact functional groups on commercial IC columns are proprietary, the manufacturer does qualitatively indicate the hydrophilicity of the ion exchange sites, which are summarized in Table 6.1. The "ultra-low" hydrophobicity designation for the AS16 suggests that OH^- is an effective eluent on this column. Indeed, the selectivity $K_{OH,\ Br}$ is 3.6 on AS16,[25] indicating that the AS16 resin retains hydroxide ion more strongly than the bromide ion.

In the fundamental studies of overload in reversed phase chromatography discussed above, the "first and foremost" condition that determines peak shape under overload conditions is the relative retention of the analyte *vs.* strong mobile phase component. For a weakly retained eluent (*e.g.*, borate), this condition is sufficient to dictate that the peaks will be tailed.[13, 20] However, if the mobile phase component is more strongly retained than the analyte, overload peaks may either be tailing or fronting.[13, 20] Whether fronting or tailing is observed depends on the *first system peak* of the mobile phase. If the first system peak of the mobile phase component appears before the analyte peak in the chromatogram, as is observed in IC,[34] the overload peaks will be fronting.[13, 20]

Qualitatively, the fronting behaviour observed in Figure 6.4 can be explained in the light of the competitive Langmuir isotherm. Again, the key consideration is that both the A^- and E^- act as eluents. In Figure 6.1C, the injected A^- acts as a weaker eluent than the displaced E^-. Thus, the analyte within the high concentration zone elutes down the column more slowly than if it would be by E^- Under these conditions, the peak maximum observed under overload conditions (Figure 6.1C) elutes *after* the retention time under analytical conditions (Figure 6.1A). As a result, at the column exit, the detector shows a gradual front and a sharp trailing edge, as observed in Figure 6.4.

6.3.4. Generality of Selectivity Coefficients for Predicting Peak Shapes

In the following sections, we evaluate the utility of selectivity coefficients for predicting peak shapes under overload conditions.

6.3.4.1. Bromide Overload on an AS23 Column with Various Monovalent Eluents

The AS23 is an ultra-low hydrophobicity column with alkanol amine quaternary groups.[3] We investigated overload of bromide on the AS23 using hydroxide, bicarbonate and acetate eluents (Figure 6.5). Both fronting and tailing were observed for bromide on the AS23. With 25 mM NaOH, the overloaded bromide peak fronted (S = -0.5). This is the shape which would be predicted based on the selectivity coefficient $K_{OH,\ Br}$ of 2.7, *i.e.* fronting is predicted if the eluent ion is more strongly retained that the analyte. The fronting is less pronounced than obsersed on the ultralow hydrophobicity AS16 column ($K_{OH,\ Br}$ of 3.6) where the S = -1.2 (Sec. 6.3.2).

Acetate and bicarbonate are weak eluents as judged by the selectivity coefficients, $K_{Bicarb,\ Br}$ = 0.99 and $K_{Acetate,\ Br}$ = 0.41 respectively. Thus similar to borate (Sec. 6.3.1, Figure 6.2), both acetate and bicarbonate eluents show highly tailed overload peaks. However, despite the difference in the selectivity coefficient for acetate and bicarbonate, the skewness are comparable (S = 1.14 vs. 1.11 respectively).

6.3.4.2. Overload of Chloride, Bromide and Nitrate on AS18 Column

The manufacturer describes the AS18 as a "low hydrophobicity" column. In contrast, the AS16 and AS23 columns discussed in Sec. 6.3.3 and 6.3.4.1 are “ultra-low hydrophobicity” columns. Measurements of $K_{OH,A}$ for a variety of analytes confirms these qualitative descriptions of the resins.[25] Figure 6.6 shows

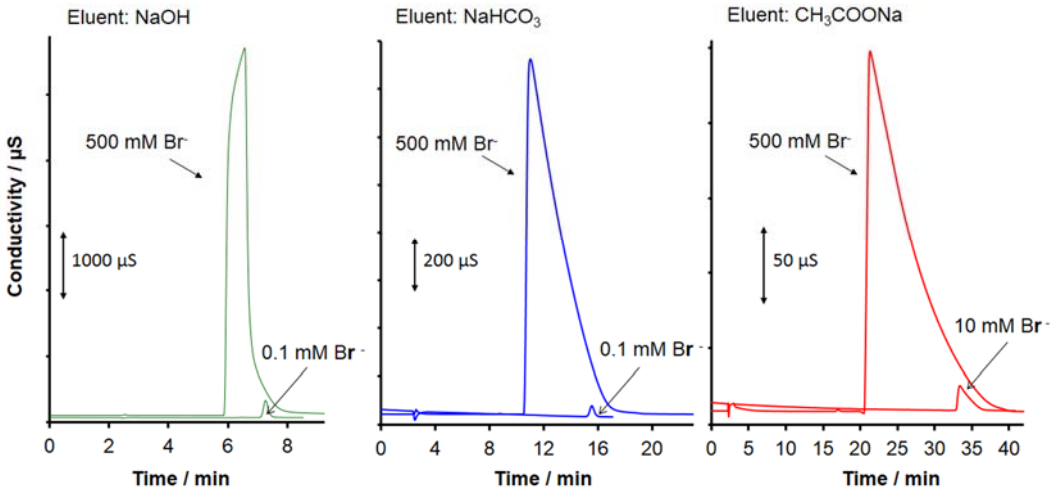

Figure 6.5. Overload profiles of bromide ion using three different eluents on an IonPac AS23 column (250 x 4 mm i.d.). Conditions: eluent, 25 mM NaOH, 25 mM $NaHCO_3$ and 25 mM CH_3COONa at 30 °C; Flow rate, 1.0 mL/min; injection volume, 20 µL; suppressed conductivity detection in recycle mode.

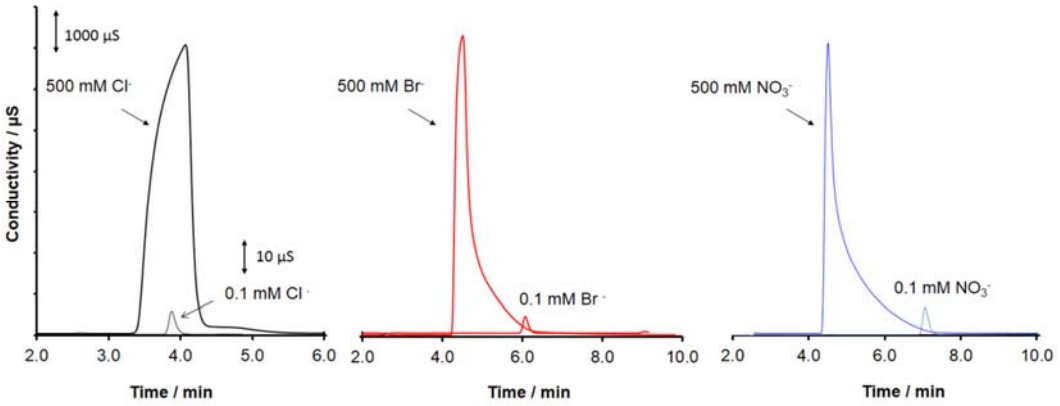

Figure 6.6. Overload profiles of chloride, bromide and nitrate ion on an IonPac AS18 (250 x4 mm i.d.) column with sodium hydroxide eluent. Conditions: eluent, 1.0 mL/min of 32 mM NaOH at 30 ºC; 20 µL injection; suppressed conductivity detection in recycle mode.

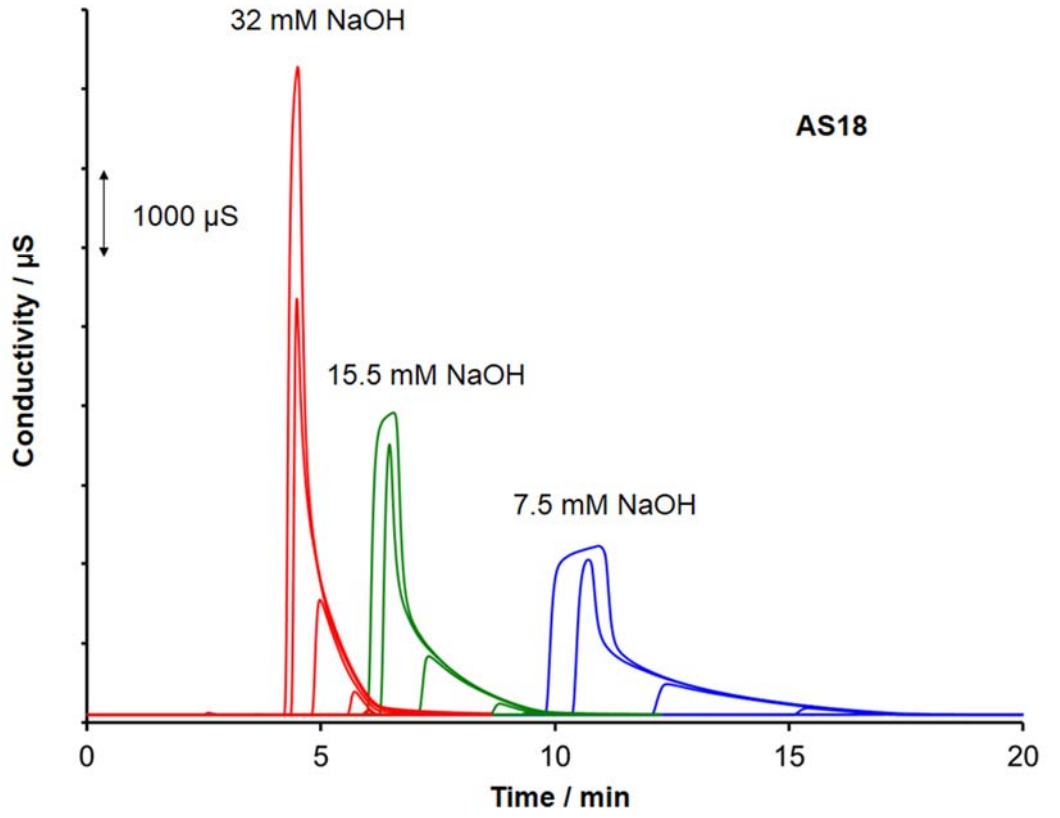

Figure 6.7. Overload profiles of bromide ion on an IonPac AS18 column (250 x4 mm i.d.) with sodium hydroxide eluent. Conditions: eluent, as indicated at 1.0 mL/min at 30 ºC; Br^- concentration: 0.1, 1, 10, 100, 300 and 500 mM, suppressed conductivity detection in recycle mode; Injection volume: 20 µL.

the overload behaviour of Cl^-, Br^- and NO_3^- under trace (0.1 mM) and overload conditions (500 mM) on the AS18 column. On the low hydrophobicity AS18 column, the weakly retained chloride peak is fronted (S = -0.77) whereas moderately retained bromide (S = 0.6) and nitrate (S = 0.9) peaks are tailed. This behaviour is consistent with the relative strengths of the affinity of hydroxide with respect to each analyte anion. The $K_{OH,A}$ for chloride, bromide and nitrate on the AS18 are 5.8, 2.1, and 1.6 respectively.[25] Since hydroxide ion has a strong affinity on the AS18 resin with respect to the chloride, the overload peak is fronted as predicted from the discussion of Figure 1(C). On the other hand, hydroxide has a comparable affinity as the nitrate and bromide ions on the AS18 resin. As observed with borate/bromide on the AS16 column (Section 6.3.1) and bicarbonate/bromide on the AS23 column (Section 6.3.4.2), such a condition results in peak tailing. The peak shape for bromide does not change with respect to change in the hydroxide concentration (Figure 6.7).

From the above test cases (Figures 6.2, 6.4, 6.5, 6.6 and 6.7) we can conclude:

a. If the $K_{E,A}$ is small (< ~2), a tailing peak will be observed under overload conditions.
b. If the $K_{E,A}$ is large (> ~2), a fronting peak will be observed with a given monovalent eluent and monovalent anion.
c. Additionally, the peak shape (fronting vs. tailing) does not depend on the concentration of the monovalent eluent. This last observation does not hold with a divalent eluent, as will be discussed below.

6.3.5. Overload Peak Shapes with a Divalent Eluent

Carbonate-bicarbonate is the most widely used eluent in suppressed ion chromatography because of its powerful elution properties (at low concentration) and buffering properties.[23, 35]

Figure 6.8 shows the overload behaviour of bromide on the AS23 column using four concentrations of a 10:1 carbonate-bicarbonate eluent. At low total concentrations of carbonate-bicarbonate (2.5 to 5 mM), all bromide overload peaks are *fronted* ($S \sim -1.3$). As the eluent concentration is increased to 10-25 mM total carbonate, the peak shape switches to *tailing* ($S \sim 0.5$). Similarly, in Figure 6.9, the peak profile on the AS16 resin also evolves from severe fronting ($S \sim -1.3$) at low concentration of total carbonate to classical tailing at 25 mM carbonate. This peak shape transition with carbonate eluents in Figures 6.8 and 6.9 is in stark contrast to what was seen with monovalent eluents (Figures 6.2 and 6.7), where the peak shape was either *always* fronting or *always* tailing, and did not depend on the eluent concentration.

An anion exchange resin interacts more strongly with a divalent anion than a monovalent ion by the principles of electroselectivity.[36-38] This principle states that a doubly charged ion will create a larger Donnan potential between the resin phase and the aqueous phase, leading to its stronger attraction than a singly charged ion. Thus, in the carbonate-bicarbonate system, CO_3^{2-} is the strong eluting ion, despite both bicarbonate and hydroxide ions also being present.[29, 35] For instance, on the Dionex AS4A, which contains alkanol quaternary ammonium groups, the inter-eluent selectivity ($K_{carbonate,\ bicarb.}$) is 13.8 and $K_{bicarb,\ hydroxide}$

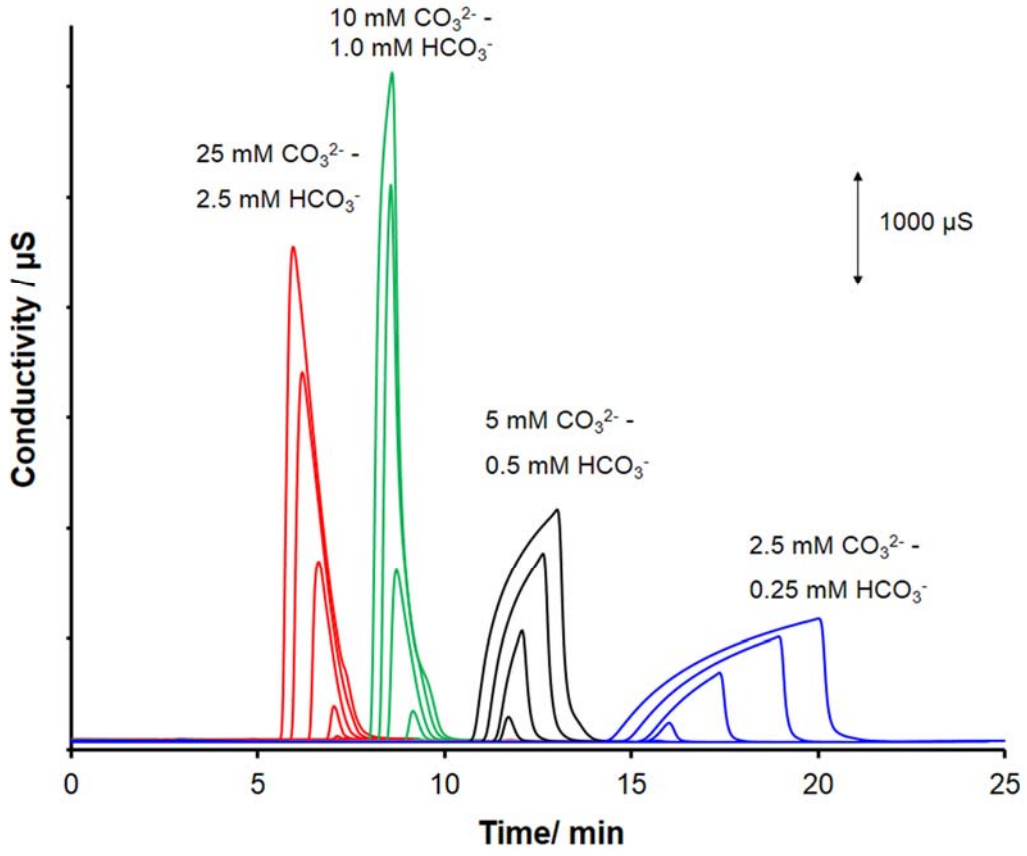

Figure 6.8. Overload profiles of bromide ion on the IonPac AS23 (250 x 4 mm i.d.) column as a function of sodium carbonate-bicarbonate concentration. Conditions: eluent, Na_2CO_3-$NaHCO_3$ in 10:1 ratio at 1.0 mL/min at ambient temperature; Br^- concentrations of 0.1, 1, 10, 100, 300 and 500 mM with 20 µL injection; suppressed conductivity detection in recycle mode.

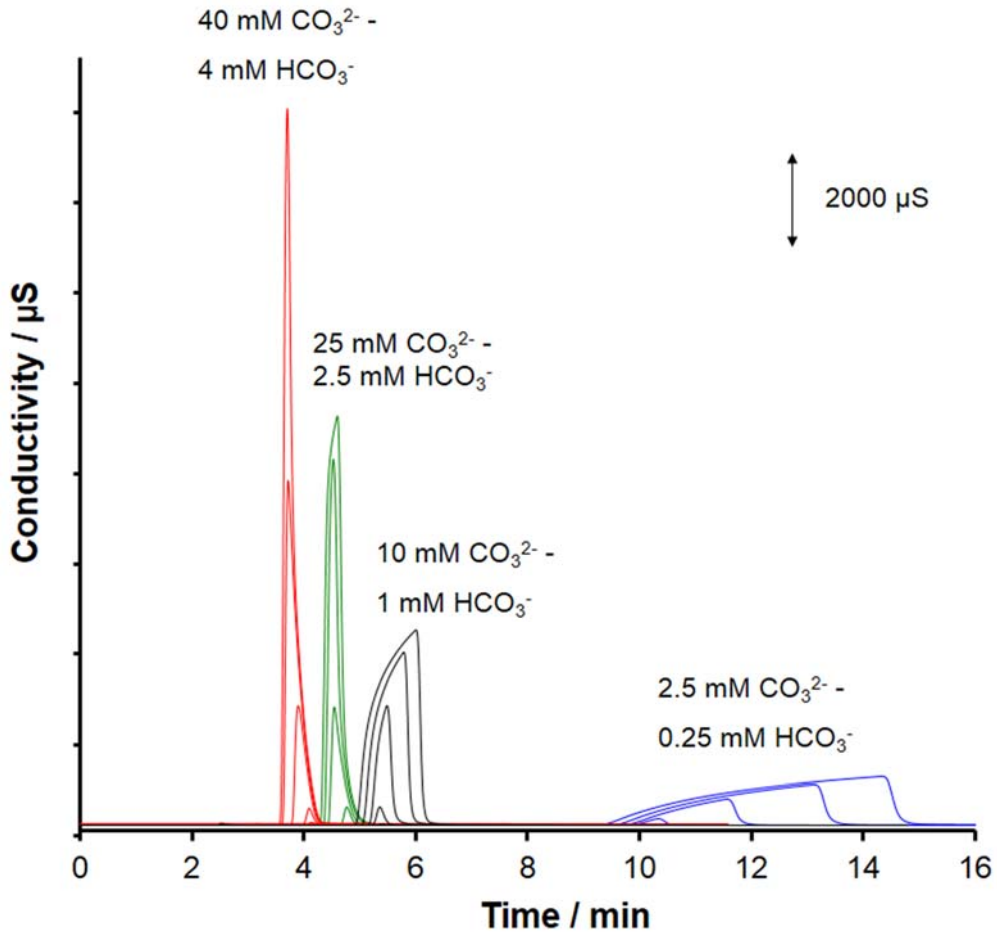

Figure 6.9. Overload profiles of bromide ion on the IonPac AS16 (250 x 4 mm i.d.) column as a function of sodium carbonate-bicarbonate concentration. Conditions: eluent, Na_2CO_3-$NaHCO_3$ in 10:1 ratio at 1.0 mL/min and room temperature; Br^- concentrations of 0.1, 1, 10, 100, 300 and 500 mM with 20 µL injection; suppressed conductivity detection in recycle mode.

= 1.54.[35] Thus, CO_3^{2-} plays the main role over all other monovalent eluent anions in the carbonate-bicarbonate system by an order of magnitude.

Based on Section 6.3.3, if the affinity of an eluent anion for the stationary phase is higher than that of the analyte ion, fronted peaks will be observed. This is what is seen with low concentrations of total carbonate on both the AS23 and AS16 (Figures 6.8 and 6.9).

However, in these figures a peak shape transition from fronting to classical tailing is seen at higher carbonate concentrations. This is due to the change in multivalent selectivity with ionic strength. This is a well-known occurrence in the ion-exchangers (in water purification) literature where sulfate ion tends to elute earlier than chloride in high ionic concentration waters.[37, 39, 40] The electroselectivity reversal[37] can be explained in terms of the Donnan potential. At low ionic strength, the resin attracts the anion in the mobile with a force, which is proportional to the analyte's charge density. As the ionic strength is increased, the absolute value of this Donnan potential decreases and at a certain point becomes zero. As a result, the resin loses its preference for the multivalent anion. Thus, each anion exchanger has a specific inversion point where it will lose the affinity of the divalent anion over the monovalent anion, depending on the nature (cross-link and functional group) of the resin. This effect is quantified by equation 6.3, which shows that the retention of a multi-valent ion is more strongly dependent on the eluent strength than a monovalent ion.[21, 24]

To investigate the effect of ionic strength on the relative retention of CO_3^{2-} and Br^- a series of separations were performed in which these two ions were

treated as analytes and increasing concentrations of a hydroxide eluent were used. Figures 6.10 and 6.11 plot the log *k* for CO_3^{2-} and Br^- against the log [NaOH] on the AS23 and AS16 columns, respectively. The plot shows that as the NaOH concentration (hence the ionic strength) is increased, the anion exchanger resin loses its affinity for the divalent anion (carbonate) relative to the monovalent ion (bromide). Indeed, the slopes in Figures 6.10 and 6.11 are near the ideal slopes predicted by equation 6.3. At higher ionic strengths (higher [NaOH]) elution order *reversal* occurs between the two ions. The intersection point of the lines corresponds to the critical ionic strength where electroselectivity reversal occurs. From the log *k* and log [NaOH] plot, we can extract the critical ionic strength at which the bromide and carbonate ion would reverse their elution order (the intersection point of two lines). In the case of AS23 (Figure 6.10), the critical crossover ionic strength is 19 mM. That is, at an ionic strength lower than 19 mM, the AS23 column retains CO_3^{2-} more strongly than Br^-, which at a higher ionic strength CO_3^{2-} will be more weakly retained than Br^-.

Considering again the reversal in peak shape seen in Figure 6.8, at low carbonate concentrations the ionic strength is low and the eluent ion (CO_3^{2-}) is more strongly retained than the analyte (Br^-). As was discussed in Section 6.3.3, under such conditions peak fronting is observed. As the eluent concentration in Figure 6.8 is increased, a transition in overload peak shape is observed between 5 mM CO_3^{2-}/5 mM HCO_3^- (I=15.5 mM) and 10 mM CO_3^{2-}/1 mM HCO_3^- (I=31 mM). The critical ionic strength that is observed for this AS23 column (Figure 6.10) is 19 mM. Thus, when the ionic strength of the carbonate eluents exceeds 19

mM, the eluent ion (CO_3^{2-}) is more weakly retained than the Br^- analyte, and so peak tailing is observed.

The AS16 column shows a similar pattern where the electroselectivity reversal between bromide and carbonate occurs at an ionic strength of ~30 mM (Figure 6.11). Thus, fronting is expected for carbonate eluents of ionic strength below 30 mM and tailing would expected for higher ionic strength carbonate eluents. This general trend is observed in Figure 6.9, but the precise transition in peak shape does not occur precisely at the critical ionic strength. Peak fronting is observed in Figure 6.9 for the 10 mM CO_3^{2-}/1 mM HCO_3^- eluent which has an ionic strength (I = 31), slightly greater than the 30 mM critical ionic strength determined in Figure 6.11.

Thus, the behaviour of carbonate eluent is consistent with the ideas developed in the Section 6.3.4. Simply put, if the eluent anion is more strongly retained than the analyte anion, the analyte will definitely produce fronting peaks under overload conditions, as observed with low concentrations of carbonate eluent. Conversely, if the eluent is less strongly retained, as in the case of high carbonate eluents, peak tailing may be observed. However, as was concluded in Section 6.3.4.2, the transition between peak fronting and peak tailing does not occur exactly at the conditions predicted by theory, but at conditions close to those predicted.

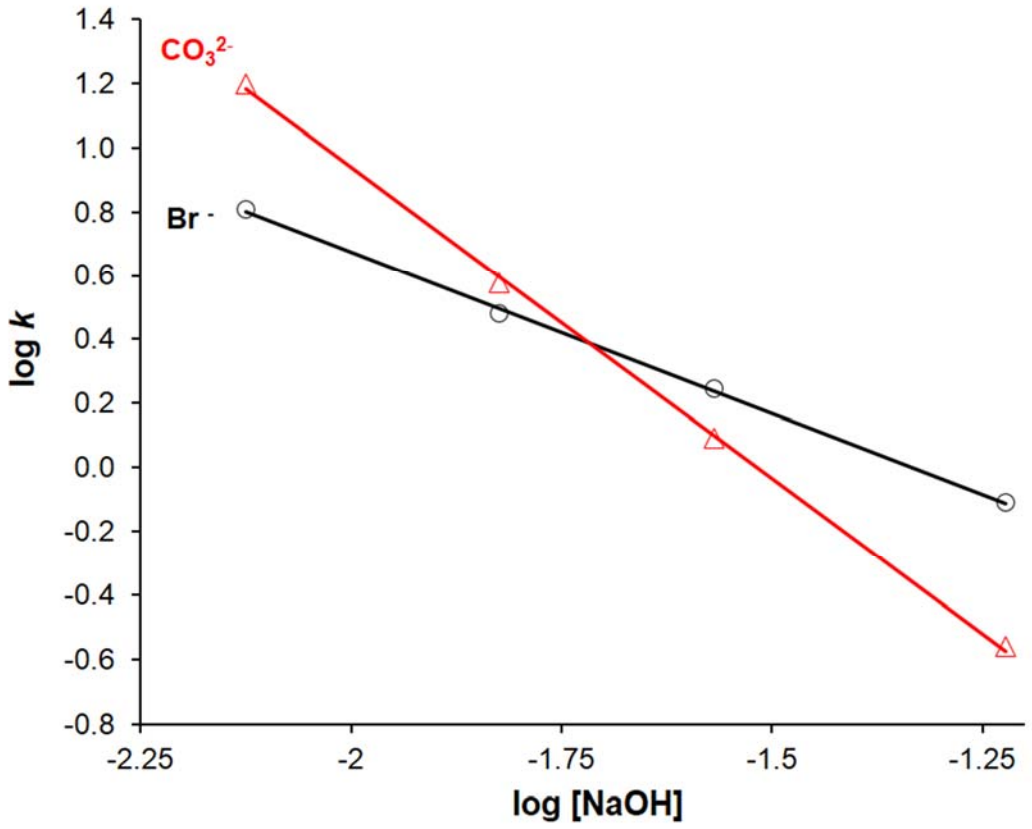

Figure 6.10. Retention behaviour of bromide and carbonate ion on a log *k vs.* log [NaOH] plot using an AS23 (250 x 4 mm i.d.) column. The horizontal line (blue) separates the fronting and the tailing regions. Conditions: eluent, NaOH at 1.0 mL/min, analyte concentration: 0.1 mM Br^- (○) and 2.5 mM CO_3^{2-} (Δ), 20 µL injection loop, and suppressed conductivity detection in recycle mode. The slopes for CO_3^{2-} and Br^- are -1.94 and 1.00, respectively.

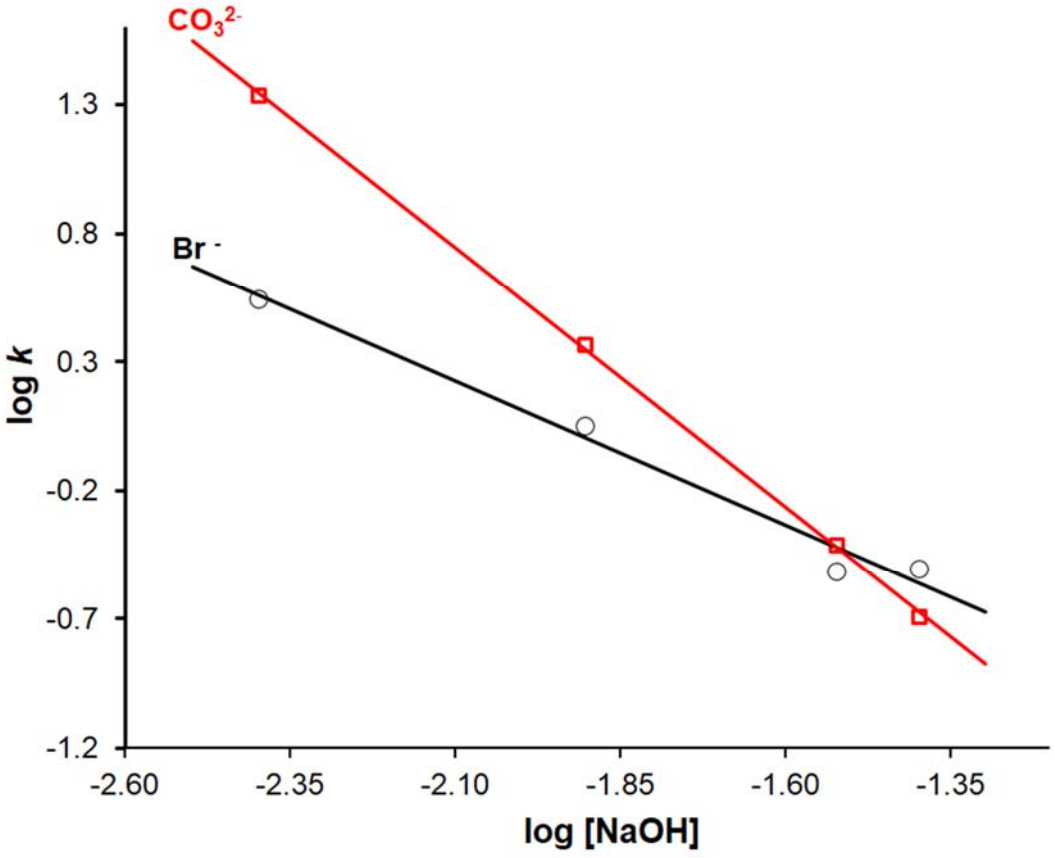

Figure 6.11. Retention behaviour of bromide and carbonate ion on a log *k vs.* log [NaOH] plot using an IonPac AS16 (250 x 4 mm i.d.) column. The horizontal line (blue) separates the fronting and the tailing regions. Conditions: eluent, NaOH at 1.0 mL/min; analyte concentrations of 0.1 mM Br^- (○) and 2.5 mM CO_3^{2-} (□); 20 µL injection loop; suppressed conductivity detection in recycle mode. The slopes for CO_3^{2-} and Br^- are -2.02 and 1.11, respectively.

6.3.6 Analytical Significance of Tailing *vs.* Fronting on Analytical Columns

The fronting or tailing of the major component will affect the shape and retention time of adjacent trace peaks.[41, 42] If the major component exhibits tailing, its peak maximum will shift to earlier time with concentration overload (*e.g.*, Figure 6.2). Any analyte eluting just before the shock wave (sharp front of a tailed peak) will be "displaced" by the shock wave to yield a sharpened peak at an earlier retention time .[43] On the other hand a trace peak which elutes just after the overload peak will experience tag-along effects which smear the trace analyte underneath the overloaded matrix peak.[43] Thus overloaded tailing peaks are undesirable in cases where a trace peak is eluting adjacent to the overloading peak on both sides.

Fronting peaks shift their retention times to a later retention time (*e.g.*, Figure 6.4). Any trace component that elutes after the fronting overload peak can be "displaced" to a longer retention time.[42] On the other hand, a trace peak which elutes before the fronting peak can be "pulled back" and broadened at longer retention times.[42]

This work has demonstrated that both tailing and fronting can be observed in IC with the same column. Future studies will be performed to determine how the overload peak shape of the major component affects the analysis of other trace components with the sample.

6.4 Conclusions

Concentration overloading phenomenon in chromatography has both theoretical and practical significance. In the case of IC eluents, competitive Langmuir isotherms offer a realistic picture of the process occurring inside the column. This work showed a simple criterion of the relative retention of the analyte anion and eluent ion for predicting peak shapes under overload conditions. When the eluent ion is less retained than the analyte ion, peak tailing is observed. If the eluent ion is more retained that the analyte ion, peak fronting occurs. Eluents such as borate and bicarbonate are always weakly retained, and so they always exhibit tailed peaks under overload conditions. Hydroxide is more complicated. Recent column development efforts have sought to make hydroxide a more effective (*i.e.*, more retained) eluent through the creation of more hydrophilic anion exchange sites. However, such hydrophilic IC columns will be more prone to exhibiting peak fronting.

For monovalent eluents and monovalent analytes the peak shape does not change with eluent concentration. With divalent eluents such as carbonate, the peak shape of the overloaded analyte may change with eluent concentration due to the effect of electroselectivity. This effect states that the IC retention of a multivalent ion is more strongly affected by the ionic strength of an eluent than a monovalent ion. Thus, the relative retention of the carbonate eluent and a monovalent analyte will switch at a critical eluent ionic strength. Regardless, of this complexity, the ultimate rule governing overload peak shape in IC remains the same: if the eluent ion is less retained than the analyte ion, peak tailing is

observed; whereas if the eluent ion is more retained that the analyte ion, peak fronting occurs.

6.5 References

1. C. A. Lucy, M. F. Wahab, *LC GC North America* **2013**, *31*, 38-42.
2. S. Fisher, R. Kunin, *Analytical Chemistry* **1955**, *27*, 1191-1194.
3. C. Pohl, C. Saini, *Journal of Chromatography A* **2008**, *1213*, 37-44.
4. J. Weiss, D. Jensen, *Analytical and Bioanalytical Chemistry* **2003**, *375*, 81-98.
5. P. Zakaria, C. Bloomfield, R. A. Shellie, P. R. Haddad, G. W. Dicinoski, *Journal of Chromatography A* **2011**, *1218*, 9080-9085.
6. R. Lin, K. Srinivasan, C. Pohl, *LC GC Europe* **2011**, *24*, 322-333.
7. H. P. Wagner, B. V. Pepich, K. S. Chris Pohl, Brian De Borba, Rong Lin , D. J. Munch, *U. S. Environmental Protection Agency* **2009**.
8. S. Ghodbane, G. Guiochon, *Journal of Chromatography* **1988**, *444*, 275-291.
9. F. Gritti, G. Guiochon, *Journal of Chromatography A* **2012**, *1254*, 30-42.
10. F. Gritti, G. Guiochon, *Journal of Chromatography A* **2009**, *1216*, 63-78.
11. Jack Cazes, R. P. W. Scott, *Chromatography Theory*; CRC Press, Marcel Dekker Inc. : New York, 2002.
12. U. D. Neue, *HPLC Columns, Theory, Technology and Practice*; John Wiley & Sons Inc.: New York, 1997.
13. T. Fornstedt, G. Guiochon, *Analytical Chemistry* **1994**, *66*, 2686-2693.
14. C. A. Lucy, P. W. Carr, *Journal of Chromatography* **1991**, *556*, 159-168.
15. R. Arnell, P. Forssen, T. Fornstedt, *Analytical Chemistry* **2007**, *79*, 5838-5847.
16. S. Golshan-Shirazi, G. Guiochon, *Analytical Chemistry* **1989**, *61*, 2373-2380.

17. S. Golshan-Shirazi, G. Guiochon, *Analytical Chemistry* **1989**, *61*, 2380-2388.

18. S. Golshan-Shirazi, G. Guiochon, *Analytical Chemistry* **1989**, *61*, 462-467.

19. G. Guiochon, A. Felinger, D. G. Shirazi, A. M. Katti, *Fundamentals of Preparative and Nonlinear Chromatography*, 2nd ed.; Elsevier Academic Press: Amsterdam, Netherlands, 2006.

20. T. Fornstedt, G. Guiochon, *Analytical Chemistry* **1994**, *66*, 2116-2128.

21. J. E. Madden, N. Avdalovic, P. E. Jackson, P. R. Haddad, *Journal of Chromatography A* **1999**, *837*, 65-74.

22. J. Madden, P. R. Haddad, P. Hajos, *Trac-Trends in Analytical Chemistry* **1996**, *15*, 531-537.

23. H. Small, *Ion Chromatography*; Plenum Press, New York: New York, 1989.

24. J. E. Madden, P. R. Haddad, *Journal of Chromatography A* **1998**, *829*, 65-80.

25. C. Liang, C. A. Lucy, *Journal of Chromatography A* **2010**, *1217*, 8154-8160.

26. P. R. Haddad, P. E. Jackson, A. L. Heckenberg, *Journal of Chromatography* **1985**, *346*, 139-148.

27. V. Maurino, C. Minero, *Analytical Chemistry* **1997**, *69*, 3333-3338.

28. D. L. Strong, P. K. Dasgupta, K. Friedman, J. R. Stillian, *Analytical Chemistry* **1991**, *63*, 480-486.

29. R. W. Slingsby, C. A. Pohl, *Journal of Chromatography* **1988**, *458*, 241-253.

30. S. Golshan-Shirazi, G. Guiochon, *Analytical Chemistry* **1988**, *60*, 2634-2641.

31. A. M. Katti, M. Diack, M. Z. El Fallah, S. Golshan-Shirazi, S. C. Jacobson, A. Seidel-Morgenstern, G. Guiochon, *Accounts of Chemical Research* **1992**, *25*, 366-374.

32. C. A. Pohl, J. R. Stillian, P. E. Jackson, *Journal of Chromatography A* **1997**, *789*, 29-41.

33. H. F. Walton, R. D. Rocklin, *Ion Exchange in Analytical Chemistry*; CRC Press, Boca Taton, 1990.

34. H. Sato, *Analytical Chemistry* **1990**, *62*, 1567-1573.

35. P. Hajos, O. Horvath, V. Denke, *Analytical Chemistry* **1995**, *67*, 434-441.

36. J. S. Fritz, *Journal of Chromatography A* **2005**, *1085*, 8-17.

37. G. Boari, L. Liberti, C. Merli, R. Passino, *Desalination* **1974**, *15*, 145-166.

38. R. E. Barron, J. S. Fritz, *Journal of Chromatography* **1984**, *316*, 201-210.

39. S. Subramonian, D. Clifford, *Reactive Polymers* **1988**, *9*, 195-209.

40. D. Muraviev, R. K. Khamizov, N. A. Tikhonov, J. G. Morales, *Industrial & Engineering Chemistry Research* **2004**, *43*, 1868-1874.

41. C. A. Lucy, L. Gureli, S. Elchuk, *Analytical Chemistry* **1993**, *65*, 3320-3325.

42. C. A. Lucy, T. L. Luong, S. Elchuk, *Journal of Chromatography* **1991**, *546*, 27-36.

43. G. Guiochon, M. Z. El Fallah, S. Golshan-Shirazi, *Journal of Chromatography A* **1990**, *511*, 1-15.

CHAPTER SEVEN. Conclusions

7.1 Conclusions and Prospects

The research presented in this thesis revolved around the factors that control the resolution of a chromatographic separation, namely the efficiency *N* and selectivity factor *α*. For that purpose, new carbonaceous stationary phases for separating ionic and polar compounds were developed. The modified carbon based phases provided a different selectivity for polar molecules. The synthesized stationary phases were characterized *via* surface analysis techniques and chromatographic performance. Once the column chemistry was designed, the efficiency *N* of a given stationary phase was improved in two ways: a) by employing small particles; and b) by optimizing packing of the particles. Additionally, to obtain a deeper fundamental understanding of peak shapes of ionic analytes, this thesis also probed the factors that lead to distortion of a peak profile under overload conditions.

Chapter 2 reviewed the state of the art approaches for achieving fast and high-resolution separations of inorganic and small organic ions.[1] Faster ion chromatography (IC) separations can be achieved by reducing the length of columns packed with large particle sizes (> 5 µm), by compromising the efficiency on polymeric phases. More recently, commercial columns employing 4 µm in 15-25 cm long columns were introduced.

Commercial IC has yet to produce columns packed with 2-3 µm particles to compete with UHPLC. Carbon clad zirconia particles are available in 2-3 µm

sizes. However, carbon does not easily lend itself to surface modification. The research described in Chapter 3 was a two pronged approach: a) to devise a generic and convenient strategy for modifying carbon surfaces; and b) to use the high efficiency ion chromatography phase in a short column.[2] The idea was to "transfer" the chemistry of commercial (polymeric) agglomerated phases onto a carbonaceous phase. An agglomerated anion exchanger was created by grafting benzene sulfonic acid on the carbon clad zirconia using diazonium chemistry followed by adsorbing a layer of custom made Dionex polycationic latexes. The 5 cm column provided lower plate heights (*e.g.* than the commercial counterpart column for organic ions) but a reduced plate height of ca. 6 was observed for organic ions. The commercial column also produced reduced plate heights of 5-6. A well packed column shows reduced plate heights around 2. This implied that the packing of 3 µm particles were not optimized. This chapter showed the feasibility of using particles smaller than 4 µm in ion chromatography. However, the poor reduced plate heights indicated that further research refinements in packing of the "charged" particles were needed. Additionally, this work gave insight into the best approach for modifying carbon based phases. These approaches have subsequently been employed to create new highly stable carbon based stationary phases with a novel selectivity. One example will be given in Chapter 5.[3]

As summarized in Chapter 2, over the past few years Dionex, the world leader in IC, has been working on small (< 5 µm) polymeric particle IC. In a collaborative project with Dionex, a model 4.4 µm polymeric substrate was

chosen to investigate the fundamental processes that control column packing. Packing is a closely guarded secret by column manufacturers, and so the literature provided very little guidance. Chapter 4 rationalized the packing behaviour of small polymeric charged particles in HPLC columns.[4]

Due to their small size, IC particles behave very much like colloids. Chapter 4 showed that high *ionic strength* slurries are detrimental for packing due to agglomeration of the particles. Thus, slurry conditions should promote a dispersed suspension, *i.e.*, slurry should be at low ionic strength with low valency counter-ions. However, such dispersed slurries of charged particles show non-Newtonian rheological properties, *i.e.* the concentrated slurry solidified when shear forces acted on it, but liquefied when pressure was removed from the consolidated bed. This was the first time that shear thickening process was reported in the chromatography literature. In addition to discovering the shear thickening properties of the suspension of charged particles, Chapter 4 also demonstrated how to minimize this undesired property, *i.e.*, by heating the slurry. Using this packing approach, reduced plate heights as low as 2 were obtained for the 4.4 μm agglomerated phase. Personal communications with Dionex have informed us that they have modified some of their packing procedures in light of these results. There is certainly a bright future for small particle ion chromatography to compete with UHPLC's speed and high resolution. Subsequent studies with carbonaceous phases in Chapter 5 have demonstrated that the conclusions made on these polymeric charged particles are relevant to charged

stationary phases made of different materials. A personally invited tutorial is being prepared for packing HPLC columns in *Analytica Chimica Acta*.[5]

In addition to efficiency *N*, the selectivity factor α is a critical chromatographic property. Separation of highly polar compounds is very difficult in reversed phase chromatography. Hydrophilic interaction liquid chromatography (HILIC) is the fastest growing separation mode in the industry, as it can retain polar compounds.[6] Extensive experiments were designed to modify porous graphitic carbon (PGC) particles based on the methodologies developed in Chapter 3. The goal was to convert the highly hydrophobic "super reversed phase" PGC surface into a polar HILIC phase. The porous graphitic carbon surface was decorated with benzoic acid groups using the diazonium salt of 4-aminobenzoic acid. This modification converted the PGC into a polar hydrophilic surface – a requirement in HILIC. This was first report of HILIC on a modified PGC in the literature.[3] After synthesis and optimization of the packing procedure, the surface and chromatographic properties of this new phase were studied. This new class of HILIC phase is *different* from 35 silica and polymeric phases tested. Personal communications with Thermo Scientific, the manufacturer of PGC, stated that they had made four attempts to modify PGC for chromatographic purposes, without much success.

This work has opened avenues for making carbon based HILIC or mixed mode HPLC stationary phases. For instance, I have synthesized a novel hybrid silica and modified graphitic phase, which combines the good characteristics of both silica and carbon. Chromatographic characterization of this phase is

underway by my collaborator (M. E. A. Ibrahim). Preliminary results are that this hybrid phase retains the high efficiency of silica phases, while keeping the unique retention properties of the modified carbon phase.[7] A major chromatography company (Phenomenex, USA) has shown interest in exploring this hybrid phase.

Finally, returning to efficiency, an often overlooked factor that can lead to poor efficiency is overloading of the column by the analyte. Under overload conditions, the peak shape changes from symmetric high efficiency peaks to fronted, tailed or even split peaks. While asymmetrical peaks are often seen with low capacity ion chromatography columns, no studies of this behaviour existed in the literature. My goal for Chapter 6 was to find out a "predictable" trend for the peak shape, under overload conditions, with a given eluent. Three commercial columns with different ion exchange chemistries were studied with common IC eluents. It was determined that the overload behaviour was characteristic of a competitive Langmuir isotherm. As such, a simple peak shape criterion was found to be valid in all cases. If the eluent anion is more *strongly* retained than the analyte ion on an ion exchanger, the analyte peak is *fronting*. On the other hand, if the eluent is more *weakly* retained on the stationary, the analyte peak always *tails* under overload conditions.[8] This work has very important consequences in terms of stationary phase design in IC and for predicting the behaviour of trace analytes when other components are present in high concentrations. The trace peaks shift their retention time because of overloading effects. A new graduate student in our group (M. H. Naeeni) is currently studying this peak interaction behaviour. These peak interaction effects are also important in two dimensional liquid

chromatography (for heart cutting purposes). As was discussed in Chapter 2, two dimensional IC is a promising solution for the analysis highly complex ionic samples, which have disproportionate amounts of analytes.

Overall, the body of knowledge presented in this thesis will be useful in both fundamental and practical aspects of the design and packing of stationary phases employed in the separation of ionic and highly hydrophilic compounds. We expect to see exciting new phases based on small particles, which offer very unique selectivity, and high efficiency along with high speed. This is the goal, which separation scientists have been successfully pursuing over the last 50 years and will continue to do so in the times to come.

7.2 References

1. C. A. Lucy, M. F. Wahab, *LC GC North America* **2013**, *31*, 38-42. **Reprinted** in *LC GC Europe*, **2013**, *26,* 38-42. (**Invited**).
2. M. F. Wahab, C. A. Pohl, C. A. Lucy, *Analyst* **2011**, *136*, 3113-3120.
3. M. F. Wahab, M. E. A. Ibrahim, C. A. Lucy, *Analytical Chemistry* **2013**, *85*, 5684-5691.
4. M. F. Wahab, C. A. Pohl, C. A. Lucy, *Journal of Chromatography A* **2012**, *1270*, 139-146.
5. M. F. Wahab, C. A. Lucy, *Analytica Chimica Acta* **(Invited, to be submitted in November 2013)**.
6. R. E. Majors, *LC-GC North America,* **2009**, *27*, 956-966.
7. M. E. A. Ibrahim, M. F. Wahab, C. A. Lucy, *Analytica Chimica Acta* **(work in progress)**.
8. M. F. Wahab, J. K. Anderson, M. Abdelrady, C. A. Lucy, *Anaytical Chemistry* **(under revision)**.